

学位论文

王 静

目次

1. 主論文

NMR studies on the structure and function relationships of proteins by using artificial structural perturbations

(構造摂動を利用した NMR によるタンパク質の構造機能相関研究)

王 静

2. 公表論文

Allosteric breakage of the hydrogen bond within the dual-histidine motif in the active site of human Pin1 PPIase

Jing Wang, Naoya Tochio, Ryosuke Kawasaki, Yu Tamari, Xu Ning, Jun-ichi Uewaki, Naoko Utsunomiya-Tate, and Shin-ichi Tate

Biochemistry, (2015) 54 5242-5253

Redox-sensitive structural change in the A-domain of HMGB1 and its implication for the cisplatin modified DNA

Jing Wang, Naoya Tochio, Aya Takeuchi, Jun-ichi Uewakia, Naohiro Kobayashi, and Shin-ichi Tate.

Biochemical and Biophysical Research Communications (2013) 441,701-706.

3. 参考論文

The C113D mutation in human Pin1 causes allosteric structural changes in the phosphate binding pocket of the PPIase domain through the tug of war in the dual-histidine motif

Xu,N., Tochio,N., Wang,J., Tamari,Y., Uewaki,J., Utsunomiya-Tate,N., Igarashi,K., Shiraki,T., Kobayashi,N., and Tate,S.

Biochemistry (2014) 53 (34) 5568-78

主論文

Contents	Page
Chapter I	
General introduction	1
Chapter II	
Allosteric breakage of the hydrogen bond within the dual-histidine motif in the active site human Pin1 PPIase	
Abstract	5
1. Introduction	6
2. Materials and methods	11
3. Results and discussion	17
4. Discussion	28
5. Conclusions	36
Chapter III	
Redox-sensitive structural change in the A-domain of HMGB1 and its implication for the cisplatin modified DNA	
Abstract	64
1. Introduction	65
2. Materials and methods	68
3. Results and discussion	72
4. Conclusions	76
Chapter IV	
General Conclusions	87
Acknowledgments	89
References	90

Chapter I

General Introduction

The function of a protein can be only interpreted from its structure. However, the protein structure is not rigid, but rather dynamic with several timescale motions. Generally, proteins achieve a fine balance between a define structure and maintaining a high population of flexibility. The structure of a protein has to be enough stable to organize a functional regions or to form a specific protein-protein interaction interfaces. Meanwhile, the protein has to be flexible enough to let the substrate into the active site or undergo conformational changes to response to several functions etc.

From a thermodynamics point of view protein structure is kept under subtle thermodynamic balance. Protein folding to make a specific structure from an extended string of amino acids associates with huge entropy loss, which is compensated by the chemical bonds energies within the protein molecule, which contribute as enthalpy to the folding free energy¹. The free energy for maintaining protein structure is usually on the order of 10 kcal/mol, being the amount of the chemical bonding energy comparable for a few number of hydrogen bonds². The folding/unfolding processes of many protein takes place within milliseconds at room temperature. Protein structures are labile and, therefore, readily change by even a little perturbation to the molecule; which perturbations are single amino acid change to the native sequence, chemical modification, chemical compound binding, and interaction

with other protein^{3, 4}.

As it is well recognized in the observations in the physics researches, perturbations to the target system give fruitful outcomes that are never gained by just looking at the target. It is also the case in exploring the structure-function relationships, perturbing protein structure in some ways could give us newer insights that have not been ever gained from the observations on naturally occurring proteins.

Nature uses the labile structural properties of proteins to regulate their functions within cells: post-translational modifications including phosphorylation, acetylation, methylation, and ubiquitination are not just protein tagging, but they also change the structure to some extent^{5, 6}. In addition, the amino acid replacement to the naturally occurring sequence will change the structure, and sometimes such structural alteration by mutation (or amino acid change) will cause inheritable diseases⁷⁻⁹.

Because protein structure is labile, it fluctuates in solution; the thermal energy in protein solution at room temperature is enough to allow the structure to sample various different conformations¹. The protein structural fluctuation or dynamics is determined by its spatial structure. The structural perturbation to the structure, thus, will also change the structural dynamics. Protein structure and dynamics are intimately interrelated and it is in general hard to discriminate their roles in biological functions¹⁰⁻¹².

Artificial structural perturbation to protein give the changes to discriminate the functional roles of structure from dynamics¹³. Structural perturbation we need for the purpose can be carried out by the site specific

amino acid mutation and chemical modification³. The changes in the structure and dynamics of protein caused by the perturbation will convey profound insights into how the protein uses them, if we could analyze the changes in dept. That is what I aimed to do by extensively using NMR in my Ph.D. research project.

In the course of my Ph.D. research, I focused on two different types of proteins: one is the prolyl-cis/trans-isomerase that constitutes an important reaction in the phosphor-mediated signal transduction pathways in cells. The other is the DNA binding protein HMGB1 that is known to also work as an ‘alarmin’ to let the cells know that something lethal reactions occur in the neighboring cells. In either case, the structural perturbation in combination with the extensive NMR analyses gave us more profound structure–functional aspects that have not been ever gained.

In Charppter II, I present the Peptidyl-prolyl isomerase (PPIase) Pin1, which is an essential enzyme that specifically catalyzes the phosphorylated-Ser/Thr-Pro motifs. The residues C113-H59-H157-T152 form a hydrogen bond network in the active site. An interesting study from computer simulation has shown that protonation of C113 rearranges the hydrogen bonding network, meanwhile, changing the tautomeric states of adjacent histidines (H59 and H157). We employed two Pin1 PPIase mutants to mimic the protonation state of C113 to see how the change in C113 modulates the active structure, dynamics and function. Here, we proposed a schemes for the dynamics hydrogen bond based on the experimental and theoretical studies (Fig.II-7). Mutation to C113 caused changes in the tautomer states of H59 according to

the amino acid type, thus, altered the dynamics in the hydrogen bond network. In both cases, the tautomer state changes eventually broken the hydrogen bond between the dual-histidine. The solution structure, dynamics, H/D exchange rates and the activity for mutants altogether were found to be consistent with our proposed dynamics in the hydrogen bond network.

In chapter III, I present HMGB1 (high-mobility group B1), which is a ubiquitously expressed bifunctional protein. HMGB1 changes its functions according to the redox states, in both intra- and extra-cellular environments. Two cysteines, Cys23 and Cys45, in the A-domain of HMGB1 forms a disulfide bond under oxidative conditions. The structure of the oxidized A-domain in HMGB1 has not been solved, therefore, the molecular mechanism for the functional changes in reposed to the redox states of HMGB1 remains elusive. To advance our understanding of the redox-dependent functional change of HMGB1, we solved the oxidized A-domain structure and compared with the reduced one. We solved the oxidized A-domain structure and compared with the reduced one. There found notable structure in the loop between helices I and II. In particular, the flipped phenyl ring at Phe38, at the C-terminal edge of the inter-helix loop, relative to that in the reduced form was remarkable. Phe38 is the key residue interacting into cisplatin-[d(GpG)] intrastrand crosslink site, as shown in the X-ray complex structure of the reduced A-domain of HMGB1 with the cisplatinated DNA. In the complex structure, the oxidized A-domain has demonstrated that the phenyl ring could not readily intercalate into the cavity by the guanine bases (Fig.III-1), which could explain the reduced affinity of the oxidized HMGB1 to the cisplatinated DNA.

Chapter II

Allosteric breakage of the hydrogen bond within the dual-histidine motif in the active site human Pin1 PPIase

Abstract

Pin1 is the phosphorylation-dependent *cis-trans* peptidyl-prolyl isomerase (PPIase), which specifically catalyze the phosphorylated-Ser/Thr-Pro motifs. The residues C113-H59-H157-T152 form a hydrogen bond network running across the active site. Theoretical study has shown that protonation states of C113 rearranges the hydrogen bonding in the network, with switching the tautomeric states of adjacent histidines (H59 and H157) that are referred as 'dual-histidine motif' [Barman,A. and Hamelberg,D. (2014) *Biochemistry*, 53, 3839-3850]. In the present work, we found the C113A and C113S Pin1 mutants altered the protonation states of H59 according to the respective residue type replaced with C113, and the changes in both mutants resulted in the hydrogen bond breaking within the dual-histidine motif. In the C113A mutant, H59 was in the exchange between ϵ - and δ -tautomers. The C113S mutant showed H59 is exchanging between ϵ -tautomer and imidazolium. The present results experimentally demonstrated that the residue change at 113 site can modulate the dynamics in the hydrogen bond network. This ensures C113 can role as a pivot to drive the concerted function among the residues in the hydrogen bond network as theoretically predicted.

1. Introduction

Peptidyl-prolyl *cis-trans* isomerases (PPIases) constitute a family of enzyme that catalyze the *cis-trans* peptide bond of proline residue in their target proteins^{14, 15}. Pin1 is a member of the parvulin family of PPIases, but it specifically rotates the ω -bond of Pro in the sequence of phosphorylated Ser (pSer) or phosphorylated Thr (pThr). Ser/Thr-Pro motifs are phosphorylated by Pro-directed protein kinases¹⁶. The Pro-directed protein kinases work in coupled with Pin1 isomerization to pSer/pThr-Pro motifs to regulate diverse signaling processes in cells¹⁷⁻¹⁹. Disordering of Pin1 is, therefore, implicated in various diseases, which makes Pin1 focused as a potential therapeutic target²⁰⁻²³.

Pin1 consists of two domains: phosphor-peptide binding domain (WW domain) and catalytic domain (PPIase domain) and those two domains are connected by a flexible linker²⁴. Crystal structures of Pin1 in the complex with Ala-Pro peptide gave the first insights into how the PPIase domain binds to the target motif, although the bound peptide does not contain the canonical pSer/pThr-Pro motif. In the crystal structure, sulfate ion was captured by the basic residues including K63, R68 and R69 in the active site loop²⁴. The sulfate ion was at the corresponding position to the phosphate in the canonical motif predicted from the dipeptide structure in the crystal²⁴. The three basic residues are, therefore, recognized engaging in the substrate binding: the three basic residues are referred as 'basic triad' in the following text. The role of the basic triad in phosphate recognition was confirmed by another crystal structure of Pin1 PPIase domain in the complex with the

ligand mimicking inhibitor²⁵. In the crystal structure, Pro in the motif stays at the hydrophobic pocket comprising of F134, M130 and L122²⁴. There are ionizable residues surrounding to the target Pro peptide bond in the substrate, which are the residues of C113, H59 and H157²⁴.

From the crystal structure of Pin1 PPIase, C113 was proposed to play as a nucleophile attacker to the substrate²⁴. In the mechanism, deprotonation from C113 thiol by spatially neighboring H59 imidazole ring allows the nucleophile attack to the carbonyl carbon in the substrate peptide to prompt *cis-trans* isomerization²⁴. The site-directed mutations to C113, however, resulted in controversial results against the mechanism^{9, 24}. In spite of the lack of nucleophilic group, C113A mutant keeps the catalytic activity, although it reduces the activity by 130-fold²⁴. In addition, the C113D and C113S mutants retain the isomerization activities without having nucleophile attack moiety⁹. Those results made the covalent mechanism mediated by C113 attack questionable.

Studies using kinetic isotope effects proposed a more feasible mechanism, in which the twisted amide configuration that occurs at a transition state in isomerization is stabilized by the intramolecular hydrogen bonding within the substrate, as found for the other types of PPIases including FKBP and cyclophilin^{26, 27}. The mechanism does not assume a nucleophile attack by C113, but it emphasizes the proper positioning of the active site residues around the substrate is essential; in especial, the basic triad binding to phosphor-moiety and Q131 hydrogen bonding to the carbonyl oxygen of Pro in substrate are focused²⁶.

The high-resolution crystal structure on Par14, a Pin1 homologue, demonstrated that the ionizable residues in the active site form a hydrogen bond network running across the active site²⁸. The residues in the hydrogen bond network are structurally super-positioned to C113, H59, H157 and T152 (listed in the connecting order in the hydrogen bonding network) in Pin1²⁸. Par14 has an aspartate instead of a cysteine at the 113 site²⁸. C113D mutant Pin1 PPIase, mimicking the Par14 active site, showed reduced isomerization rate relative to the wild-type²⁹. NMR analysis has shown that D113 made a tighter hydrogen bond to H59 via carboxylate oxygen in D113 with destabilizing the hydrogen bond between H59 and H157²⁹. Unbalancing the hydrogen bonding in the network destabilized the active site structure and disorganized the basic triad structure in the active loop. The allosteric structural change to the basic triad could explain the reduced binding affinity for the C113D mutant to phosphor-peptide, thus its lowered isomerization rate²⁹. The result has shown the properly balanced hydrogen bonding network (C113-H59-H157-T152) is essential for the efficient isomerization²⁹.

The nucleophile attack of thiolate in C113 does not seem plausible. The high chemical reactivity of C113, however, assures there exists a thiolate in free Pin1: Juglone (5-hydroxynaphthoquinone) selectively makes a covalent bond to C113 with keeping C57 intact in Pin1³⁰, and C113 is oxidized under the condition that C57 remains unmodified³¹. The role of the C113 thiolate in the context of the hydrogen bond network was proposed by Barman and Hamelberg³². They theoretically showed that C113 should stay in a thiolate form in the absence of substrate, while it will be protonated in the complex

with substrate. In their simulation, they predicted that the altered protonation to C113 will change the tautomeric state of the spatially neighboring H59, and it further rearranges the hydrogen bonding to H157 and T152³². They emphasized the C113-triggering cooperative protonation change among the residues in the hydrogen bond network can energetically explain the cis to trans isomerization in the active site of Pin1 PPIase³².

C113 mediated dynamic rearrangement of the hydrogen bonding network, which Barman and Hamelberg proposed, relies on the coupled changes in the protonation states of the spatially neighboring H59 and H157; these histidines are conserved among the parvulins, thus, referred to as ‘dual-histidine motif’³². The imidazole ring of histidine has two nitrogen atoms, N^{ε2} and N^{δ1}. The imidazole ring can be in two neutral forms and a charged state according to the pH and/or the local environment. Two neutral imidazole forms are designated as δ-tautomer (protonated to N^{δ1}) and ε-tautomer (protonated to N^{ε2}) according to the protonated position. In a charged state, two nitrogen atoms are protonated to make cationic imidazole ring (imidazolium). In general, protonation of histidine is not obviously observed in X-ray crystal structure. Instead, NMR can discriminate the three states of the imidazole ring based on the ¹⁵N^{ε2} and ¹³C^{δ2} chemical shifts that significantly change according to the protonation states^{33, 34}. The C113 mediating dynamic changes in protonation to dual-histidine motif, therefore, can be seen by NMR, which motivated us to study the dynamic rearrangement of the hydrogen bond network by changing the amino acid type at the 113 site.

The C113A and C113S Pin1 PPIase mutants were used in this work. Both of the mutants have about 10% activities relative to the wild-type^{9, 35}. In the context of the C113 mediated hydrogen bond dynamics by Barman and Hamelberg, C113S mutant can mimic the thiol form of C113, while C113A mutation could mimic the active site structure with a broken C113-H59 hydrogen bond. Using the mutants, we intended to see how the change in C113 modulates the active site structure and dynamics through altering protonation to H59 and H157. We found each amino acid change to C113 caused different changes to the protonation state of H59, respectively. In both cases, the change in H59 protonation state eventually broke the hydrogen bond between H59 and H157, thus cut the hydrogen bond network in the middle. The disrupting the hydrogen bond network explains the reduced structural stabilities of both proteins relative to the C113D mutant; the C113D mutant keeps the hydrogen bond network and moderately reduced its structural stability²⁹.

Overall, we could observe the structure and dynamics of the conserved histidines, H59 and H157, which sensitively change according to the residue type at the 113 site in Pin1 PPIase. The present results support the theoretical description that the hydrogen bond network including dual-histidine motif is dynamically modulated according to the chemical states of C113. C113 roles as a trigger to cooperatively reorganize the hydrogen bonds within the network in the active site of Pin1.

2. Materials and methods

Plasmids

Pin1 cDNA was reported previously (Gene Bank accession number NM_006221), and the wild-type cDNA were prepared by our previously students. Pin1 and mutants cDNAs to be cloned into pET28a expression vector (Merck Chemicals, Germany) at *Nde*I and *Eco*RI cloning sites that the Pin1 would have a 6X His-tag at N-terminal, PCR-based site-directed mutagenesis of HMGB2 was performed using QuikChange (Stratagene) and KOD-plus mutagenesis (Toyobo). The mutant's sequences were verified by automated DNA sequencing.

Protein Expression and purification

Pin1 mutants were purified from *E. coli* grown in M9 minimal medium supplemented with 50 µg/ml kanamycin at 37 °C with shaking at 140rpm until the optical density up to OD₆₀₀ = 0.6. For NMR measurement, medium also contained ¹⁵NH₄Cl and ¹³CD-glucose. IPTG (isopropyl β-D-thiogalactopyranoside) was then added to the medium to induce protein expression (final conc. 0.5 mM) for 15 h. were harvested and re-suspended in 100 ml buffer solution (50 mM Tris-HCl, pH 8.0). The cells were broken by sonication and the soluble fraction was collected by the centrifugation at 14,000 rpm at 4 °C for 20 min. Polyethylenimine (PEI) was put into the supernatant to a final concentration of 0.1% to remove the DNA and RNA contaminants by applying another centrifugation at 14,000 rpm at 4 °C for 20 min. The collected supernatant was applied to TALON® column (TAKARA

Bio). After the flow through to the column with the buffer solution (50 mM Tris-HCl, pH8.0), the column was further washed with the 200 mL solution containing 50 mM Tris-HCl, pH8.0 and 25 mM imidazole. His6X-tagged protein was eluted with the other buffer solution (50 mM Tris-HCl, pH 8.0 and 400 mM imidazole). The collected His6X-tagged protein was subjected to dialysis against 50 mM sodium phosphate buffer, pH 6.0. After the dialysis, 80-unit thrombin protease solution (GE Healthcare) was put into the protein solution to remove the His6X-tag from the PPIase domain; the proteolysis reaction was done at 20°C for overnight. The reactant was applied to cation-exchange column HiTrap SP FF (GE Healthcare) equilibrated with 50 mM sodium phosphate buffer, pH 6.0. PPIase domain was eluted by the NaCl gradient from 0 M to 1 M in 50 mM sodium phosphate buffer, pH 6.0, using BioLogic DuoFlow™ HPLC system (Bio-Rad). The collected fractions containing PPIase were subjected to the extensive dialysis against the desired buffer solutions according to the purposes for use.

Thermal stability tests for the mutant PPIases by circular dichroism(CD)

The change in the molar ellipticity at 222 nm was used to monitor the thermal denaturing process on a JASCO-720W spectrometer. The sample buffer consisted of 50 mM sodium phosphate (pH 6.0), 100 mM Na₂SO₄ and 1 mM DTT. The protein concentration was adjusted to 2 μM. The temperature was changed over the range of 20-80 °C, with an increment rate at 1 °C/min.

NMR spectroscopy and structure determination.

Structures of the C113A and C113S Pin1 PPIase mutants were determined according to the standard methods using the uniformly $^{13}\text{C}/^{15}\text{N}$ -labeled samples³⁶. All the NMR data were collected on a Bruker Avance II spectrometer equipped with a triple-resonance cryogenic probe operating at 700.33 MHz for the ^1H resonance frequency. In both of the mutants, protein was dissolved in a buffer solution consisting of 50 mM sodium phosphate (pH 6.6), 100 mM Na_2SO_4 , 5 mM ethylenediaminetetraacetic acid (EDTA), 1 mM DTT, and 0.03% NaN_3 . The protein concentrations were adjusted to 1.0 mM (C113A) and 0.4 mM (C113S), respectively; the solubility of the C113S mutant was limited. Sample temperature was set at 299 K for all NMR experiments, unless otherwise noted. Data processing and analysis were done with the programs NMRPipe³⁷ and KIJIRA³⁸ running with NMRview³⁹, respectively. CYANA utility to achieve the automatic NOE assignments was used^{40, 41}. The backbone dihedral angle restraints were generated with TALOS+⁴². The 50 lowest-target function CYANA structures were subjected to the explicit water refinement using the program XPLOR-NIH with distance and dihedral restraints⁴³. The 10 lowest-energy structures resulted from the calculation with XPLOR-NIH were validated by the program PROCHECK-NMR⁴⁴. The structural statistics for the C113A and C113S mutants are summarized in Table II-1. The programs PyMOL (DeLano Scientific, San Carlos, CA) and MOLMOL⁴⁵ were used for the structural analyses and figure generation.

The resonance assignments and the structural data for the C113A and C113S mutants were deposited in BMRB and PDB databases, respectively. BMRB accession codes are 11587 (C113A) and 11588 (C113S). PDB entries

are 2RUQ (C113A) and 2RUR (C113S). The backbone ^1H - ^{15}N resonance assignments of the HSQC spectra for the mutants are available as supplemental data (Figure II-1).

Cis-trans isomerization rates.

The *cis-trans* isomerization rates for C113A and C113S mutants were done by using 2D ^1H , ^1H -EXSY spectroscopy^{46, 47}. The sample contained 2 mM Cdc25C phosphopeptide with 50 μM PPIase mutants (C113A or C113S). The sample solution contained 50 mM Tris-HCl (pH 6.8), 1 mM DTT, and 0.03% NaN_3 . The experiments were done at 295 K on a 700 MHz NMR spectrometer. The mixing times (t_{mix}) were set to 2, 5, 10, 15, 25, 35, 50 (twice), 75, 100 (twice), 200, 300, and 400 ms. The net exchange rate, k_{EX} , was estimated to fit the equation below (eq. 1) to the ratios of the trans-to-cis exchange cross-peaks against the trans diagonal peaks. In estimating the k_{EX} values, we simultaneously used the buildup profiles from the signals for pT5 CH3, pT5 HN, and V7 HN for fitting, as in a global fitting manner.

$$\text{ratio}(t_{\text{mix}}) = \frac{[1 - e^{-(k_{\text{CT}} + k_{\text{TC}})t_{\text{mix}}}]k_{\text{TC}}}{k_{\text{CT}} + k_{\text{TC}}e^{-(k_{\text{CT}} + k_{\text{TC}})t_{\text{mix}}}} \quad (1)$$

where k_{CT} and k_{TC} are adjustable parameters in fitting and the net exchange rate, k_{EX} , is defined as $k_{\text{EX}} = k_{\text{CT}} + k_{\text{TC}}$, where k_{CT} and k_{TC} are the exchange rates from *cis* to *trans* and *trans* to *cis*, respectively⁴⁶. Uncertainties in the rate constants were estimated by Monte Carlo simulations on the basis of the duplicated data.

NMR spin relaxation experiments.

All the backbone ^{15}N R_1 and R_2 relaxation rates and steady state heteronuclear ^{15}N NOE (hNOE) data were collected on a 700 MHz NMR spectrometer, operating at 700.33 MHz for ^1H resonance, at 299 K³⁶. Each peak intensity was measured by averaging over the signal intensities at the peak center and its eight surrounding points (nine-point averaging); each peak center was found by the SPARKY “pc” function (T.D. Goddard and D. G. Kneller, SPARKY 3, University of California, San Francisco). The delays for R_1 measurements (trelax) were 10.3 (twice), 153.9, 307.9, 461.8, 615.7 (twice), 769.6, 923.6, 1128.8, and 1539.3 ms, whereas the delays for R_2 (trelax) were 0.0, 16.0 (twice), 40.0, 80.0 (twice), and 160.0 ms. The spectra for R_1 and R_2 were collected in an interleaved manner. For measuring hNOEs, we recorded an interleaved pair of spectra in which ^1H saturation of 3 s was applied alternatively with the relaxation delay set to 2 s. R_1 and R_2 relaxation rate constants for each signal were determined through the function fitting using the modelXY TCL built-in function of NMRPipe³⁷. Uncertainties for R_1 and R_2 were estimated in a Monte Carlo manner on the basis of the duplicated data. The uncertainty for each hNOE value was evaluated using the RMSD value on a spectral region with no peaks, which was obtained by the NMRPipe built-in module⁴⁷. The reduced spectral density functions, including $J_{eff}(0)$, $\mathcal{J}(\omega_N)$, and $\mathcal{J}(\omega_H)$, were calculated using the software suite RELAX^{48, 49}.

H/D exchange rates.

The amide proton/deuteron exchange (H/D exchange) rates were

measured with extensively lyophilized samples; the sample solution (the C113A or C113S Pin1 PPIase mutants in 50 mM sodium phosphate (pH 6.6), 100 mM Na₂SO₄, 5 mM EDTA, 1 mM DTT, and 0.03% NaN₃) was rapidly frozen in liquid nitrogen and placed at a vacuum chamber for approximately 12 h. The lyophilized sample was dissolved with the same volume of D₂O as it was before lyophilization, just prior to recording a series of 2D ¹H-¹⁵N HSQC spectra. The NMR measure was initiated within 10 min after dissolving the sample. One spectrum was collected for 35 min and 35 data sets were collected sequentially. No apparent spectral difference was observed between the data before and after lyophilization, which ensures the preparation had no structure damage to the mutants. H/D exchange rates were determined through the peak intensities on a series of 2D spectra as described in the previous work²⁹.

3. Results

The C113S mutant is less active in isomerization than the C113A mutant.

EXSY experiments were used to determine the isomerization rates for the C113A and C113S mutants^{17, 34} (Figure II-2). The C113A mutant showed reduced but measurable isomerization rates by EXSY (Table II-2). The isomerization rates were not determined for the C113S mutant; no exchange signals were observed on the spectra with the mixing time set up to 1 sec (Figure II-2). The C113S mutant has the *cis* to *trans* isomerization rate, k_{CT} , much smaller than 1 sec^{-1} (Table II-2).

Protease-free assays for the C113A and C113S mutants reported their relative enzyme activity (k_{cat}/K_m) were 6% and 4% to the wild-type, respectively³⁵. The other results showed the C113S mutant has 1% relative enzyme activity, while the C113D mutant retains 25% relative activity⁹. The reported results demonstrated that C113S mutation has severer detriment to the PPIase, than the C113D and C113A mutations; which is consistent with the NMR results that C113S mutant has lower isomerization activity while the C113D mutant keeps (Table II-2).

C113A mutation caused greater long range structural impact than C113S.

The backbone ^1H and ^{15}N chemical shift changes, $\Delta\delta$, by C113A and C113S mutations were compared (Figure II-3). Both mutants showed the similar $\Delta\delta$ profiles demonstrating the obvious spectral changes for the residues in β_1 , β_3 - β_4 loop, and β_4 , which parts are distant from the mutation site in the α_2 - α_3 loop. It is noted that the C113A mutant showed the greater

spectral changes for the residues in the β 3- β 4 loop and β 4 than the corresponding changes in the C113S mutant (FigureII-3A).

The parts having shown the significant spectral changes include the residues in the hydrogen bond network connecting C113-H59-H157-T152 (FigureII-3, right).¹⁶ This implies the distal spectral changes are propagated through the hydrogen bond network.

Comparing the solution structures of the wild-type, C113A and C113S Pin1 PPIase domains supports the spectral changes; the C113A mutant has induced significantly different structures in β 3- β 4 loop and β 4 from the corresponding parts in the wild-type and the C113S mutant (Figure II-4A).

C113A and C113S mutations disarranged the basic triad.

Both the C113A and C113S mutants have the disordered basic triad, comprising of K63, R68, and R69, relative to the wild type (Figure II-5). The basic triad interacts to the phosphate upon Pin1 binding to substrate²⁶. The disordered basic triad in the C113A and C113S mutants explains their diminished binding to phosphor-substrate; their bindings to substrate were too weak to measure with the isothermal titration calorimetry (ITC). It was also the case for the C113D mutant that changed the basic triad and showed severely reduced substrate affinity²⁹.

The active loop (β 1- α 1 loop) harboring the basic triad in the C113S mutant has rigid backbone structure showing hNOE values over 0.8 (Figure II6-B). The C113A mutant has also rigid active loop except for the C-terminal part including the residues W73-Q75, which part has significant structural

flexibility as shown by the lower hNOE values (Figure II-6-A). In the wild-type Pin1 PPIase structure, W73 indole ring is buried in the cavity formed by α 2- α 3 helices.¹¹ As seen in the structure comparison, the C113A mutant apparently changed the α 2- α 3 loop structure (Figure II-4A), which released the W73 indole ring from the inter-helix cavity (Figure II-4B). This structural change specifically found to the C113A mutant explains the reduced hNOE values for the residues W73-Q75 in the C113A mutant (Figure II-6A).

Protonation states of the histidines were changed in the C113A and C113S mutants.

H59 and H157 are the highly conserved among the parvulin PPIase domains. The histidines are referred to as ‘dual histidine motif’⁵⁰. The histidines engage in the hydrogen bond network, in which H59 and H157 are in ϵ - and δ -tautomers, respectively^{28, 29}. Our previous work showed impairing the hydrogen bond between H59 and H157 destabilized the structure²⁹. The change in the protonation states of the histidines, which is theoretically predicted to happen according to the state of C113³², should have significant impact on the structure and dynamics. According to the simulation³², the amino acid change to C113 should change the protonation states of H59 and H157.

The imidazole rings of H59 and H157 in the C113A mutant gave no correlations on the multi-bond ^1H - ^{15}N HSQC spectrum, while the corresponding histidines in the C113S mutant showed faint but detectable signals (Figure II-7A). The spectra observed for the histidines in these

mutants are quite different from those for the wild-type; the histidines in the wild-type gave clear correlations on the spectrum (Figure II-7A)²⁹. The apparent spectral changes for the histidines in the mutants imply that their histidines are in the quite different states from those in the wild-type.

The imidazole $^{15}\text{N}^{\epsilon 2}$ and $^{15}\text{N}^{\delta 1}$ chemical shifts can be used to distinguish its protonation states³³. H59 $^{15}\text{N}^{\epsilon 2}$ in the C113S mutant showed a broadened signal around 180 ppm, suggesting H59 imidazole ring is fully protonated to form imidazolium (Figure II-7A). The imidazolium usually gives four signals as observed for H3 in the N-terminally attached GSHM segment from the construct (Figure II-7A). H59 $^{15}\text{N}^{\epsilon 2}$ broadened signal may imply the H59 is in a chemical exchange between ϵ -tautomer (literature value: $\delta^{15}\text{N}^{\epsilon 2} = 167.5$ ppm)³³ and imidazolium state (literature value: $\delta^{15}\text{N}^{\epsilon 2} = 176.5$ ppm)³⁹. This is supported by the $^{13}\text{C}^{\delta 2}$ chemical shift at 118.3 ppm for H59 in the C113S mutant (Figure II-7D). As literature values, imidazole ring in ϵ -tautomer gives $^{13}\text{C}^{\delta 2}$ at 117.9 ppm, while imidazolium gives $\delta^{13}\text{C}^{\delta 2} = 120.0$ ppm^{33, 50}. Imidazole $^{13}\text{C}^{\delta 2}$ for H59 in the C113S mutant is observed at ^{13}C chemical shifts between ϵ -tautomer and imidazolium state (Figure II-7D). The $^{13}\text{C}^{\delta 2}$ signal for H59 was significantly weak relative to the corresponding signal in the wild-type (Figure II-7B), suggesting the H59 imidazole is in the chemical exchange at the intermediate rate in the NMR chemical shift time scale. The state of H59 in the C113S mutant is quite different from that in the wild-type, as clearly seen in comparing with the wild-type spectrum, where H59 $^{13}\text{C}^{\delta 2}$ resonates at around 116 ppm, typical position for ϵ -tautomer (Figure II-7B).

H157 in the C113S mutant showed broadened $^{15}\text{N}^{\epsilon 2}$ signal around 250

ppm, showing H157 is in δ -tautomer (literature value: $\delta^{15}\text{N}^{\epsilon 2} = 249.5$ ppm) (Figure II-7A).²¹ The $^{13}\text{C}^{\delta 2}$ for H157 resonates at 129.6 ppm close to the literature value for δ -tautomer (127.1 ppm) (Figure II-7D)⁵⁰. The broadened ^1H - ^{15}N correlation for H157 imidazole ring in the C113S mutant, therefore, is presumably caused by the imidazole ring fluctuation at the rate to facilitate the ^{15}N transverse relaxation (Figure II-7A).

The C113A mutant did not give any correlations for H59 and H157 on the multi-bond ^1H - ^{15}N HSQC spectrum (Figure II-7A). On a ^1H - ^{13}C HSQC spectrum for the C113A mutant, H157 $^{13}\text{C}^{\delta 2}$ signal was observed, while H59 did not give any correlation (Figure II-7C). Based on the $^{13}\text{C}^{\delta 2}$ chemical shift (130.5 ppm), H157 is a δ -tautomer (Figure II-7C)^{33, 50}. The loss of any ^1H - ^{15}N correlation for H157 is also ascribed to the ring fluctuation that accelerates imidazole ^{15}N transverse relaxation with keeping in a δ -tautomeric state.

We could not detect ^1H - $^{13}\text{C}^{\delta 2}$ correlation for H59 in the C113A mutant on a spectrum (Figure II-7C). It was not possible to detect the signal, even on a spectrum drawn with the threshold down to the thermal noise level (Figure II-8). Instead, the ^1H - $^{13}\text{C}^{\epsilon 1}$ correlation was clearly observed for H59, 137.0 ppm (Figure II-8). It is known that $^{13}\text{C}^{\epsilon 1}$ chemical shift does not change according to the tautomeric states; according to the literature, $^{13}\text{C}^{\epsilon 1}$ chemical shift remains 139.6 ppm irrespective of the tautomeric states of the imidazole ring⁵⁰. On the other hand, $^{13}\text{C}^{\delta 2}$ chemical shift varies according to the tautomeric states: the literature values are 117.9 ppm (ϵ -tautomer) and 127.1 ppm (δ -tautomer)⁵⁰.

For H59 in the C113A mutant, the ^1H - ^{13}C correlation for $^{13}\text{C}^{\epsilon 1}$ was

observed, while the signal for $^{13}\text{C}^{\delta 2}$ was not observed (Figure II-8). This peculiar results can be explained if we consider the imidazole ring is chemically exchanging between ϵ - and δ -tautomers. If the exchanging rate is close to the chemical shift differences between ϵ - and δ -tautomers, the ^1H - $^{13}\text{C}^{\delta 2}$ signal becomes broadened to make its signal too weak to be detected⁵¹. On the other hand, ^1H - $^{13}\text{C}^{\epsilon 1}$ signal can be observed even the imidazole ring is under the chemical exchanging, because the $^{13}\text{C}^{\epsilon 1}$ shift does not change according to the tautomeric states⁵⁰. Therefore, it is insisted to describe that H59 in the C113A is under the chemical exchange between ϵ - and δ -tautomers.

In the C113S mutant, H59 is elucidated to be primarily in the imidazolium state with chemical exchanging to ϵ -tautomer to make the signal broadened, based on the observed $^{15}\text{N}^{\epsilon 2}$ and $^{13}\text{C}^{\delta 2}$ chemical shifts (Figures II-7A and 7D). The signals for H59 in the C113A mutant was not detected on neither ^1H - ^{15}N HSQC nor ^1H - ^{13}C HSQC spectra (Figures II-7A and 7C), which is different observation from the case for the H59 in the C113S mutant. It is, therefore, presumable to consider H59 in the C113A mutant is in the other type of chemical exchanging; H59 should be in the exchange between ϵ - and δ -tautomers. Otherwise, H59 in the C113A mutant should give the similar signals as observed for the C113S mutant.

In the structure determination for both of the C113A and C113S mutants, we fixed H59 in ϵ -tautomer, without considering it in the chemically mixed states. Although it seems too simplified for assuming H59 in only ϵ -tautomer, we could successfully determine the structures without any serious violations

from the experimental restraints.

C113A and C113S mutation caused different structural changes in the active site.

The C113A and C113S mutations have different the active site structures to each other (Figure II-9). Expanded view of the active site in the C113S mutant showed that the imidazole rings of H59 and H157 are in the different orientations from those in the wild-type, while the corresponding histidines in the C113A mutant keep the similar orientation (Figure II-9A). Comparing the distributions of χ_2 -angles for the histidines H59 and H157 among the 10-lowest energy NMR structures (Figure II-10) assures the change in the imidazole ring orientations in the C113S mutant is statistically significant (Figure II-9B, Table 3).

Structural changes caused by C113A and C113S mutations were compared through the C α atom positions relative to the wild-type (Figure II-11A). The profiles for the C α displacement showed they shared the major structural changes to the β 1- α 1 loop. The C113A mutant had additionally altered the structure near the β 3- β 4 loop (Figure II-11A), which is consistent with the enhanced H/D exchange rates and the significantly reduced signal intensities for the corresponding residues characteristically observed for the C113A mutant (Figures II-12 and 13). The C113A mutation affects the residues further distant from the mutation site in comparison to the C113S.

The inter-residue C α distances among the selected residues in the active site were compared (Figure II-11B). In the C113A mutant, S115-H59

distance was shortened, while the residues A113 and S154 are put apart relative to the corresponding distances in the wild-type (Figure II-11B). The increased distance between the residues A113 and S154 in the C113A mutant resembles the change to the active site structure of the wild-type, which was theoretically predicted to occur when C113 becomes thiol-form³². In the simulation by Barman and Hamelberg, the C113-S154 distance is increased associated with the change in H59 protonation from ϵ - to δ -tautomer by forming the hydrogen bond between S115 and H59³². The shortened S115 C α -H59 C α distance observed in the C113A mutant may suggest the hydrogen bond was formed between S115 and H59, as predicted in the simulation³².

C113S mutation does not change the spatial arrangement of the focused residues in the active site (Figure II-11B). S115 may form a hydrogen bond with S113, instead of H59, as theoretically predicted in the wild-type having thiol-form C113³². The C113S mutant, therefore, maintains the narrow active site entrance as in the wild-type in the absence of substrate, which is a keen structural difference from that of the C113A mutant.

The changes in the structural dynamics by C113A and C113S mutation.

The changes in the structural dynamics were apparent for both the C113A and C113S mutations, which were seen by the reduced spectral densities^{52, 53}. The C113A mutation caused the increased $J_{eff}(0)$ values for most of the residues in the PPIase domain; $J_{eff}(0) = J_{eff}(0) [C113A/S] - J_{eff}(0) [wild\ type]$ (Figure II-14A). It should be noted that the residues with increased $J_{eff}(0)$ values are primarily clustered in the $\beta 1$ - $\alpha 1$ loop (Figure II-

14A). The increase in the $J_{eff}(0)$ value implies that the corresponding residue has promoted backbone motion in μsec - msec time regime relative to the wild-type⁵². The loss of the hydrogen bonding between C113–H59 by the C113A mutation may have destabilized the active site structure to induce the backbone fluctuation to the residues in the active site (Figure II-14A). In contrast to the case of C113A, the C113S mutant showed rather randomly distributed $\Delta J_{eff}(0)$ values (Figure II-14B); the C113S mutation did not induce the backbone motions for the active site residues in μsec - msec time scale.

The profile of $\Delta \mathcal{J}(\omega_N) = \mathcal{J}(\omega_N) [\text{C113A/S}] - \mathcal{J}(\omega_N) [\text{wild-type}]$ for the C113S mutant differed from those for the C113A mutant (Figures II-14C and 14D). The C113S mutant showed positive $\Delta \mathcal{J}(\omega_N)$ values for most of the residues, while for the C113A mutant, $\Delta \mathcal{J}(\omega_N)$ values were in the less biased distribution (Figures II-14C and 14D).

To characterize the significance of the $\Delta \mathcal{J}(\omega_N)$ distribution, we used the Lipari-Szabo maps for $\Delta \mathcal{J}(\omega_h)$ and $\mathcal{J}(\omega_N)$ ⁴². The Lipari-Szabo maps are compared among for the wild-type, the C113A and C113S mutants (Figure II-15A); most of the residues show the plots close to the rigid isotropic tumbling curve or the ' $\tau_e = 0$ ' line: the ' $\tau_e = 0$ ' line is defined by the line passing through the point on the rigid isotropic tumbling curve at the overall correlation time ($\tau_m = 9.5 \text{ nsec}$) to the origin (Figure II-15B). The rigid isotropic tumbling curve is drawn on the axes of $\mathcal{J}(\omega_N)$ and $J_{eff}(\omega_h)$ by the spectral density function for the rigid body isotropic tumbling,

$$J(t) = \frac{2}{5} \left(\frac{t}{1 + \omega^2 t^2} \right) \quad (2)$$

where t can be changed from 0 to infinity⁴². In the Lipari-Szabo model-free

formalism, the spectral density function for the motion of a given N-H bond vector is described by,

$$J(\omega) = \frac{2}{5} \left(\frac{S^2 \tau_m}{1 + \omega^2 \tau^2} + (1 - S^2) \frac{\tau}{1 + \omega^2 \tau^2} \right) \quad (3)$$

$$1/\tau = 1/\tau_m + 1/\tau_e \quad (4)$$

where S^2 is a measure of the spatial restriction of the internal motion, τ_e is the correlation time to describe the time scale of the internal motion, τ_m is the rotation correlation time for the overall molecule tumbling⁵⁴.

The rotational correlation time τ_m for Pin1 PPIase was determined to 9.5 nsec, giving in the isotropic rigid tumbling end point ($J^{rigid}(\omega_N)$, $J^{rigid}(\omega_H)$) = (0.20, 0.02) (Figure II-15B).

In the present cases where most of the plots are spread close to the rigid isotropic tumbling curve or the ' $\tau_e = 0$ ' line, the increase in $\mathcal{J}(\omega_N)$ value is primarily ascribed to the decrease in τ_e value without changing S^2 (Figure S8B). The correlation time τ_e represents how rapidly the backbone N-H bond vector moves on the tumbling molecule: at the isotropic rigid-body tumbling end point ($J^{rigid}(\omega_N)$, $J^{rigid}(\omega_H)$), τ_e becomes infinity, implying no significant internal motion happens⁵⁵. On the other hand, τ_e approaches to zero, the internal N-H bond vector motion becomes very rapid relative to the overall tumbling correlation time, τ_m . In the plots for the difference in the spectral densities, the bars for the residues in nearly the extreme narrowing limit ($\mathcal{J}(\omega_N) < 0.2$) are marked in red (Figure II-14).

In comparing the histograms showing the $\mathcal{J}(\omega_N)$ values, the C113S mutant shows significantly different distribution from those of the others, the wild-type and the C113A mutant (Figure II-15C). The increased $\mathcal{J}(\omega_N)$ values

observed for the residues in the C113S mutant, therefore, implies that overall the C113S mutant structure has reduced local backbone motions in the nsec-psec time regime relative to the wild-type and the C113A mutant (Figure II-14D).

4. Discussion

Barman and Hamelberg has theoretically demonstrated the hydrogen bonding network in the active site of Pin1 PPIase is dynamically modulated according to the protonation state of C113³². They insisted that C113 stays as a thiolate form in substrate-free state, while it becomes protonated or thiol form upon binding to cis substrate³². They have also shown the change in the active site structure and dynamics associated with the rearranging the hydrogen bond network facilitates the isomerization process through the free energy calculation³². Their theoretical insights into the Pin1 PPIase isomerization mechanism arose the interests in seeing how the amino acid change to C113 modulated the hydrogen bond network, which drove the present works using two types of C113 mutants of Pin1 PPIase domain.

Our previous work on the C113D mutant has shown that D113 alleviates the hydrogen bond between H59 and H157 (dual histidine motif), which resulted in the reduced structural stability of the active site to disorder the basic triad structure in the active loop, which binds to phosphor-moiety in substrate²⁹. The C113D mutant did not alter the protonation to H59 and H157; H59 and H157 in the C113D mutant keeps ϵ -and δ -tautomer, respectively, as they are in the wild-type²⁹. The C113D was not an appropriate example to see the dynamic change in the hydrogen bonding network in associate with the protonation changes in histidines predicted by Barman and Hamelberg.

To gain the experimental insights into dynamic hydrogen bond network

in Pin1, we carried out the research on the C113 mutants of Pin1 with the C113A and C113S mutants. The C113A removes the reactive thiol or thiolate group at the 113 site, while C113S may chemically mimic the thiol form of C113 in the wild-type. In this work, we intended to explore how the residue change at the 113 site affects the dynamics of the hydrogen bond network in the active site.

The dynamics of the hydrogen bond network changed according to the type of amino acid at the 113 position.

The changes in the dynamics of the hydrogen bond network by C113A and C113S mutations are schematically summarized (Figure II-16). In our previous work, we clearly identified the tautomeric states of H59 and H157 in the wild-type by using multi-bond ^1H - ^{15}N HSQC, which showed H59 and H157 are ϵ - and δ -tautomers, respectively (Figure II-16A)²⁹. The results are consistent with the tautomers of the corresponding histidines identified in the high resolution crystal structure of Par14, a homologous PPIase to Pin1²⁸. Our NMR result showed the hydrogen bond network exists as in the Par14 crystal structure, although NMR could not directly see if C113 is thiolate or thiol form²⁹.

As described in the RESULTS, the unusual ^1H - ^{15}N and ^1H - ^{13}C HSQC spectra for the imidazole rings in the present mutants could represent the chemical exchange between the different protonation states of H59 imidazole ring (Figures II-16B and 16C).

The C113A mutant lacks the hydrogen bond between H59 and A113, and

it may stabilize H59 in δ -tautomer by the hydrogen bonding with S115 (Figure II-16B). The hydrogen bond from S115 to H59 was theoretically predicted, in associate with the conversion from thiolate to thiol in C113 and its release from the interaction with H59³². On a ^1H - ^{15}N HSQC spectrum for C113A mutant, S115 correlation was not observed, while the neighboring S114 signal was observed, which indicating S115 is under the chemical exchanging through the interaction with H59 exchanging between ε - and δ -tautomers (Figure II-16B).

In the simulation by Barman and Hamelberg, once H59 becomes a δ -tautomer, it prompts the conversion of H157 from δ - to ε -tautomer with rearranging the hydrogen bond from H157 to T152 hydroxyl oxygen as acceptor³². The NMR results, however, showed that H157 remains in δ -tautomer in the C113A mutant (Figure II-7A). Therefore, there should be a steric clash between H59 (δ -tautomer) and H157 (δ -tautomer) (Figure II-16B). As seen in the solution structure of the C113A mutant, the distance between A113 and S154 was increased with shortening S115 - H59 distance (Figure II-11B). This might indicate S115 pulls H59 by hydrogen bonding, to release the steric clash against H157. Because the side chain contacts was alleviated due to the widened cavity entrance formed by A113 and S154, the imidazole rings of H59 and H157 keep the similar orientation as those in the wild-type (Figure II-10). The widened active site structure resembles the theoretically predicted structure occurring in the wild-type with thiol form C113³². The significantly induced structural deformation in the C113A mutant was apparent by the CD spectral change (Figures II-17A).

The C113S mutant showed the chemical exchange for H59 between the ϵ -tautomer and the imidazolium state (Figure II-17C). Based on the $^{15}\text{N}^{\epsilon 1}$ and $^{13}\text{C}^{\delta 2}$ chemical shifts, it is most probable that H59 stays preferentially at the imidazolium state (Figure II-7). The imidazolium could be stabilized by hydrogen bonding with the hydroxyl group of S113 (Figure II-16C). In addition, the S113 hydrogen bonding to H59 could be stabilized by the interaction with S115, as predicted in the simulation where S115 hydrogen bonds to thiol sulfur in C113 engaged in the interaction with substrate (Figure II-17C)³². The H157 remains in δ -tautomer, as evidenced in the NMR spectra (Figure II-7). The C113S mutant did not show any significant change to the active site backbone structure, as seen from the C α -distances among the selected residues (Figure II-11B). Because of the less significant backbone structural change in the active site in the C113S mutant, the steric clash caused by the imidazole rings of H59 (imidazolium) and H157 (δ -tautomer) was released by changing their orientation (Figure II-10).

As in the schemes for both of the mutants, the hydrogen bond between H59 and H157 will be broken transiently in exchanging between the different imidazole states of H59 (Figures II-16B and 16C). The breakage of the hydrogen bond in the dual-histidine motif explains the further reduced structural stabilities of the C113A and C113S relative to the C113D mutant (Table 2 and Figure II-17B).

It is interesting to note that the overlay of the CD spectra for the wild-type, C113D, C113A, and C113S mutants showed the isosbestic point around 208 nm (Figure II-17A). In considering of the significantly deformed active

site structure to give an open entrance architecture in the C113A mutant (Figure II-11A), we prefer to think that Pin1 PPIase domain can adopt two major conformations with different entrance forms in the active site; they open (as in the wild-type) and close (as in the C113A mutant) forms. This explains the differences in the CD spectra showing an isosbestic point among the four types of Pin1 PPIase protein (Figure II-1).

C113A and C113S mutations induced different structure dynamics.

We also found that the residue change to C113 also caused respectively different structure dynamics at various time regimes.

The C113A mutation induced additional backbone motion in msec- μ sec time regime, as evident by the increased $J_{\text{eff}}(0)$ values for most of the residues (Figure II-14A). The change was similar to that observed for the C113D mutant, but the C113A caused the significant increase in $J_{\text{eff}}(0)$ values for the residues in β_4 , which was not apparent in the C113D mutant²⁹. Impairing the structural stability in β_4 is characteristic for the C113A mutant, as evident in the enhanced H/D exchanging rate for the corresponding residues (Figure II-12A). H59 in the C113A mutant should be in the chemical exchange with changing the active site entrance structure; the active site entrance includes S154 in β_3 - β_4 loop (Figure II-16B). The exchange between the hydrogen bonding states of H59 and H157 associating with the active site structural change could explain the induced structure dynamics by C113A mutation in msec- μ sec time regime (Figure II-16B).

Based on the literature values of $^{15}\text{N}^{\epsilon_2}$ chemical shifts for ϵ^- and δ^-

tautomers, the chemical shift difference between the two states is estimated to 82 ppm^{33, 50}. In considering the chemical shift difference, the chemical exchange rate to make the signal broadened is estimated to 13,000 sec⁻¹. The exchange rate for the tautomer inter-conversion to make the ¹³C^{δ2} signal broadened is estimated to 3,600 sec⁻¹ using the ¹³C^{δ2} chemical shift difference between the ε- and δ-tautomers (9.2 ppm)⁵⁰. The loss of the signal for the H59 ¹³C^{δ2} in the C113A mutant can be explained by the tautomer-exchange with considering the additional causes including the signal intensity reduction by the addition long range ¹H-¹³C and ¹³C-¹³C spin couplings and also the ¹³C-¹³C dipolar interactions to accelerate transverse relaxation of the signal.

The C113S mutant caused different change in the structural dynamics; the change was apparent in nsec-psec time regime, as seen by the increase in $\mathcal{J}(\omega_N)$ values (Figure II-14D). The changes in $\mathcal{J}(\omega_N)$ values for the C113S mutant implies that the residues with increased $\mathcal{J}(\omega_N)$ values had reduced local motion, thus become more stiff local structure relative to the corresponding parts in the wild-type (Figure II-14D). This change could come from the tightly packed imidazole rings of H59 and H157 in the active site cavity, both of which are δ-tautomers thus in the sterically crowded in the cavity (Figure II-16C).

The observed change in the structure dynamics for each mutant can be explained by assuming the protonation dynamics of H59 and its associating change in the interaction with H157 (Figure II-16). Our proposed imidazole dynamics of H59 in the mutants, therefore, should be right, which is derived from the present NMR observation and the theoretical predictions for the

dynamics in the hydrogen bonding network by Barman and Hamelberg³².

Why the C113S mutant had lower the activity than the C113A mutant.

The C113A and C113S mutants are reported to have severely reduced isomerase activities^{9, 24}. Direct determining the isomerization rates by EXSY experiments demonstrate the C113S mutant has much reduced isomerization rate relative to the C113A mutant; actually, the EXSY experiments carried out at 295 K could not measure the rates for the C113S mutant, because its isomerization was too slow (Table II-2).

Both of the C113A and C113S mutants disordered the basic triad structure in the active loop (Figure II-5), which explains the reduced substrate affinity as we found for the C113D mutant^{29,17}. Because the isomerization rates of the C113A mutant are close to those of the C113D mutant, the reduced activity of the C113A could be explained by the disordered basic triad structure²⁹.

In considering the less apparent difference in the isomerization rates between the C113A and C113D mutants (Table II-2), it is hard to estimate the functional significance of change in the hydrogen bond dynamics associated with H59 exchanging between the tautomers (Figure II-16B); the reduced affinity of the basic triad to the phosphate could be the primal cause. On the other hand, the further reduced isomerization rates was found for the C113S mutant, which implies that the imidazole ring disorientations of H59 and H157 (Figure II-10B) and also occurrence of the imidazolium form H59 (Figure II-16C) are functionally relevant. H59 and H157 constitute the floor in the active site to hold the Pro residue in substrate, the disorientation of the

histidines may get the interaction perturbed²⁶. As seen in the crystal structure²⁶, catalytic cavity is hydrophobic to stabilize the interaction with Pro. Therefore, the charged imidazolium H59, happening in the state exchange, will reasonably diminish the substrate affinity. The two changes found in the C113S mutant explains its further reduced isomerization activity.

5. Conclusions

We using the C113A and C113S mutants of Pin1 PPIase domains, we found the dynamics in the hydrogen bond network mediated by H59 and H157 (dual histidine motif) can change according to the residue type at the 113 position. The lack or severely reduced signal intensities for H59 and H157 in the mutants clued to think over the dynamic rearrangement of the hydrogen bond network, as theoretically predicted²⁰. The plausible hydrogen bond dynamics could be derived from the ¹H-¹⁵N and ¹H-¹³C correlations (Figure II-16), although imperfect sets of their signals limited the discussion (Figure II-7). However, the solution structures, the structure dynamics, and H/D exchange rates for the mutants altogether were found to be consistent with our proposed dynamics in the hydrogen bonding among the residues A113/S113, H157 and H59 (Figure II-16), which assures our schemes for the dynamic hydrogen bond network in the mutants are right. It has to be noted, because NMR data cannot determine the protonation states of all the engaging residues, the schemes relay on the theoretical prediction, where the dynamic hydrogen bond rearrangements among the active site residues, including C113-H59-H157-T152 and S115, are described²⁰ (Figure II-16).

Overall, this work experimentally supports the view that the chemical state of C113 plays as a pivot role in reorganizing the hydrogen bond network to facilitate the isomerization process, which was originally proposed with simulations by Barman and Hamelberg¹⁶.

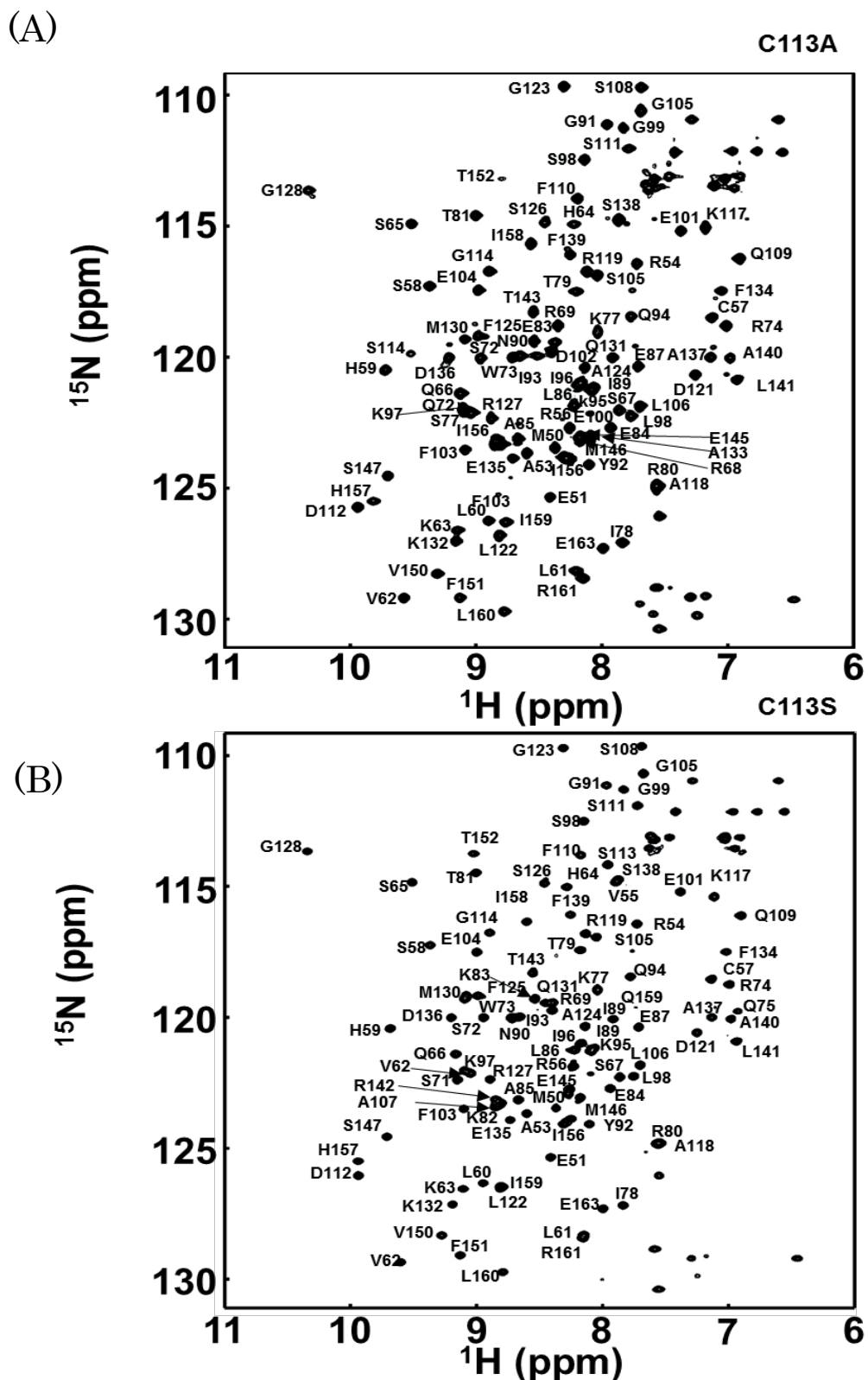


Figure II-1

2D ^1H - ^{15}N HSQC spectra for the C113A (A) and C113S (B) mutant Pin1 PPIase

domains. The resonance assignments for the backbone signals are put on the spectra.

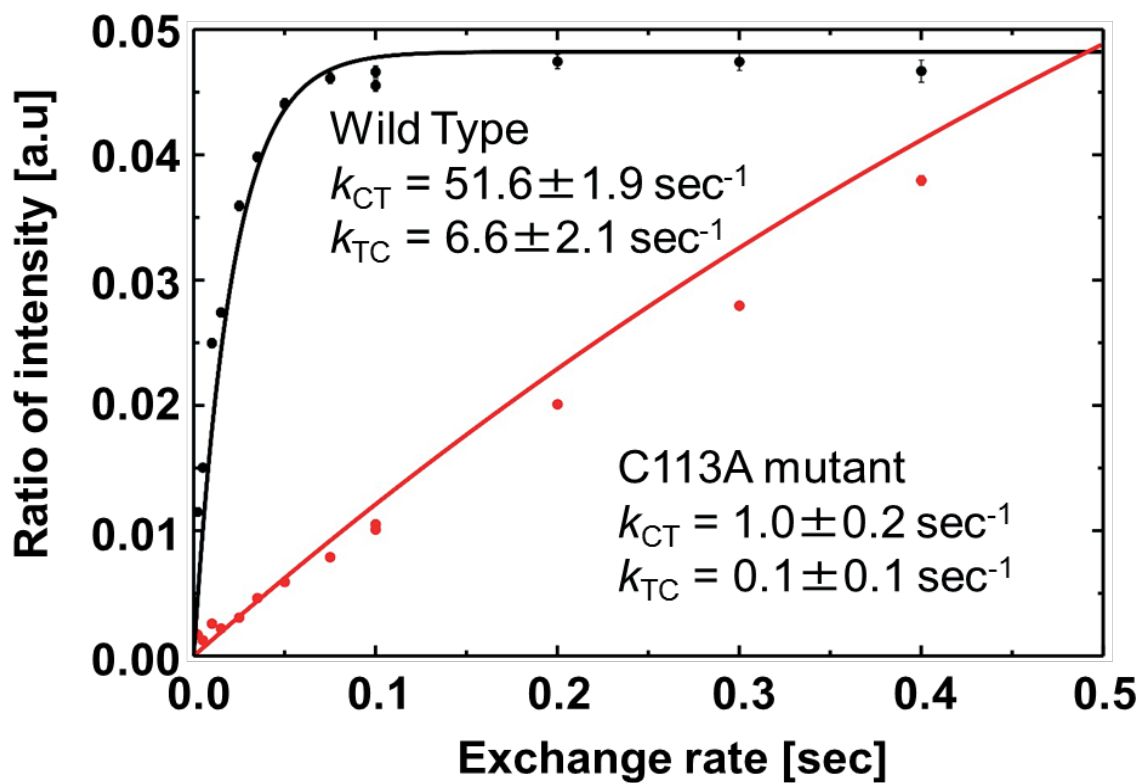


Figure II-2

Isomerization rate determination with a series of EXSY spectra. The growth of the intensity ratios of the *trans* to *cis* exchange cross peaks against the diagonal peaks for *trans* are plot for the C113A mutant (red dot). The theoretical curve optimized to fit the experimental data is drawn in a red line. For reference, the corresponding data previously reported for the wild-type is drawn in the same graph (black dot and black line).

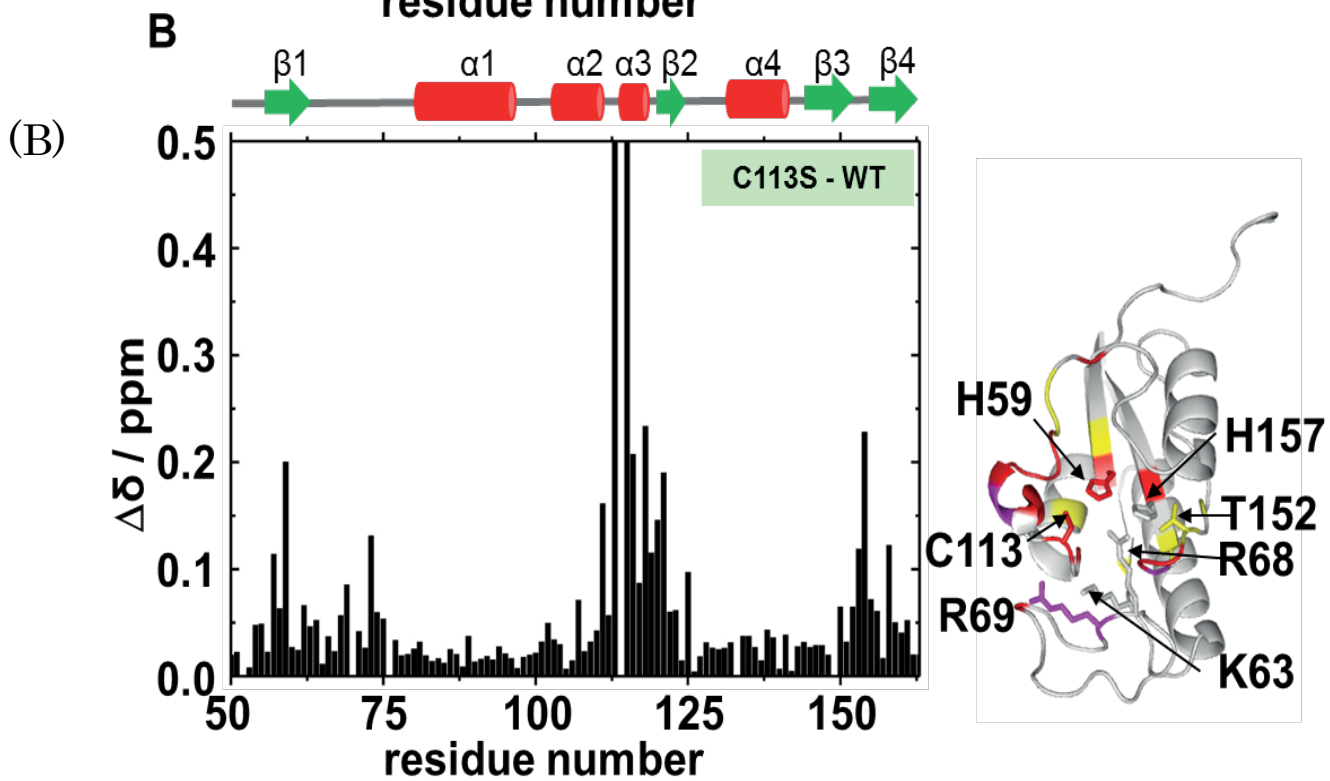
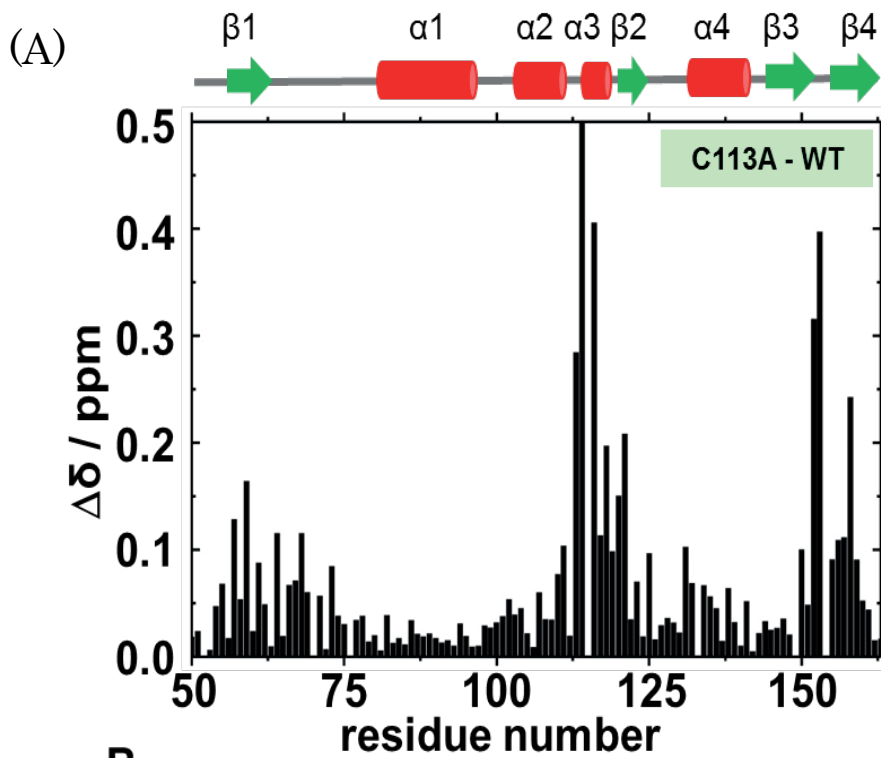


Figure II-3

Chemical shift differences for the C113A and C113S mutants relative to the wild-type.

(A) Residue-wise plot for the normalized chemical shift differences between the wild type and the C113A mutant (left). The normalized chemical shift difference for each residue is defined as $\Delta\delta = [(\Delta\delta^1\text{H})^2 + (\Delta\delta^{15}\text{N}/5)^2]^{1/2}$, where $\Delta\delta^1\text{H}$ and $\Delta\delta^{15}\text{N}$ are the chemical shift differences in the ^1H and ^{15}N dimensions, respectively. According to the magnitude of $\Delta\delta$, the residues in Pin1 PPIase structure (PDB ID: 1PIN) were colored differently: red for $> \Delta\delta_{\text{ave}} + 1\sigma$, magenta for $> \Delta\delta_{\text{ave}} + 0.5\sigma$, and yellow for $> \Delta\delta_{\text{ave}} + 0.25\sigma$, where $\Delta\delta_{\text{ave}}$ is the average value for $\Delta\delta$ and σ is the standard deviation of $\Delta\delta$ calculated over all residues (right). The residues in the hydrogen bond network and the basic triad are drawn in stick with label. (B) The plot of $\Delta\delta$ for the C113S mutant (left). Mapping of the chemical shift differences on the structure as done as in the above case (right).

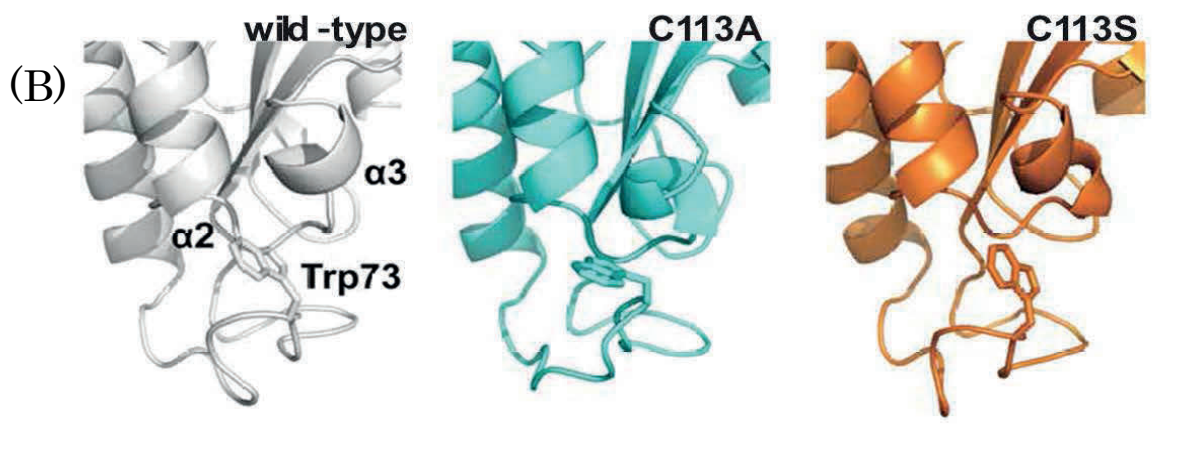
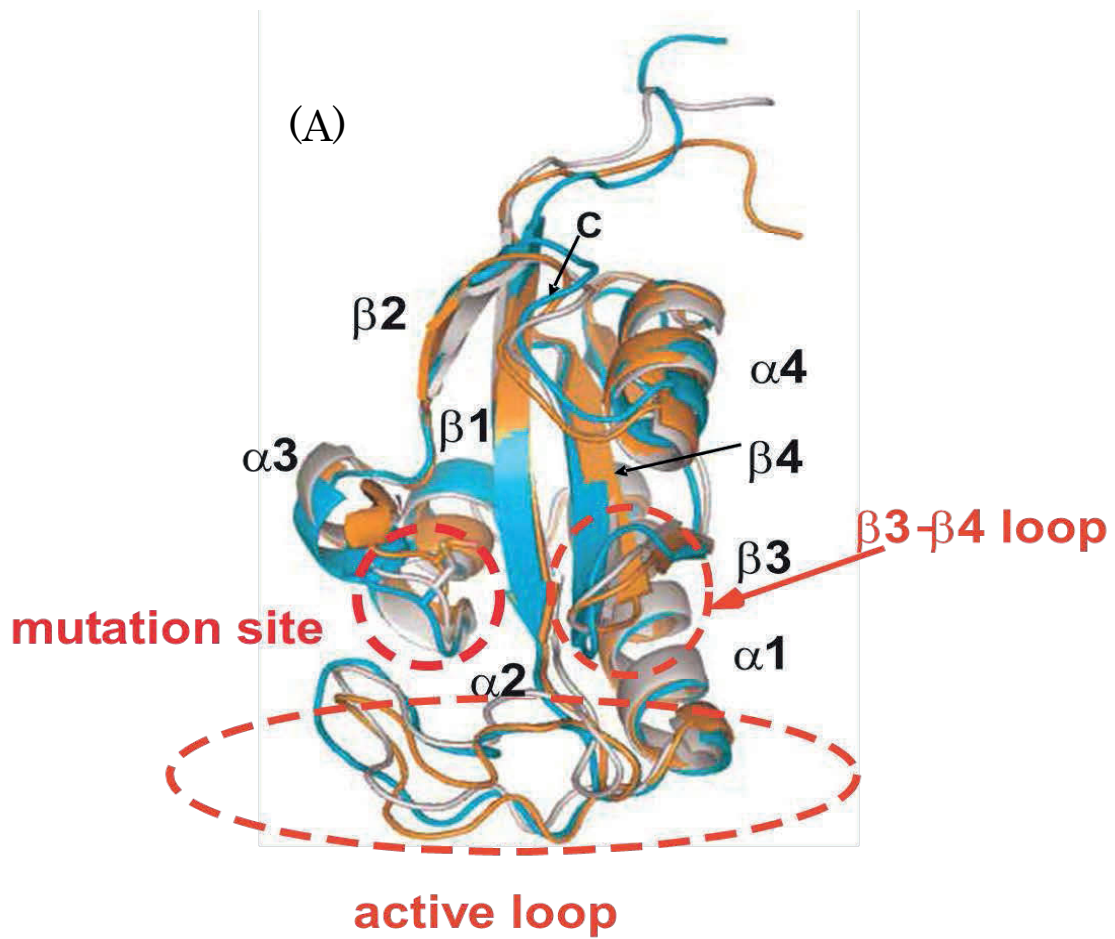


Figure II-4

Structure overlay of the wild-type, C113A, and C133S mutant Pin1 PPIase domains (A): the wild-type (gray), C113A (cyan), and C113S (orange). The close up views to compare the interaction of W73 and $\beta 2$ - $\beta 3$ helices in the active site (B): the wild-type (gray), C113A (cyan), and C113S (orange).

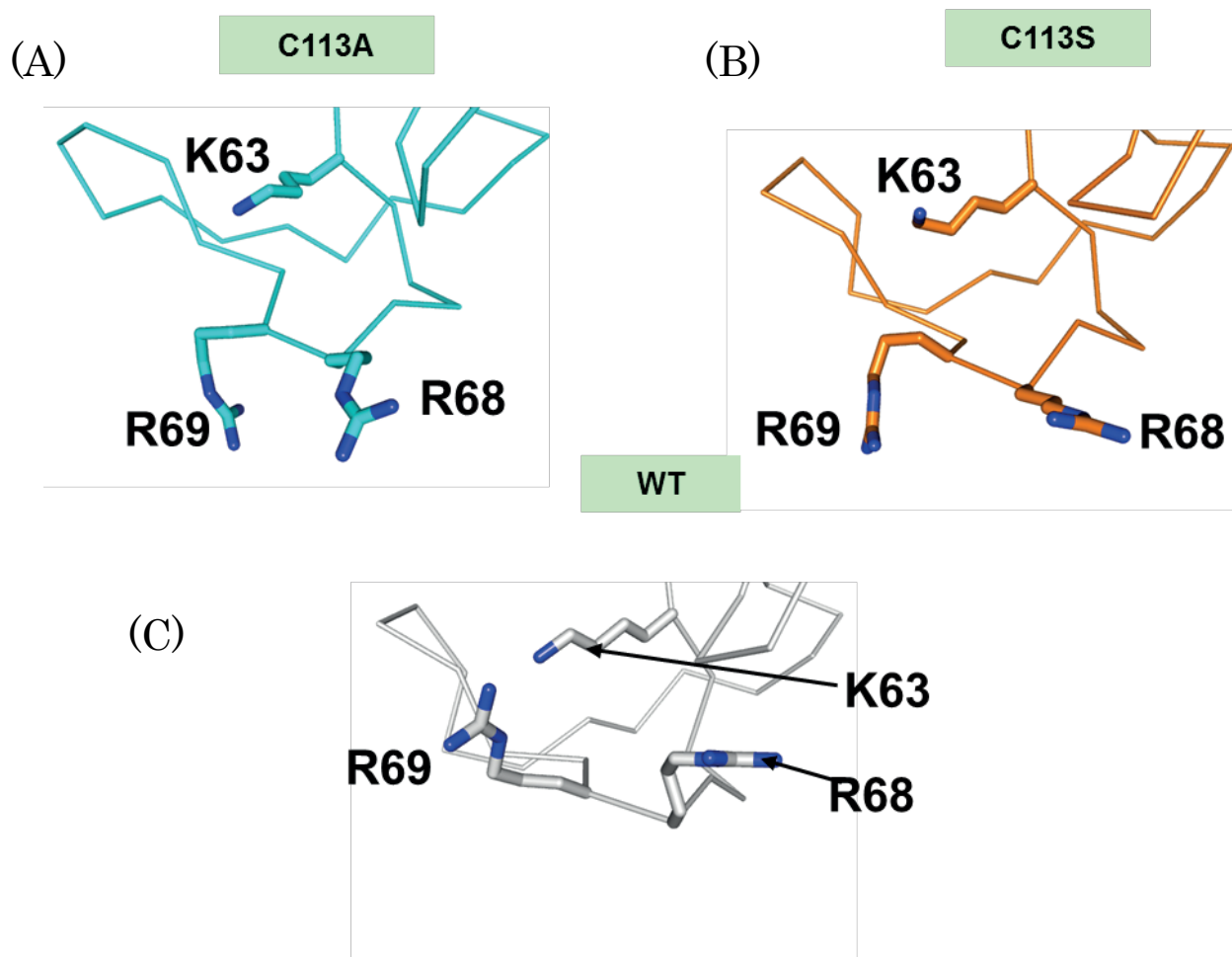


Figure II-5

Close up views of the active loop harboring the basic triad in Pin1 PPIase domain for the (A) C113A (cyan) and (B) C113S (orange) mutants with (C) the wild-type (gray). The residues in the basic triad are drawn in sticks.

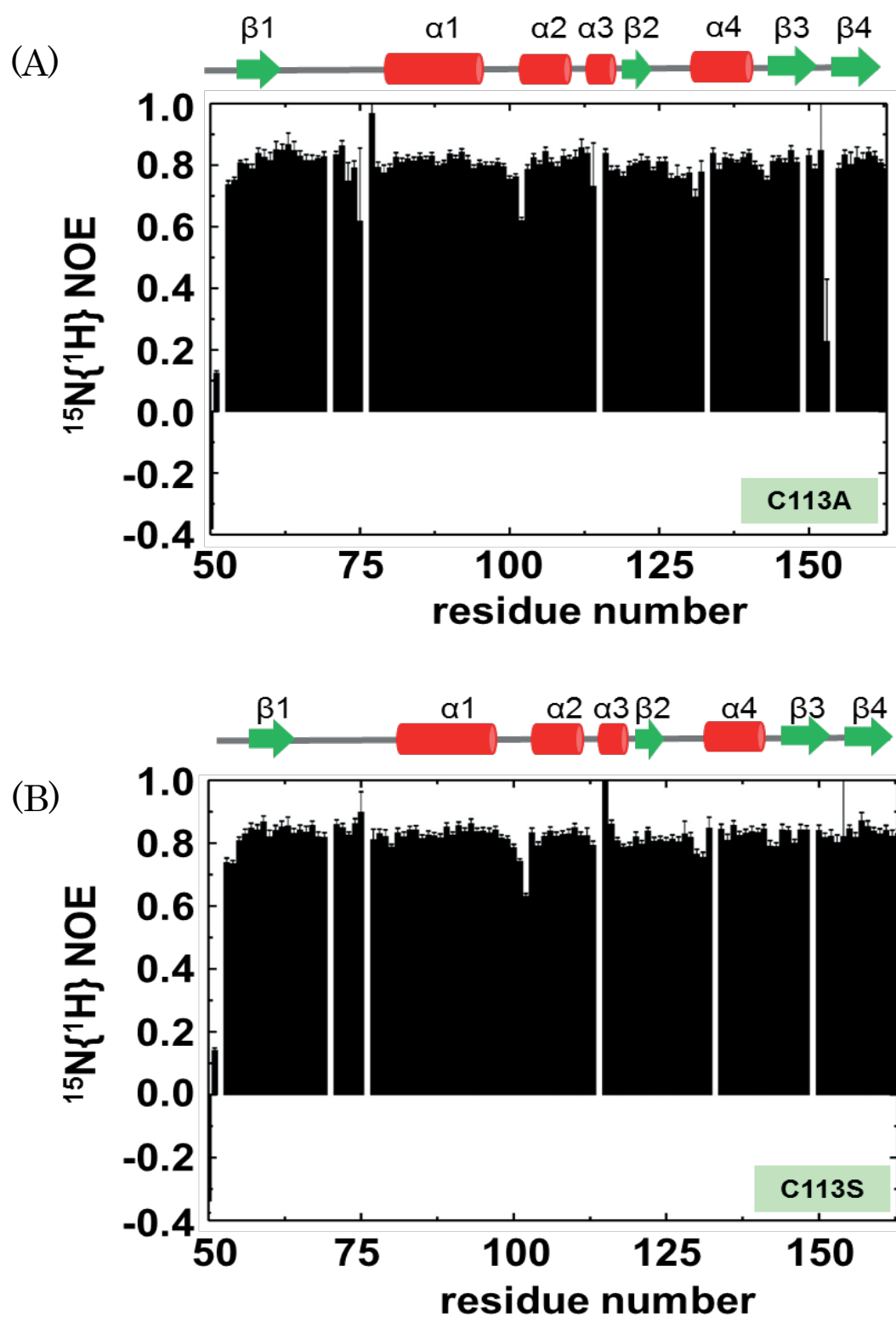


Figure II-6

$^{15}\text{N}\{$ hetero-nuclear NOE profiles for the C113A (A) and C113S (B) mutants.

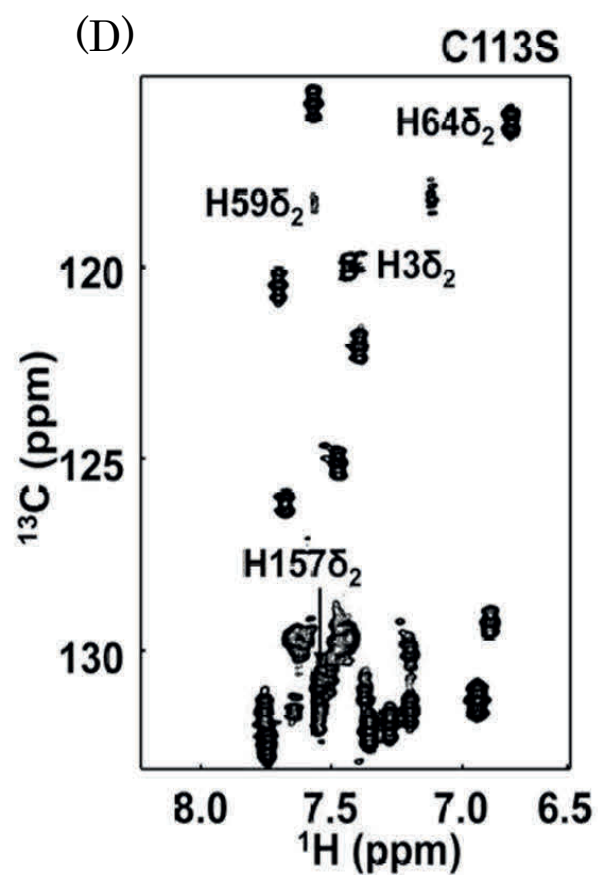
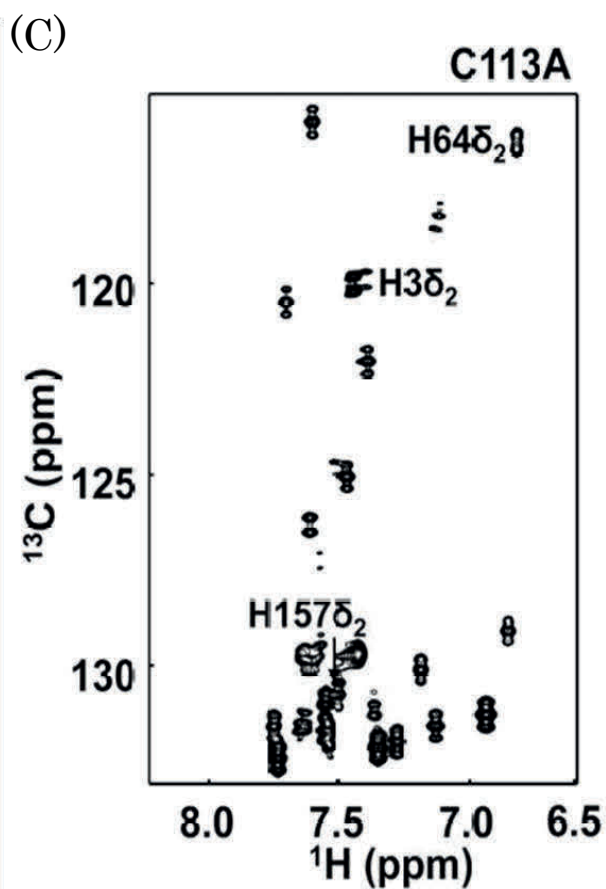
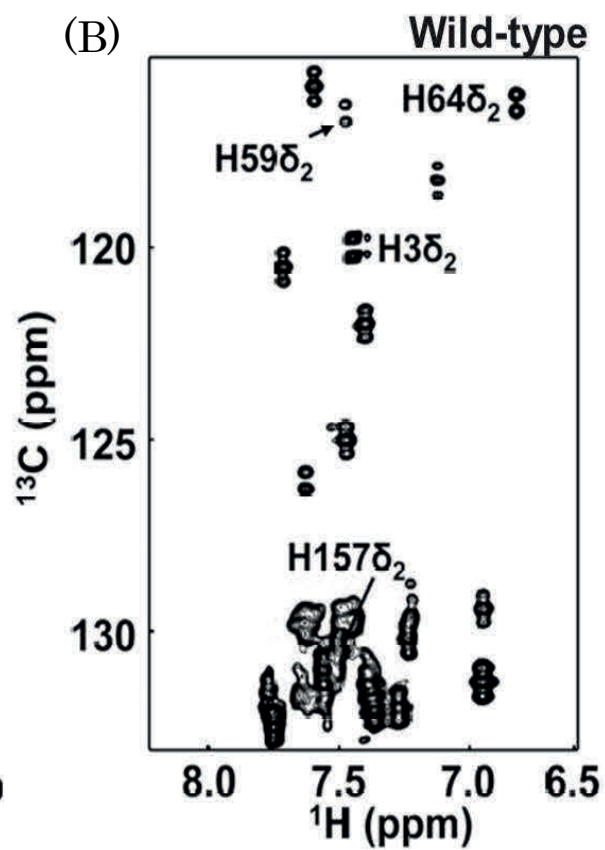
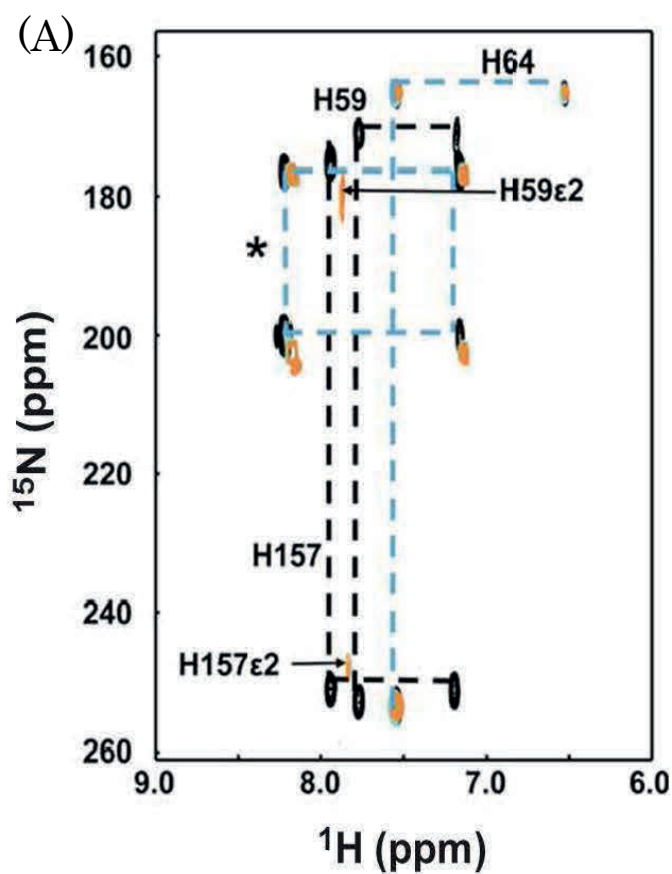


Figure II-7

^1H - ^{15}N multi-bond HSQC spectra and ^1H - ^{13}C HSQC spectra for the imidazole ring in Pin1 PPIase domain. (A) 2D ^1H - ^{15}N multi-bond HSQC spectra for the imidazole rings of the histidines in the wild-type (black), the C113A (cyan) and C113S (orange) mutants. A set of signals marked with asterisk come from the histidine (referred to as H3 in the text) in the N-terminal GSHM segment attached due to the construction. 2D ^1H - ^{13}C HSQC spectra for the wild-type (B), the C113A (C), and C113S (D) mutants.

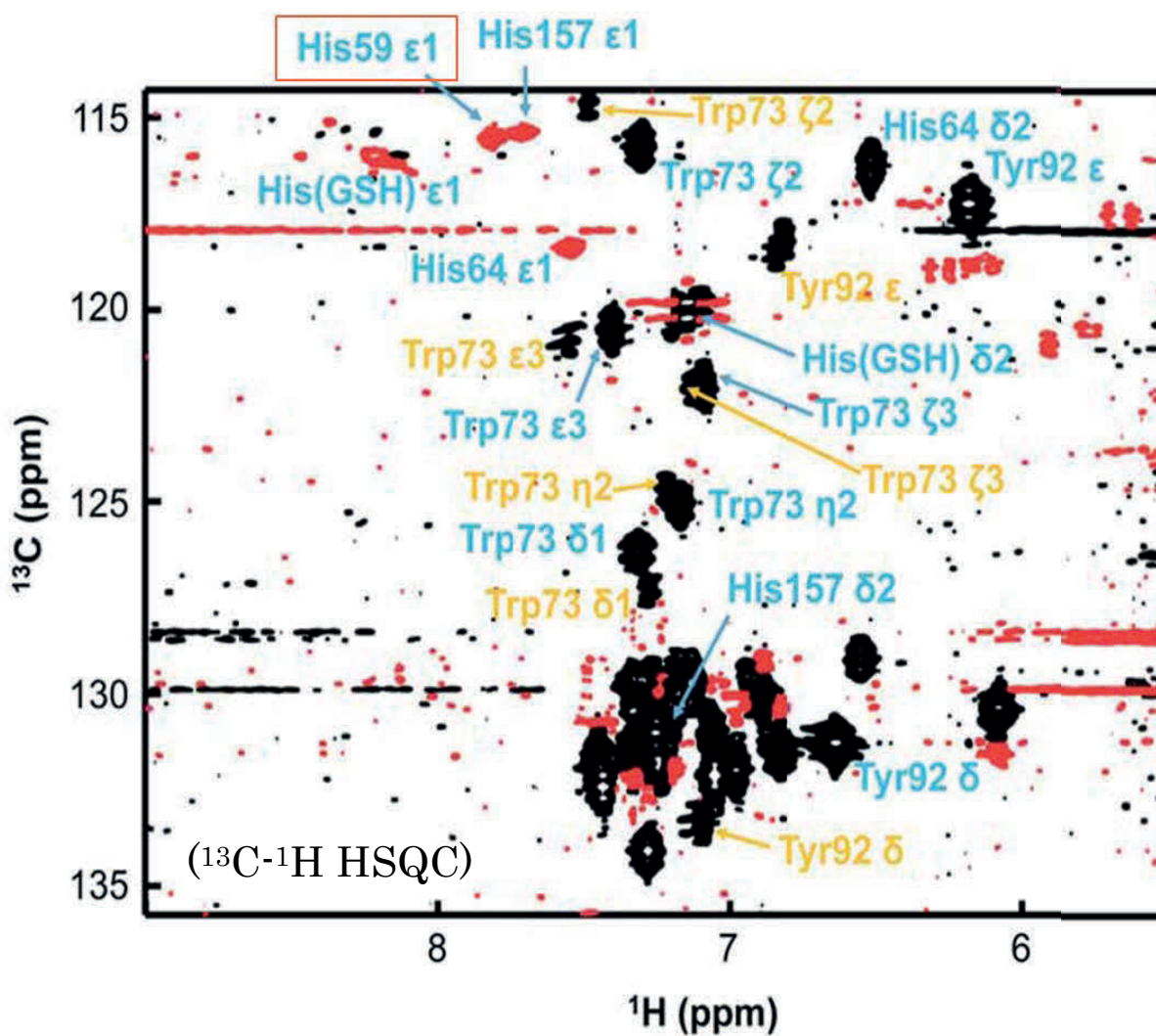


Figure II-8

2D ^1H - ^{13}C HSQC spectrum for the aromatic regions of the C113A mutant with the lowered threshold to display. The spectrum is the same as shown in Figure 4S. The resonance assignments are put on the spectrum. The signals with yellow mark come from the minor structure having alternative local conformation that is apparent under the present condition. In the present work, the minor signals were not considered.

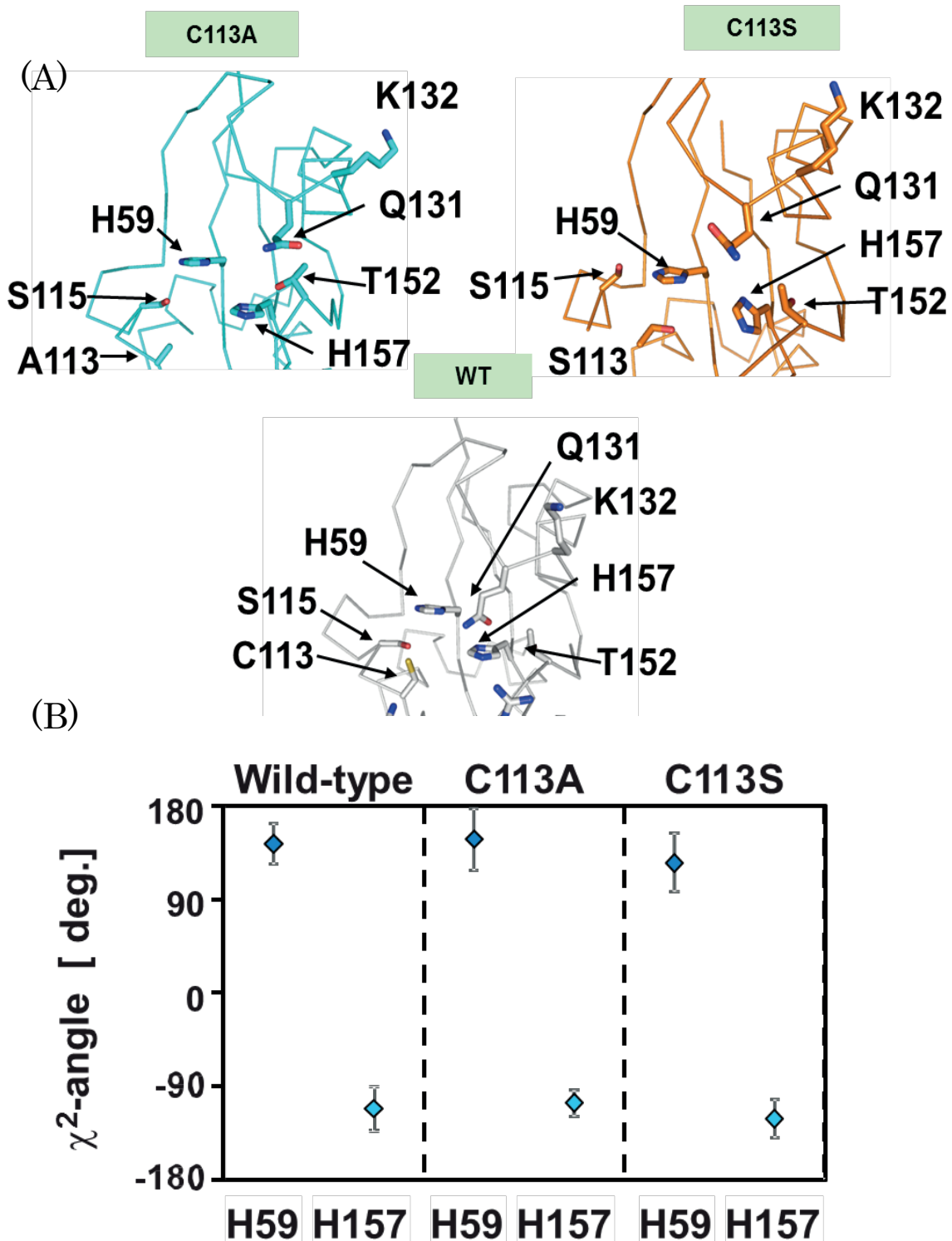


Figure II-9

Comparison of the active site structures. (A) The close up views are drawn for the C113A (cyan) and C113S (orange) mutants with the wild-type (gray). (B) The χ^2 -angle distributions for H59 and H157 among the 10-lowest energy NMR structures for the wild-type, C113A and C113S mutants.

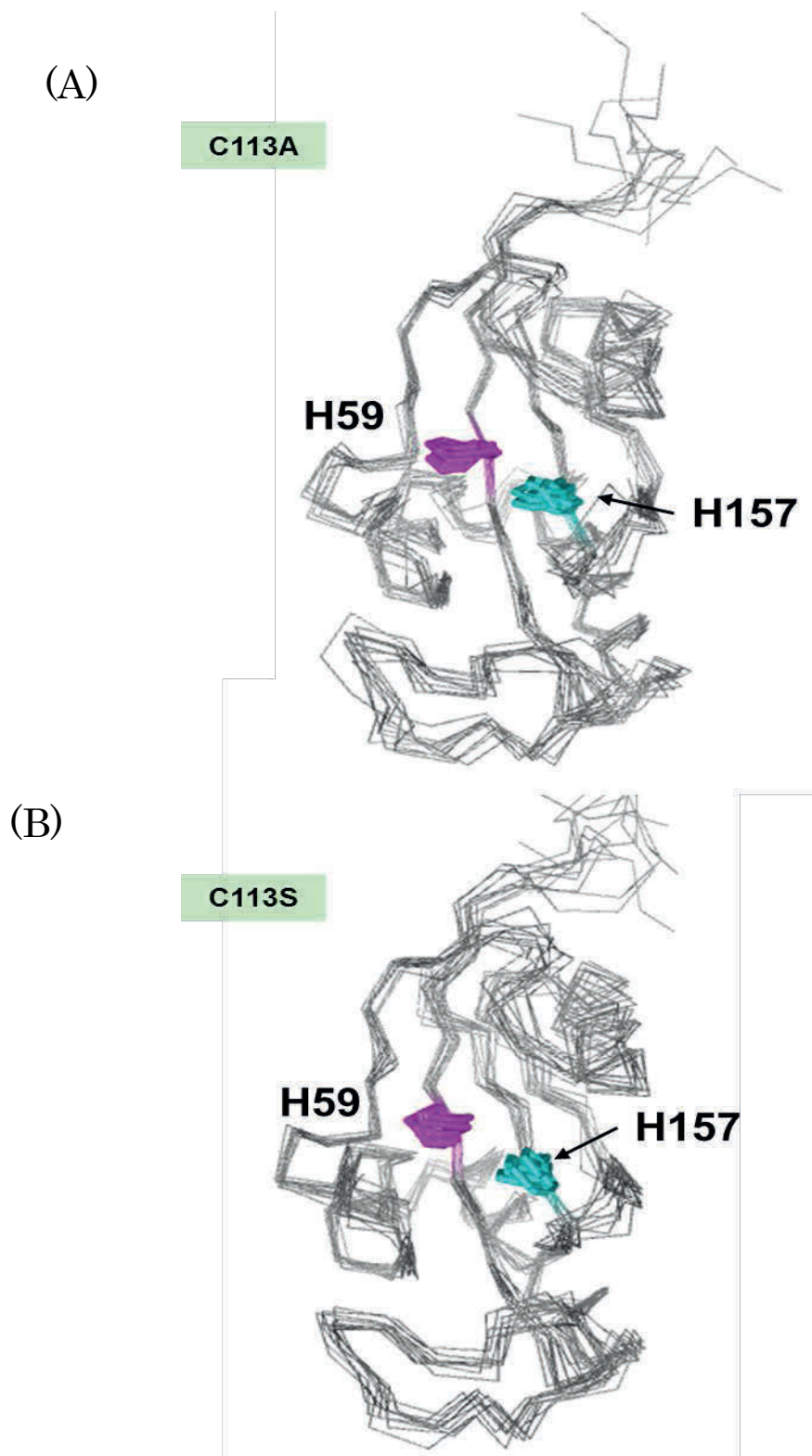


Figure II-10

The overlaid structures of 10-lowest energy NMR structures for the C113A (A) and C113S (B)

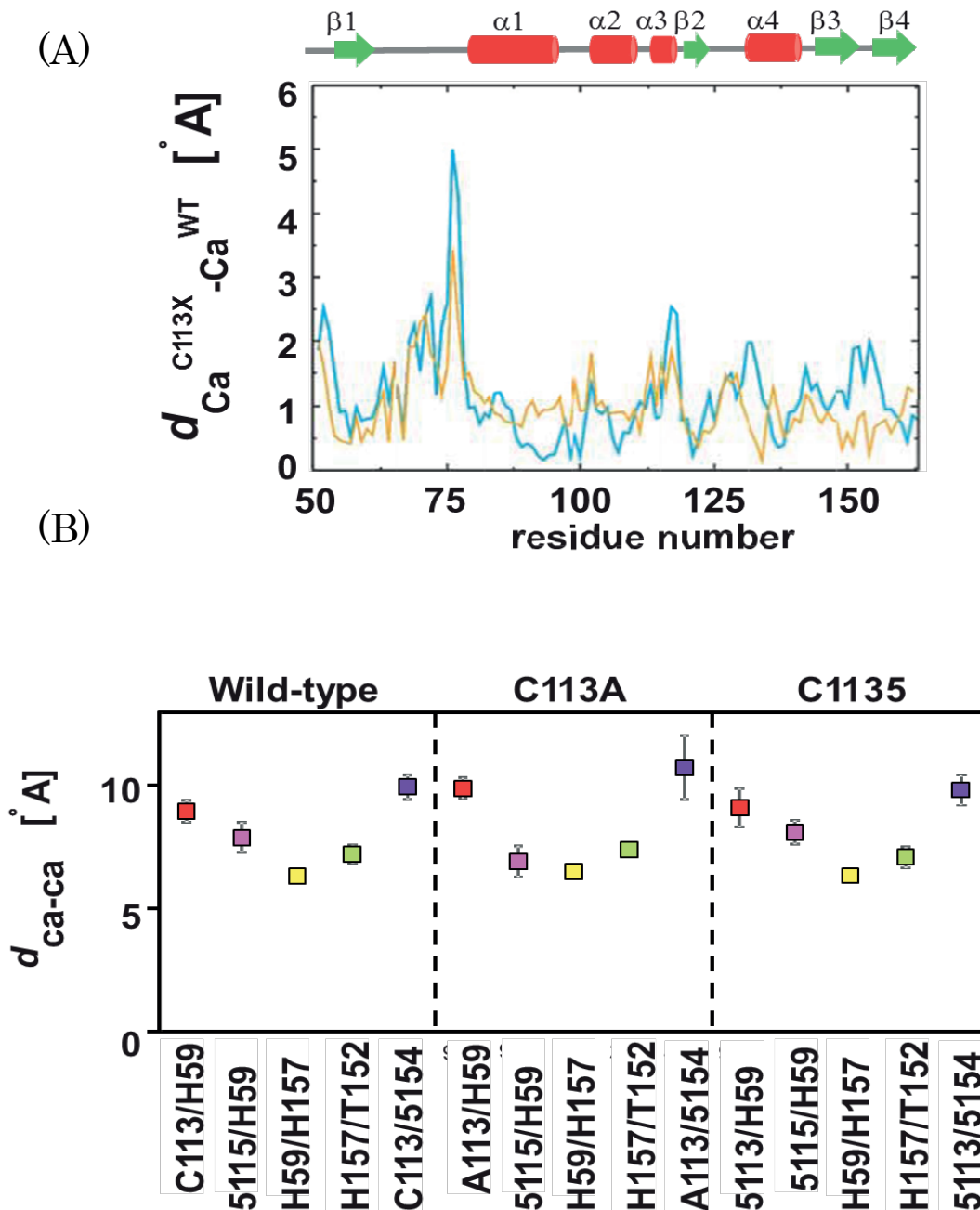


Figure II-11

Structural changes measured with Ca-Ca distances. (A) The residue-wise plot for the displacement of Ca position in the C113A (cyan) and C113S (orange) mutants relative to the corresponding Ca in the wild-type. (B) The Ca-Ca distance distributions among the 10-lowest energy NMR structures for the selected pairs of the residues in the wild-type, C113A, and C113S mutants.

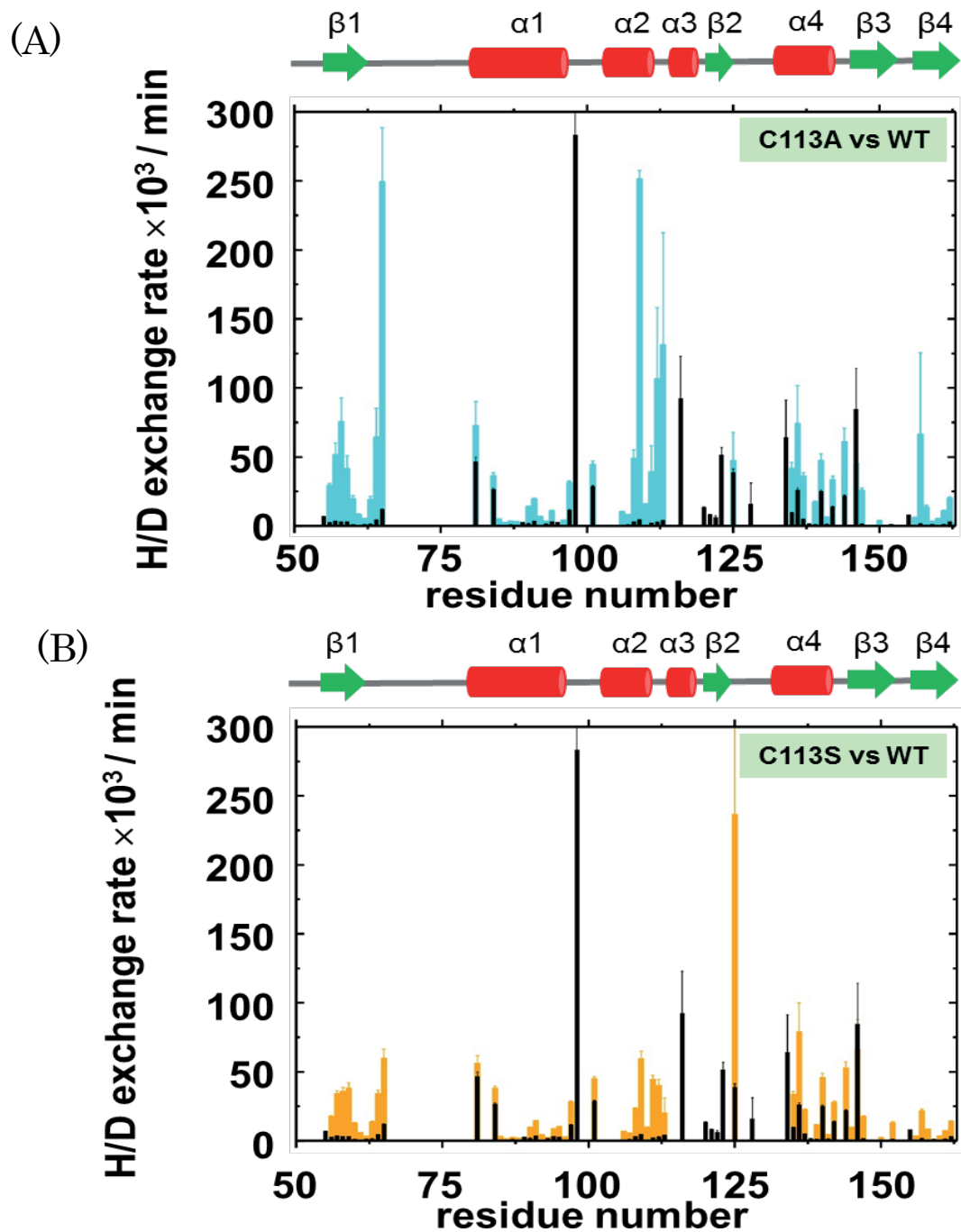
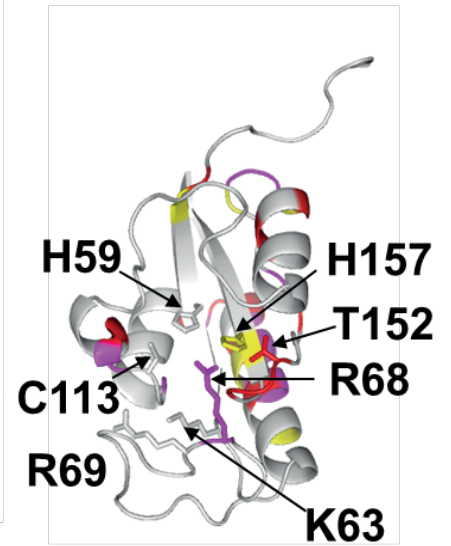
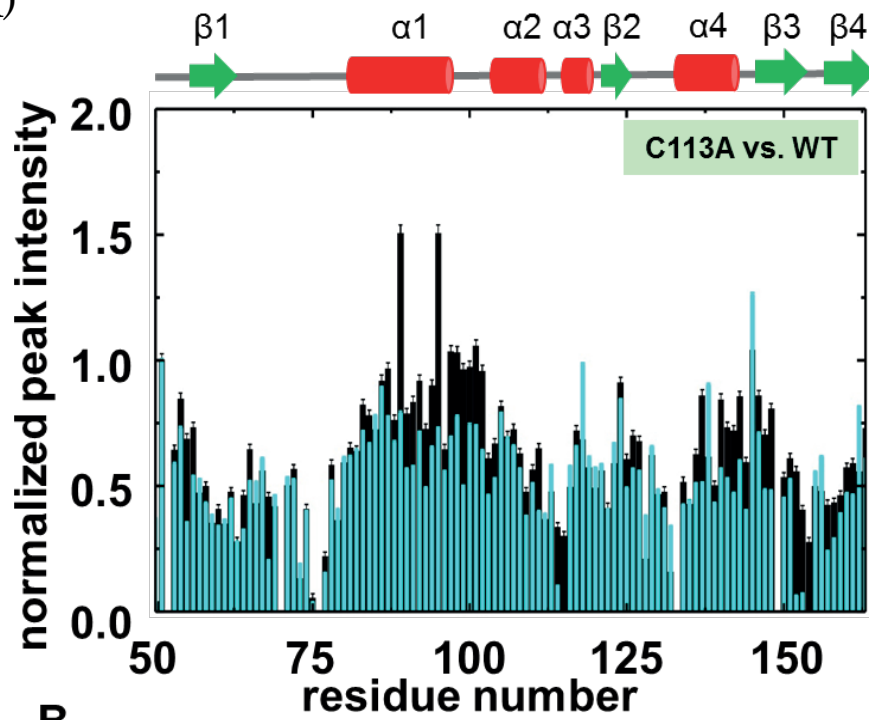


Figure II-12

The plot for the H/D exchange rates for the residues of the mutants in comparison with the corresponding values in the wild-type. The C113A mutant (cyan) with the wild-type (black) (A), and the C113S mutant (orange) with the wild-type (black) (B).

(A)



B

(B)

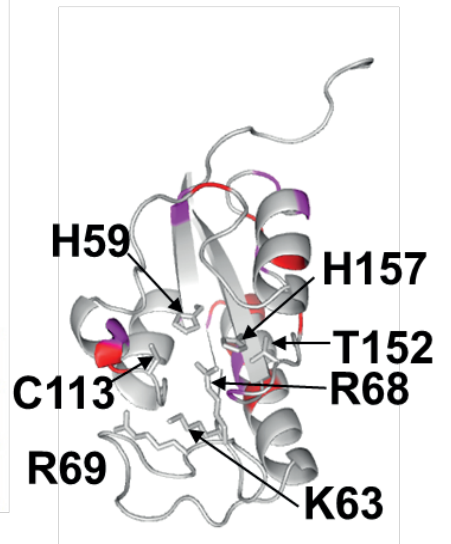
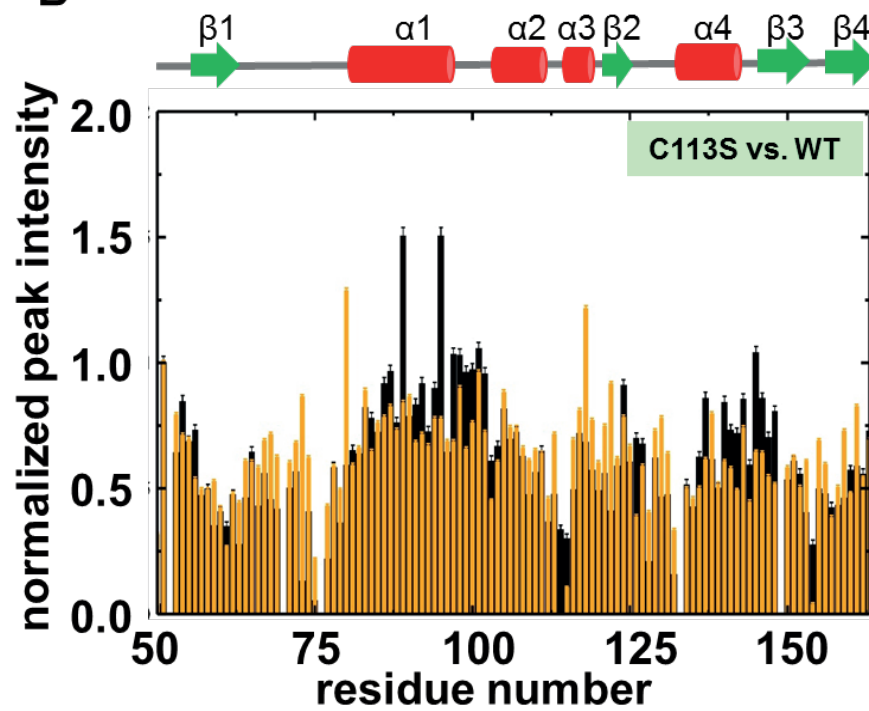
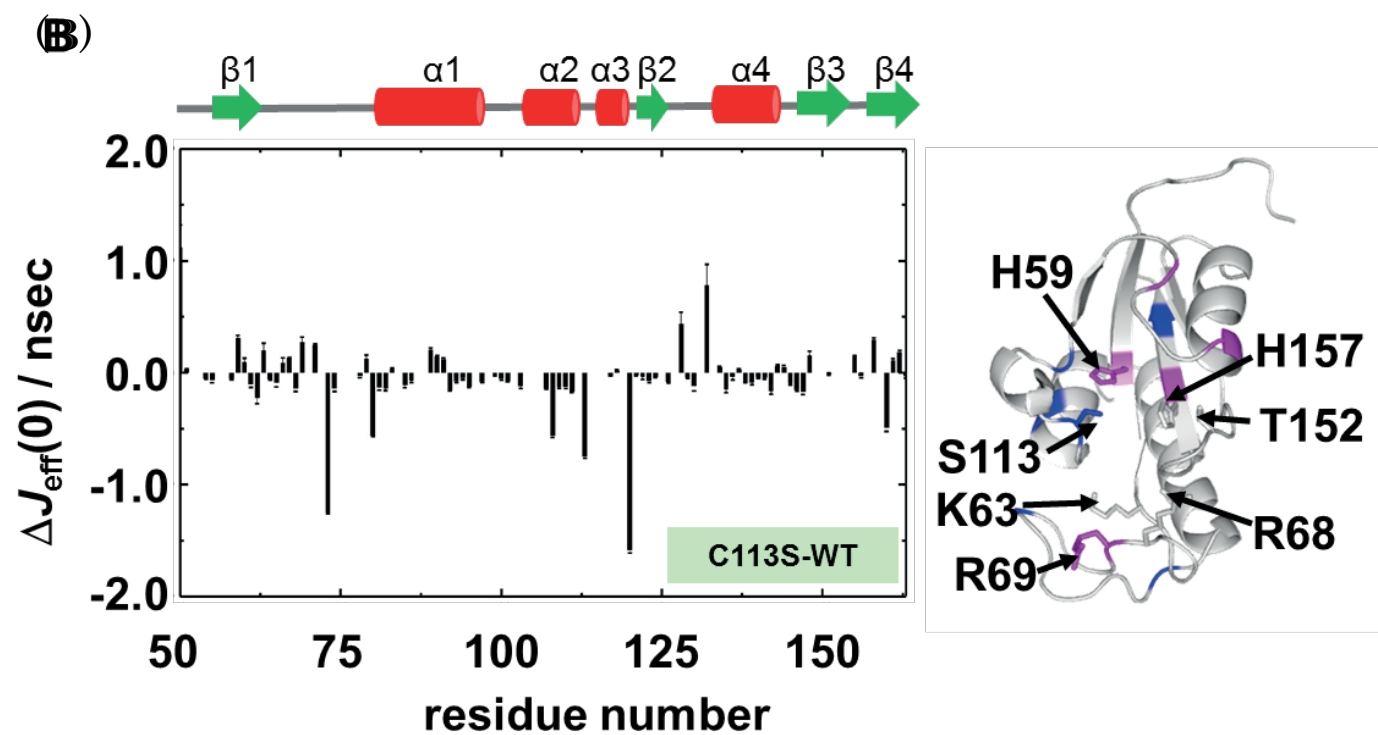
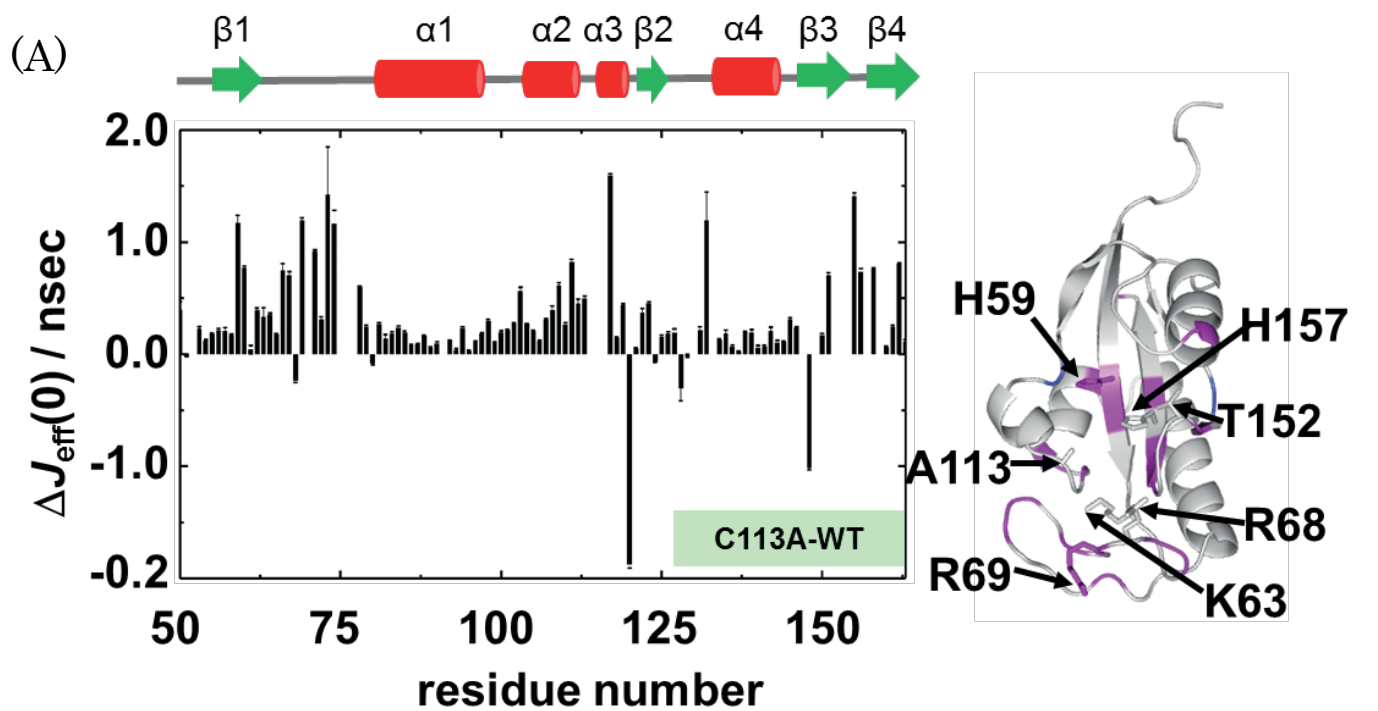


Figure II-13

The normalized intensity profiles for the C113A (cyan) (A) and C113S (orange) (B) mutants in reference to that for the wild-type (black). The normalized peak intensities were estimated by using the ^1H - ^{15}N HSQC signal for E51 to give a unit intensity by assuming that E51 amide group is fully exposed to the solvent without any interactions to the neighboring residues. The residues having significant changes in the signal intensities from the corresponding signals in the wild-type are colored on the structure (PDB ID: 1PIN) according to the magnitudes of the difference: average+ 1σ (red), average+ 0.5σ (magenta) and average+ 0.25σ (yellow).



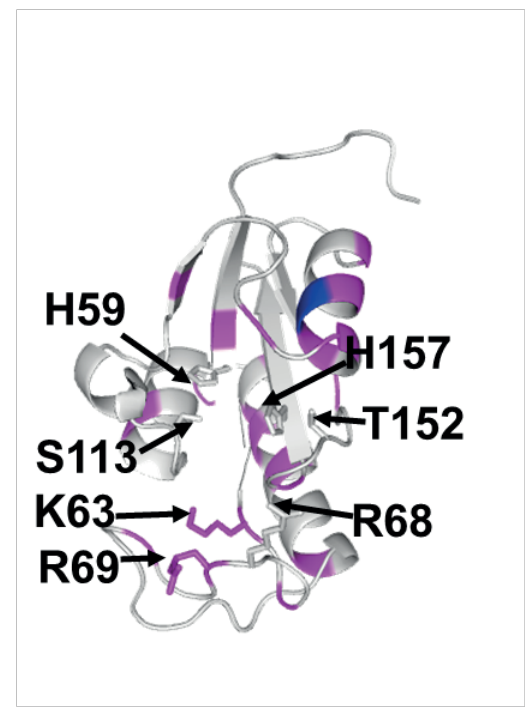
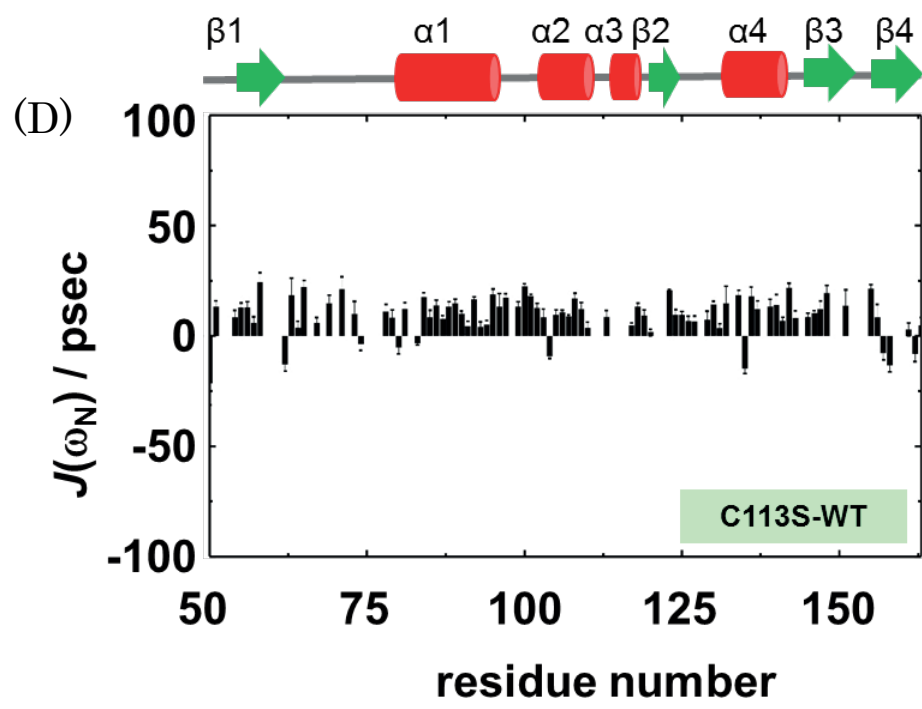
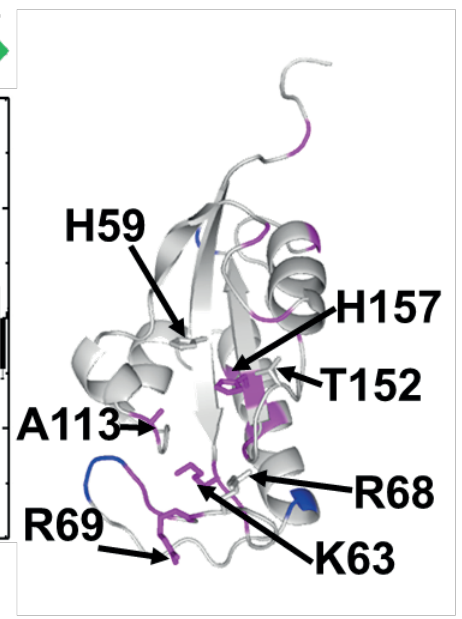
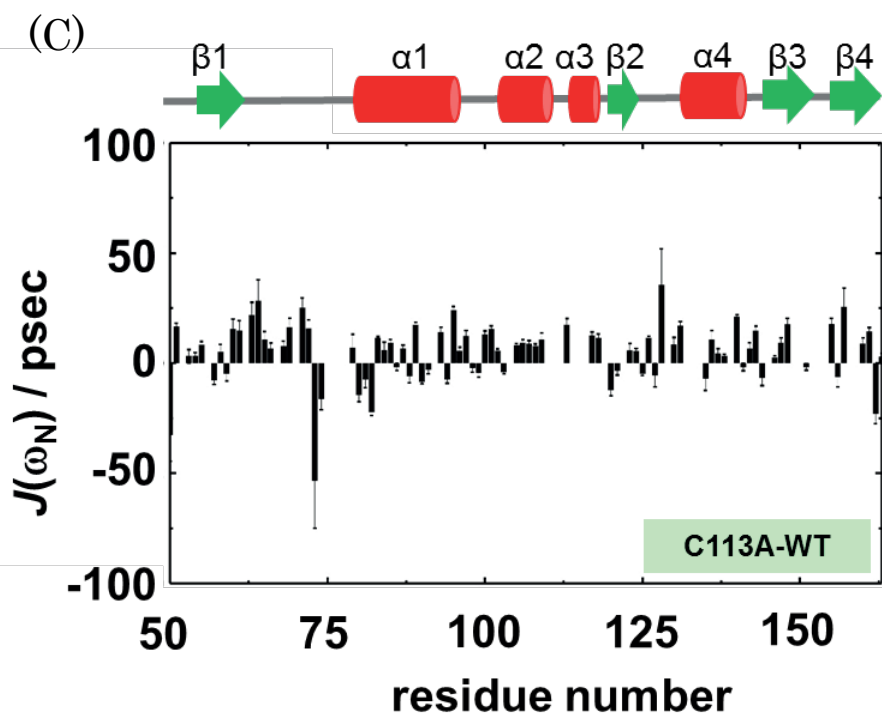


Figure II-14

Plots of the difference spectral density values. The $\Delta J_{\text{eff}}(0)$ is defined as $J_{\text{eff}}(0)^{\text{C113A/S}} - J_{\text{eff}}(0)^{\text{wild}}$, and $\Delta \mathcal{J}(\omega_{\text{N}}) = \mathcal{J}(\omega_{\text{N}})^{\text{C113A/S}} - \mathcal{J}(\omega_{\text{N}})^{\text{wild}}$. The $\Delta J_{\text{eff}}(0)$ plots are drawn for the C113A (A) and C113S (B), respectively. The $\Delta \mathcal{J}(\omega_{\text{N}})$ values are plot for the C113A (C) and C113S (D), respectively. The bars in red and black represent the corresponding residues are in the extreme narrowing limit backbone motion (red) or the others (black). According to the magnitudes of the difference spectral densities ΔJ , the residues are marked in different colors: the residues with $\Delta J > \Delta J^{\text{ave}} + 0.5\sigma$ are colored in magenta, while those with $\Delta J < \Delta J^{\text{ave}} - 0.5\sigma$ are in blue, where ΔJ^{ave} and σ are the average of the ΔJ values and the standard deviation, respectively.

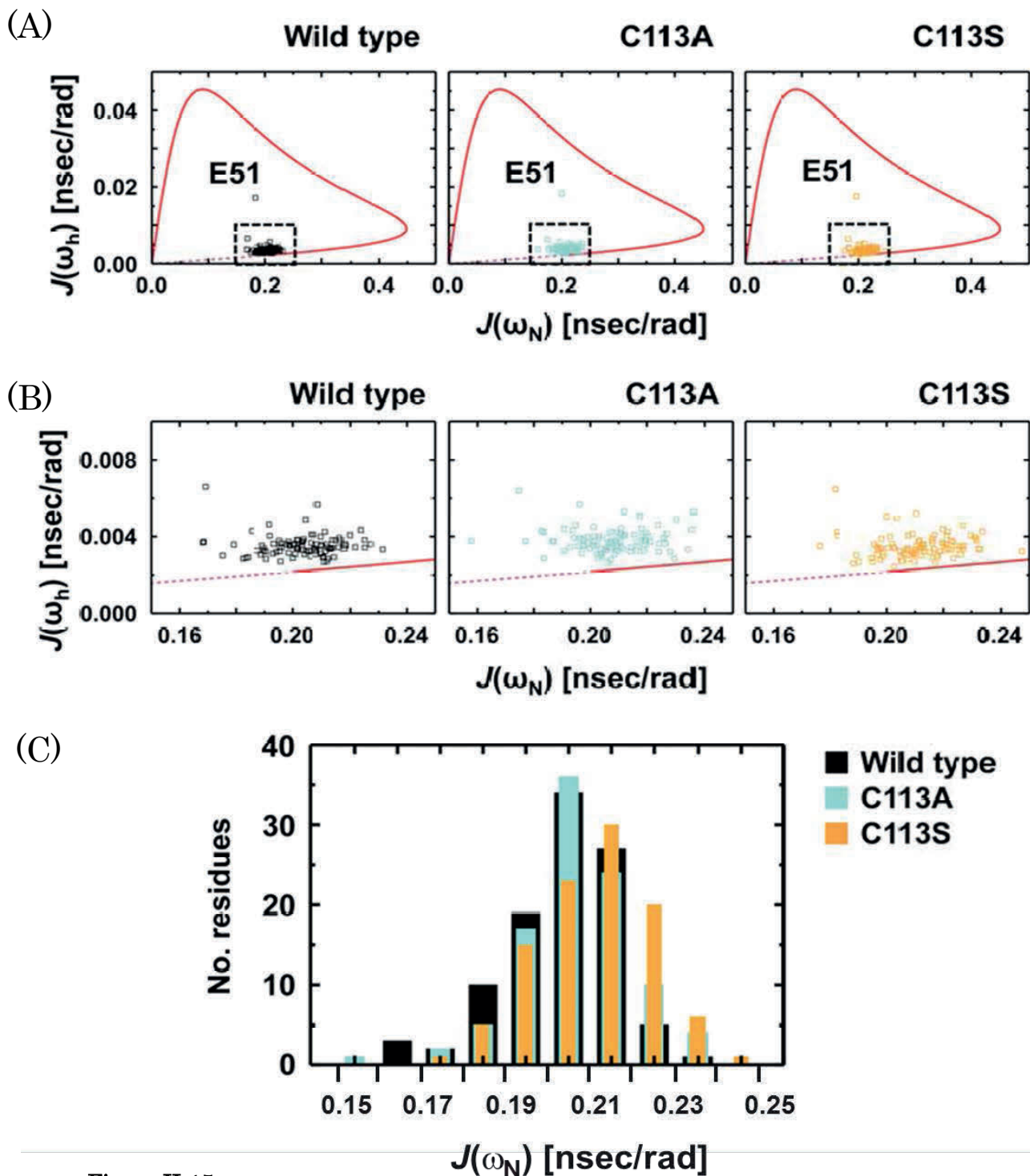
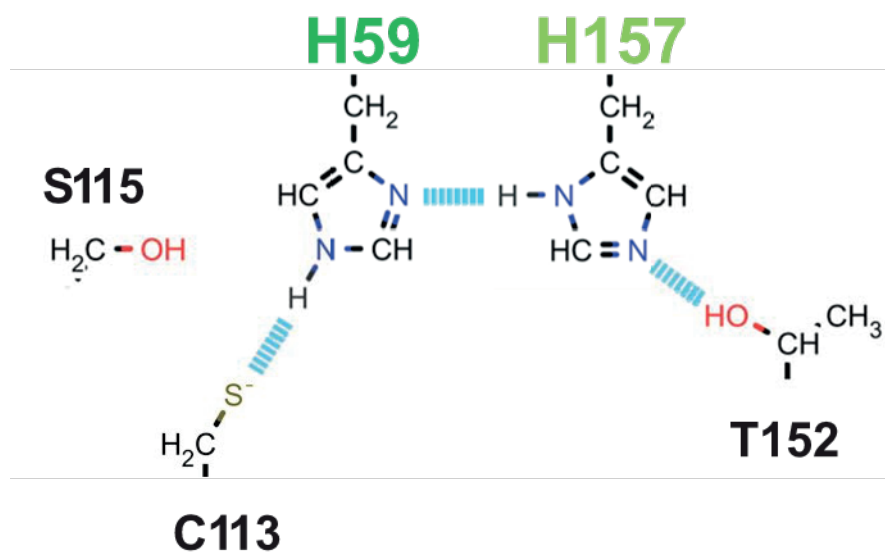


Figure II-15

The Lipari-Szabo mapping for the correlation between the spectral densities of $J(\omega_N)$ and $J(\omega_h)$ (A). The solid red curve represents the rigid isotropic tumbling curve, while the dashed line is the ' $\tau_e=0$ ' line. The parts with dotted squares in (A) are shown with expansion (B). The histograms of $J(\omega_N)$ values are shown for the wild-type, C113A, and C113S mutants (C).

(A)



(B)

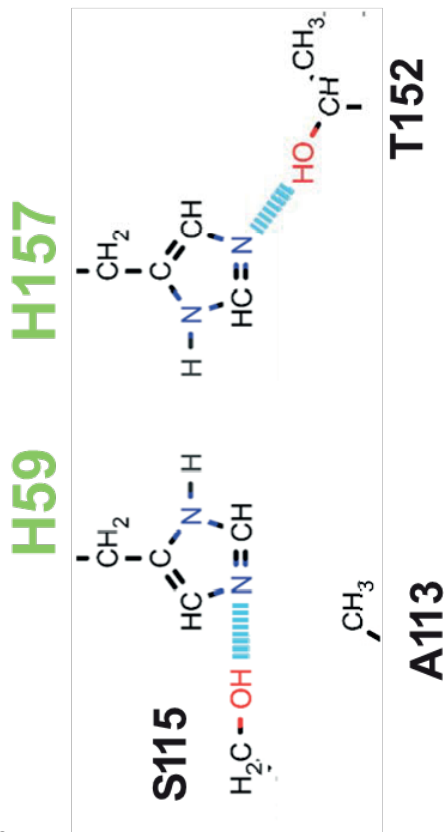
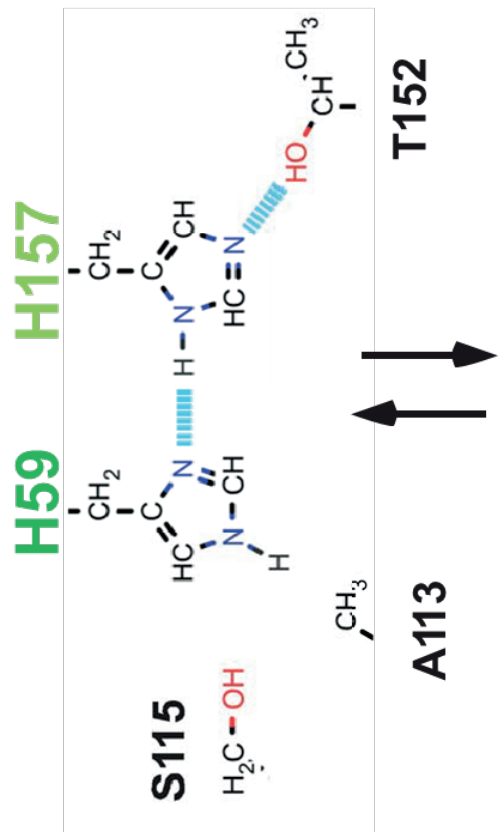
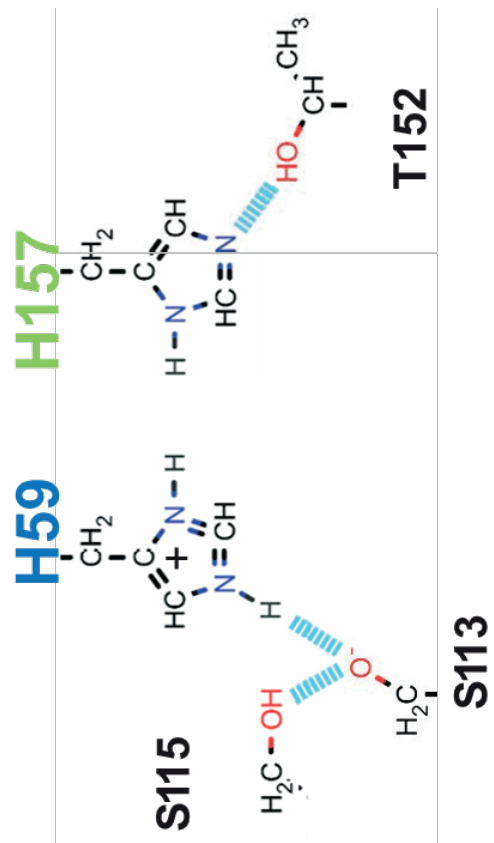
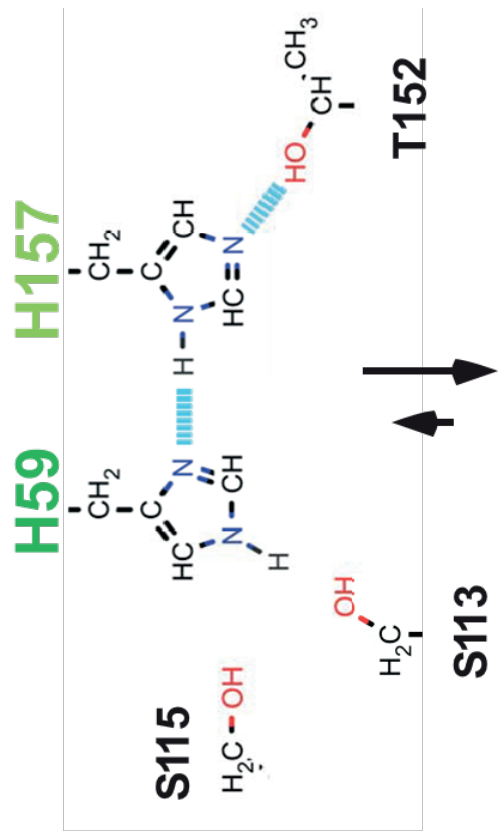


Figure II-16

Dynamics in the hydrogen bond network. The hydrogen bond network identified in the wild-type Pin1 PPIase according to the high resolution crystal structure of Par14 (A), where C113 is drawn to keep thiolate as theoretically proposed. The hydrogen bond rearrangement associated with the exchange of H59 between the ϵ - and δ -tautomers (B). The rearrangement of the hydrogen bonding in the network caused by the H59 ϵ -tautomer conversion to the imidazolium form.

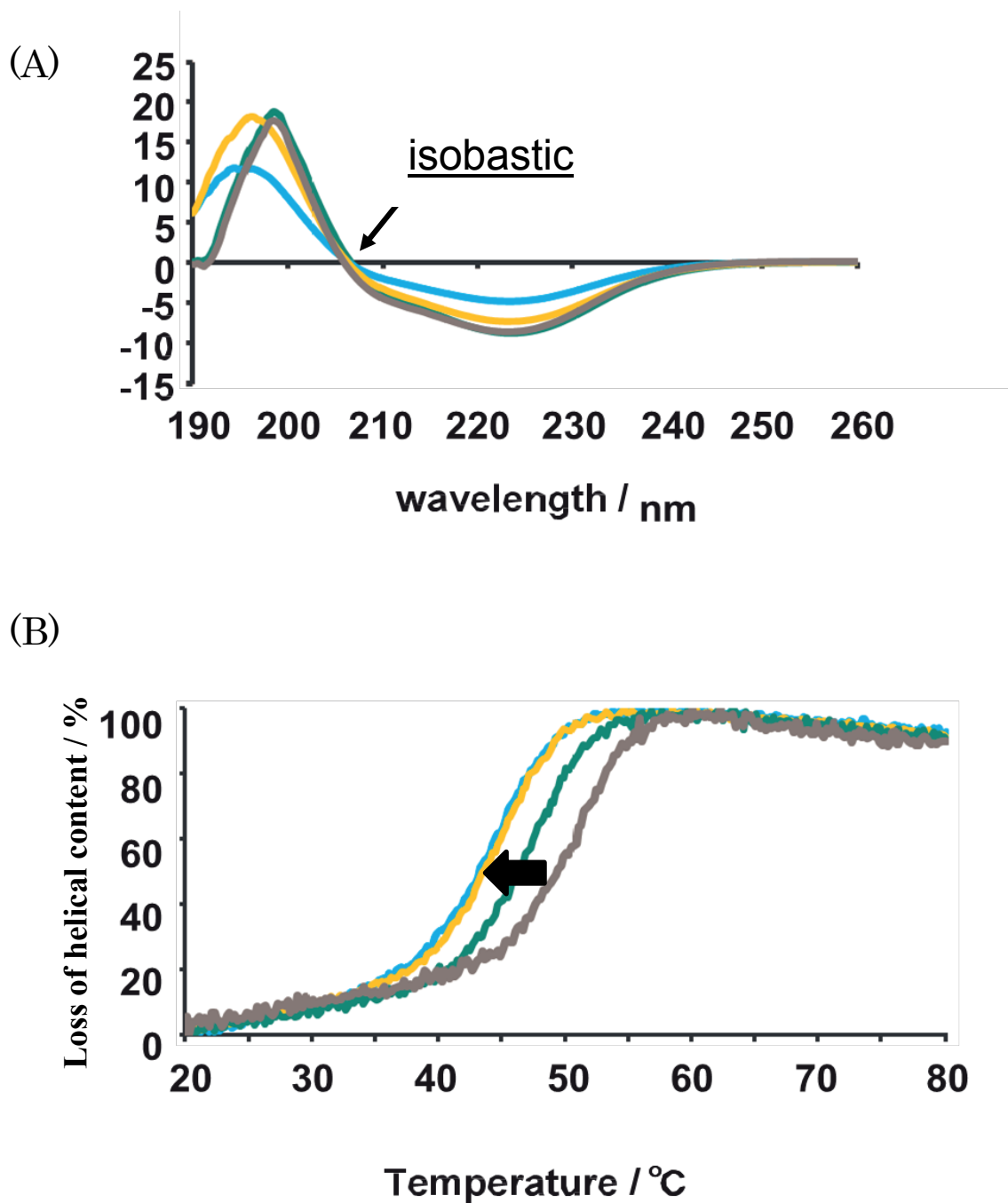


Figure II-17

Comparison of the CD spectra for the wild-type (gray), C113D (green), C113A (cyan), and C113S (orange) mutant Pin1 PPIase domains (A). The overlaid presentation of the CD spectral changes by heating the sample: the wild-type (gray), C113D (green), C113A (cyan), and C113S (orange) mutants (B).

Table II-1**Structural statistics of the final 10 structures of C113A and C113S Pin1 PPIase mutants.**

Pin1 PPIase	C113A	C113S
RMSDs from NOE upper distance restraints (Å)		
Intra-residual ($ i-j =0$) (498 for C113A; 493 for C113S)	0.000 ± 0.000	0.000 ± 0.000
Medium-range ($1 \leq i-j \leq 4$) (924; 872)	0.005 ± 0.002	0.004 ± 0.003
Long-range ($ i-j > 4$) (858; 768)	0.012 ± 0.007	0.005 ± 0.005
Total (2280; 2133)	0.006 ± 0.003	0.003 ± 0.002
RMSDs from dihedral angle restraints (ϕ and ψ) (°) (104 for C113A; 104 for C113S) ^a		
	0.032 ± 0.050	0.025 ± 0.019
RMSDs from ideal stereochemistry		
Bonds (Å)	0.005	0.005
Angles (°)	0.505	0.490
Impropers (°)	0.668	0.719
Ramachandran plot (%) ^b		
Residues in most favored regions	86.3	87.3
Residues in additional allowed regions	13.1	12.6
Residues in generously allowed regions	0.5	0.0
Residues in disallowed regions	0.1	0.1
Average RMSDs to the mean structure (Å) ^c		
Backbone (N, C α , C', O)	0.76 ± 0.18	0.85 ± 0.17
All non-hydrogen	1.30 ± 0.24	1.34 ± 0.22

^aThe angle restraints were derived from TALOS+ with the angle ranges $\pm 30^\circ$.^bFor the residues R54 – R161 in the 10-lowest energy structures.^cFor the residues in the secondary structure parts (residues R54 – V62, K82 – K97, F103 – Q109, S114 – K117, A124 – S126, K132 – S138, V150 – F151, and G155 – R161).

Table II-2**Reduced the global structural stabilities and the *cis-trans* isomerization rates of C113A****and C113S Pin1 PPIase mutants.**

Pin1 PPIase	Denaturation temperature [°C] ^a	Exchange rate from <i>cis</i> to <i>trans</i> (k_{CT}) [sec ⁻¹] ^b	Exchange rate from <i>trans</i> to <i>cis</i> (k_{TC}) [sec ⁻¹] ^b
C113A	43.2	1.0 ± 0.2	0.1 ± 0.1
C113S	43.6	Not detected	Not detected
Wild-type ^c	49.4	51.6 ± 1.9	6.6 ± 2.1
C113D ^c	46.2	0.7 ± 0.5	0.1 ± 0.0

^aDenaturation temperature was estimated by CD molar ellipticity at 222 nm.^bIsomerization exchange rates were directly determined using EXSY experiments.^cThese values were determined in our previous study.

Table II-3.**Distance and angle comparison among the wild type, C113A, and C113S Pin1 PPIase mutant.**

	Wild-type ^a	C113A	C113S
Distance (Å)			
$C\alpha^{C113/A113/S113} - C\alpha^{H59}$	8.97 ± 0.44	9.90 ± 0.41	9.10 ± 0.79
$C\alpha^{S115} - C\alpha^{H59}$	7.89 ± 0.61	6.92 ± 0.62	8.11 ± 0.48
$C\alpha^{H59} - C\alpha^{H157}$	6.31 ± 0.23	6.51 ± 0.20	6.34 ± 0.22
$C\alpha^{H157} - C\alpha^{T152}$	7.21 ± 0.37	7.41 ± 0.24	7.10 ± 0.43
$C\alpha^{C113/A113/S113} - C\alpha^{S154}$	9.95 ± 0.50	10.74 ± 1.30	9.83 ± 0.61
Angle (deg.)			
χ^2^{H59}	143.78 ± 19.66	148.10 ± 29.73	125.39 ± 28.09
χ^2^{H157}	-111.57 ± 21.49	-105.96 ± 12.62	-121.08 ± 18.50

The values referred to the means and standard deviations from the 10 lowest energy structures.

^aThe values for the wild type were estimated using our previously determined structure

Chapter III

Redox-sensitive structural change in the A-domain of HMGB1 and its implication for the cisplatin modified DNA

Abstract

HMGB1 (high-mobility group B1) is a ubiquitously expressed bifunctional protein; which acts as a nuclear protein in cells and also as an inflammatory mediator in the extracellular space. HMGB1 changes its functions according to the redox states, in both intra- and extra-cellular environments. Two cysteines, Cys23 and Cys45, in the A-domain of HMGB1 forms a disulfide bond under oxidative conditions. The A-domain with the disulfide bond shows reduced affinity to cisplatin modified DNA. We have solved the oxidized A-domain structure by NMR. In the structure, Phe38 has flipped ring orientation from that found in the reduced form; the phenyl ring in the reduced form intercalates into the platinated lesion in DNA. The phenyl ring orientation in the oxidized form is stabilized through the intramolecular hydrophobic contacts. The disorientation of Phe38 ring by the disulfide bonding in the A-domain could explain the reduced HMGB1 binding to the cisplatinated DNA.

1. Introduction

Cells use an elaborate mechanism for control of protein function in response to oxidative stress through forming disulfide bond between thiol groups ⁵⁶. In fact, various types of transcription factors were found to exhibit redox-dependent switch on their transcriptional activities^{57, 58} . Recent studies listed the proteins regulated by thiol-disulfide exchange^{59, 60} . Intriguingly, most of the proteins were abundant structural proteins, molecular chaperons, and the others that are not directly involved in the gene regulation. HMGB1 (high-mobility group B1) is one of those proteins having redox-dependent functional switch⁶¹.

HMGB1 is a ubiquitously expressed nuclear protein, which has two tandem DNA-binding domains, high-mobility group boxes A and B, and a highly acidic C-terminal tail⁶². HMGB1 functions as an architectural chromatin-binding factor that binds to DNA in a structure-specific but a sequence-independent manner, with higher affinity for unusual DNA structures, including bent, kinked or unwound duplexes ⁶³. HMGB1 also plays as an extracellular signaling molecule during inflammation, cell differentiation, cell migration and tumor metastasis; HMGB1 is released from necrotic cells or secreted by activated immune cells ⁶⁴. The released HMGB1 becomes oxidized in the oxidative extracellular space ⁶⁴⁻⁶⁶. HMGB1 has three cysteine residues. Cys23 and Cys45 in the A-domain are located in a spatial proximity ⁶⁷, and these two cysteines form disulfide bond under mild oxidative condition ⁶⁶. The other cysteine, Cys106, in the B-domain is less reactive to

oxidative modification; its thiol turns inside the structure⁶¹. The redox-dependent disulfide bond formation between Cys23 and Cys45 in the A-domain switches the HMGB1 functions in the extracellular space; the HMGB1 in the reduced form plays as a chemoattractant, while the protein with the disulfide bond roles as a proinflammatory cytokine⁶⁸. Cys106 may engage in the nuclear localization of HMGB1 inside cells ⁶¹.

The redox state of HMGB1 should be functionally relevant also in the intracellular environment, because the redox potential of the A-domain is within the range of the physiological intracellular redox potential ⁶⁶. A fraction of HMGB1 should exist in the oxidized form in cells, which could explain the variety of the cellular response to the HMGB1 engaging gene regulations ⁶⁷. The high affinity of HMGB1 to the cisplatinated DNA lesions is expected to enhance the efficacy of cisplatin, one of the widely used anticancer drugs ⁶⁹. The HMGB1 binding to the cisplatinated DNA impedes nucleotide excision repair (NER) by shielding the lesions from the repairing proteins ^{70, 71}, which thus blocks the replication and transcription in aggressively growing cancer cells to induce their cell death ^{72, 73}[17, 18]. However, the improvement of the efficacy of cisplatin as a function of HMGB1 protein levels in cells are not observed⁷⁴. The failure to correlate cell sensitivity to cisplatin with the amount of HMGB1 in cells could be ascribed to the co-existence of the oxidized HMGB1 in cells ⁶⁷; the oxidized HMGB1 with the disulfide bond between Cys23 and Cys45 has 10-fold reduced affinity to the cisplatinated DNA, thus less impeding to the NER process⁶⁷. The oxidization to HMGB1 in cells is thought to be one factor for the cisplatin

resistance of certain tumors⁶⁷.

The functional switch according to the redox state of HMGB1 in cells and in the extracellular space has been focused to gain the new biological roles of this ubiquitously expressed protein. The structure of the oxidized A-domain in HMGB1, however, has not been solved. Therefore, the molecular mechanism for the functional changes in response to the redox states of HMGB1 remains elusive. To advance our understanding of the redox-dependent functional change of HMGB1, we solved the oxidized A-domain structure by NMR. The A-domain in the oxidized form has unexpectedly large structural change in the loop between helices I and II. In particular, the flipped phenyl ring at Phe38, at the C-terminal edge of the inter-helix loop, relative to that in the reduced form was remarkable. Phe38 is the key residue interacting into cisplatin-[d(GpG)] intrastrand crosslink site, as shown in the X-ray complex structure of the reduced A-domain of HMGB1 with the cisplatinated DNA⁷⁵. The significant structural change associated with the disulfide bonding in the A-domain could explain the reduced affinity of the oxidized HMGB1 to the cisplatinated DNA.

2. Materials and methods

Expression and Purification of the oxidized A-domain of HMGB1

HMGB1 A-domain (residues from 1 to 84 of human HMGB1 protein; SwissProt accession IDP09429) was purified from *Escherichia coli*, BL21 (DE3), harboring the corresponding cDNA cloned to pET28a (Merck Chemicals, Germany). The purification for the isotopically labeled sample was done according to essentially the same way as described before⁷⁶ [21]. His6-tag at the N-terminus of the HMGB1 A-domain was cleaved by using thrombin in 30 units (GE Healthcare) during dialysis against the buffer A solution (50 mM TrisHCl, pH 8.0) at 4 °C for 16 h. The tag-cleaved A-domain was further purified by using Heparin-Sepharose (GE Healthcare) with NaCl gradient (from 0 M to 1 M) in the buffer A. Disulfide bond formation in the A-domain was done according to the protocol in the preceding work [13]; the protein was dialyzed against the buffer B (50 mM potassium phosphate with 150 mM KCl, pH 6.4) containing 5 μ M CuCl₂ for overnight at 4 °C and then redialyzed against the buffer B lacking CuCl₂. The protein concentration was determined by OD₂₈₀. Disulfide bond formation in the final sample was confirmed by the electrophoretic mobility in SDS-PAGE and also by the ¹³C β NMR chemical shifts for the Cys23 and Cys 45 residues ⁷⁷ (Figure III-1).

It is noted that throughout this manuscript, residues in HMGB1 is numbered according to the immature form that retains the initial methionine to keep the consistency with the entry in the sequence data base: the first amino acid of the mature HMGB1 is a glycine, since the first methionine encoded by the gene is cleaved off after synthesis⁷⁸, which numbering is

adopted in some literatures. The present HMGB1 A-domain fragment has additional three residues, GSH, from the expression vector at its N-terminus.

NMR spectroscopy

A standard set of NMR spectra³⁶ for the resonance assignments of HMGB1 A-domain in the buffer B were collected at 293 K on a Bruker AvanceII spectrometer operating at the ¹H resonance frequency of 700 MHz equipped with a triple resonance cryogenic probe. The ¹⁵N-¹H hetero-nuclear NOE experiments³⁶ were also done at 293 K on a 700 MHz spectrometer. The experiments for the anisotropic sample using liquid crystal were carried out at 300 K to keep the liquid crystalline media stably aligned. NMR data were processed by NMRPipe³⁷. Spectral analyses were done by using the KUIJIRA suite³⁸ running on NMRview³⁹ platform and SPARKY (T.D. Goddard and Kneller, D.G. SPARKY 3, UCSA). The chemical shifts data for the oxidized HMGB1 A-domain were deposited in the Biological Magnetic Resonance Data Bank (accession code, 11532) (Figure III-2).

Dipolar coupling measurements

Dipolar couplings (1DNH, 1DC'N, and 2DC'H) for the ¹³C/¹⁵N labeled HMGB1 A-domain in the buffer B were simultaneously measured using IPAP-HSQC spectra⁷⁹ under the selective decoupling to ¹³Cβ spins. For aligning protein, a 6% C12E5/hexanol (r = 0.96) liquid crystalline medium was used at 300 K, which gave the residual deuterium quadrupolar coupling 8.5 Hz and aligned the A-domain in the magnitudes of the axial alignment

tensor component (Da) and rhombicity (R) -8.7 Hz and 0.43, respectively.

Structure determination of the oxidized HMGB1 A-domain

Structure calculation was done with the CYANA program using the automated NOE assignment suite, CANDID^{40, 80}. The backbone dihedral angle restraints were generated by the TALOS+ program^{42, 81}. The 40 lowest-energy CYANA structures calculated with the distance and the backbone torsion angle restraints were subjected to the explicit water refinement with XPLOR-NIH^{43, 82}. In this refinement, the three types of RDCs (1DNH, 1DC'N, and 2DC'H) were added to the distance and backbone torsion angle restraints; the RDCs data were used by normalizing to the 1DNH data based on bond length and gyromagnetic ratios⁸³. The final 20 XPLOR-NIH structures were validated using the program PROCHECK-NMR⁴⁴. The final set of ensemble structure coordinates were deposited in the Protein Data Bank, under the accession code 2RTU.

2.5. Model building of the complex of oxidized A-domain in HMGB1 with cisplatinated DNA

The complex of the oxidized A-domain in HMGB1 with cisplatinated DNA was modeled on the basis of the X-ray complex structure of cisplatinated DNA and the reduced form of A-domain (PDB code 1CKT)⁷⁵. The modeling was done as follows. At first, the minimally essential pairs of the inter-molecularly contacting residues were extracted from the coordinate, which enable to

reproduce the original complex structure by the HADDOCK calculation⁸⁴. Subsequently, the same inter-molecular contact residues were used to model the oxidized HMGB1 domain A with the cisplatinated DNA by using the HADDOCK⁸⁴. The contacting residues were selected through the analysis of the inter-molecular interactions with the LIGPLOT software⁸⁵; the residues having more than one intermolecular hydrogen bond or more than five non bonded interactions were chosen. In the complex structure of the cisplatinated DNA with the reduced A-domain, the identified contacting residues were Lys12, Tyr16, Ala17, Arg24, Phe38, Ser42, Lys43, Ser46, and Trp49 in A-domain and G8, G9, A10, C11, C12, T13 in one strand and C15/T7, C8, and C9 in the other strand of the cisplatinated DNA. The docking modeling calculation was done on the HADDOCK web server⁸⁶ with the above contacting residues input as the “active” ambiguous interaction residues (AIRs)⁸⁴. For comparison, the same docking calculation was done using the reduced HMGB1 A-domain structure solved in the reductive solution condition containing 1 mM DTT (PDB code 2YRQ).

3. Results and discussion

Structure description of the oxidized A-domain of HMGB1

The determined structure of the oxidized A-domain in HMGB1 is shown in comparison with that of the reduced form reported by the other group (PDB code 2YRQ) (Figure III-3A and 4A). The structural statistics is available as a supplemental table (Table III-1). There found notable orientation change in the N-terminal part of the helix II caused by the disulfide bonding between Cys23 and Cys45 (Figure III-4A). As shown in the close up view, the inter-helix loop between the helices I and II flipping over to the concaved surface of the L-shaped structure of the A-domain (Figure III-4B). The disulfide bonding seems to pull up the N-terminus of the helix II and subsequently allows the hydrophobic interaction between the phenyl ring of Phe38 and the residues sandwiched by the helices I and II (Figure III-4C). In fact, the aromatic protons in Phe38 showed several clear NOEs to the hydrophobic residues inside the concaved surface, which confirm their contacts (Figure III-5); the corresponding NOEs were not observed in the reduced form A-domain.

The intra-molecular contacts of the Phe38 with the hydrophobic residues rather limited the flexibility of the inter-helix loop, as evidenced by the changes in the profiles for the ^{15}N (1 heteronuclear NOEs (hetNOEs) (Figure III-6). The residues in the inter-helix loop (residues 34-40) showed significantly smaller hetNOE values relative to the secondary structured parts in both reduced and oxidized forms; the corresponding inter-helix loop is more flexible than the other structured par in the psec-nsec time regimes⁸⁷. In comparing the hetNOE profiles, the inter-loop residues near the Phe38

in the oxidized form showed increased hetNOE values; the phenyl ring contact to the hydrophobic residues may have reduced the intrinsic flexibility in the corresponding residues.

Model complex of the oxidized A-domain with the cisplatin-modified DNA

The functional significance of the flipped Phe38 ring in the oxidized form was elucidated on the complex structure of the oxidized A-domain with the cisplatinated DNA modeled based on the corresponding X-ray complex structure with the reduced A-domain (PDB code 1CKT)⁷⁵.

HMGB1 A-domain specifically binds to a cisplatin1,2-intrastrand d(GpG) cross-linked (cisplatin-[d(GpG)]) DNA⁶⁹. The crystal structure demonstrated that the increased affinity of the A-domain for the cisplatinated DNA is mediated by an intercalation of the phenyl ring of Ph38 into the patinated lesion (Figure III-7)⁷⁵. The phenyl ring is inserted into a hydrophobic cavity formed by the platinum-modified neighboring guanine rings⁷⁵. The stacking interactions between the phenyl ring and its surrounding guanine bases may stabilize the overall protein-DNA complex. HMGB1 A-domain has limited affinity to the canonical double stranded DNA, while the B-domain has higher affinity to such ordinal double stranded DNA structure⁸⁸. The enhanced affinity of the A-domain to the cisplatinated DNA by the phenyl ring intercalation determines the specific binding of the full-length HMGB1 to the cisplatinated DNA.

The reduced A-domain structure solved in a DNA free-state (PDB code 2YRQ) was docked onto the cisplatinated DNA using the HADDOCK

program⁸⁴. The phenyl ring of Phe38 in the docked structure is close to that found in the X-ray structure (Figure III-7). The phenyl ring in the reduced A-domain could attain the stacking interaction with the platinated guanine bases as that in the X-ray structure by subtle ring reorientation (Figure III-7B). The model complex structure, therefore, reasonably explains the high affinity of the reduced A-domain to the displatinated DNA.

The Phe38 ring moiety in the oxidized A-domain with the flipped orientation against that in the reduced form is not allowed for intercalating into the cisplatin-[(GpG)] lesion in the model complex (Figure III-7B).

Structural explanation for the reduced binding of the oxidized A-domain to the cisplatinated DNA

As discussed above, the phenyl ring of Phe38 intercalation into the palatinate guanine bases is the key interaction to enhance the A-domain binding to the cisplatinated DNA. As seen in the model complex with the reduced A-domain structure solved in DNA free-state, the only slight reorientation of the phenyl ring achieves the stable interaction of the A-domain to the cisplatinated DNA (Figure III-7B). On the other hand, the model complex using the oxidized A-domain has demonstrated that the phenyl ring could not readily intercalate into the cavity by the platinated guanine bases (Figure III-7B). The phenyl ring stably stays on the hydrophobic core in the oxidized A-domain (Fig. 1C), which interactions are stable enough to give significant number of NOEs among the residues (Figure III-5). In addition, this phenyl ring mediating interactions limit the structural

flexibility of the inter-helix loop as shown by the hetNOE profiles (Figure III-6). Taking these spectroscopic data together, the phenyl ring could retain the flipped orientation in the complex with the cisplatinated DNA, and it cannot intercalate into the platinated lesion as shown in the model complex structure (Figure III-7B). In addition, the phenyl ring in the oxidized A-domain directs in the opposite side from the platinated guanine bases in the complex, the induced flip of the phenyl ring to enable the interaction may hard to occur upon binding to the displatinated DNA (Figure III-7B). These structure based inspection could explain the reduced affinity of the A-domain of HMGB1 to the cisplatin modified DNA.

In summary, this study has shown the significant structural difference in the oxidized A-domain of HMGB1 from that of the reduced form. The oxidized A-domain has the flipped phenyl ring of Phe38 onto the concaved surface of the L-shaped structure, whilst the ring in the reduced form extrudes to play as a wedge intercalating into the platinated lesion in the DNA. As experimentally suggested, the withdrawn form of the phenyl ring is stable enough presumably to keep the structure even in the complex with the cisplatinated DNA. The phenyl ring in the oxidized form, therefore, could not play as a wedge into the cisplatinated DNA, although the other interactings to the DNA are kept as in the complex of the reduced A-domain with the DNA. The flipped phenyl ring caused by the disulfide bonding could be the primal cause for the one-order impaired binding of the oxidized A-domain compared to the reduced form ⁶⁷.

4. Conclusions

This study has shown the significant structural difference in the oxidized A-domain of HMGB1 from that of the reduced form. The oxidized A-domain has the flipped phenyl ring of Phe38 onto the concaved surface of the L-shaped structure, whilst the ring in the reduced form extrudes to play as a wedge intercalating into the cis-platinated lesion in the DNA. As experimentally suggested, the withdrawn form of the phenyl ring is stable enough presumably to keep the structure even in the complex with the cis-platinated DNA. The phenyl ring in the oxidized form, therefore, could not play as a wedge into the cisplatinated DNA, although the other interactings to the DNA are kept as in the complex of the reduced A-domain with the DNA. The flipped phenyl ring caused by the disulfide bonding could be the primal cause for the one-order impaired binding of the oxidized A-domain compared to the reduced form.

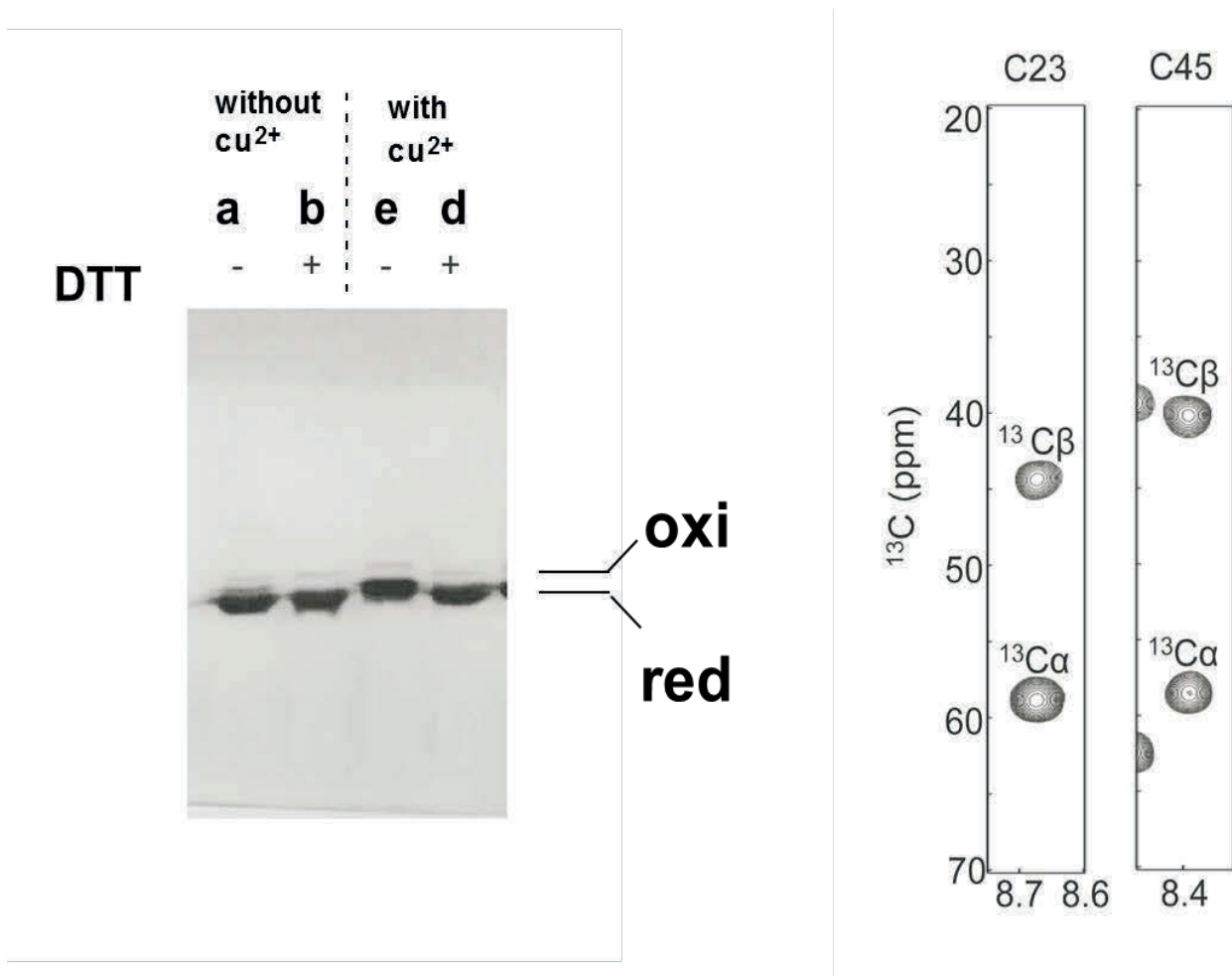


Figure III-1

Characterization of the prepared oxidized A-domain of HMGB1 (A) Oxidation of the A-domain by Cu^{2+} ion as oxidant was analyzed by the SDS-PAGE for the samples prepared with and without DTT treatment: Lanes a and b are for the sample dialyzed against the buffer solution without Cu^{2+} ion, while the lanes c and d for the protein dialyzed against the buffer solution containing 5 mM Cu^{2+} ion. The oxidized A-domain shows slower migration relative to the reduced form, as seen in the lane c in comparison to the lane d. (B) The strips of the 3D CBCA(CO)NH spectrum are shown to demonstrate the lower field $^{13}\text{C}\beta$ chemical shift values for Cys23 and Cys45; the reduced cysteine $^{13}\text{C}\beta$ resonates in the ranges of 20 – 30 ppm. Both results showed that the present preparation oxidized the A-domain almost completely.

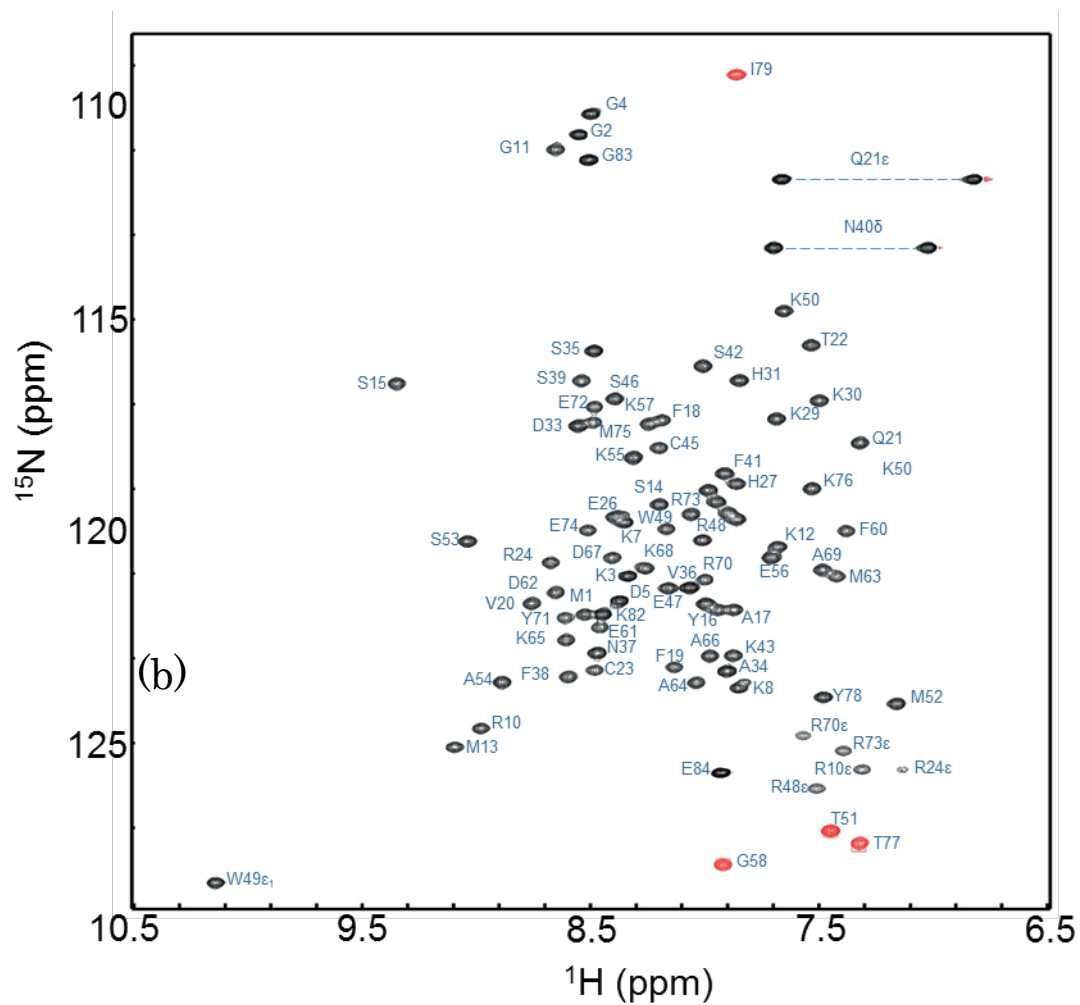


Figure III-2

^1H - ^{15}N HSQC spectrum for the oxidized A-domain of HMGB1. The resonance assignments are drawn by blue characters on the spectrum.

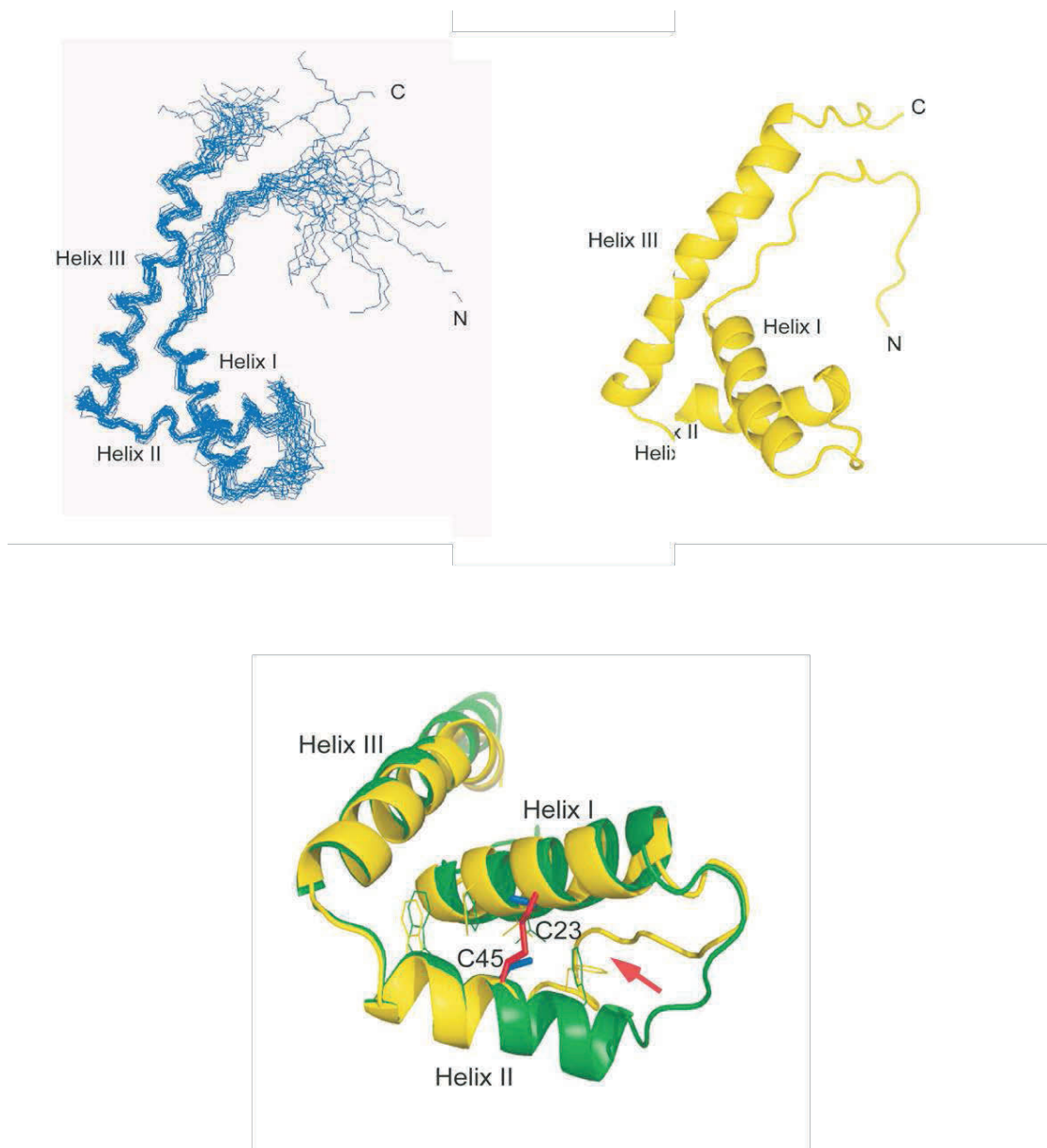


Figure III-3

Over all structure of the A-domain of HMGB1. (A) The overlay of the 20 lowest energy structures. (B) The ribbon drawing of the lowest energy structure among the final 20 structure ensemble. (C) The close up view of the structure part having shown the structural change by the disulfide bond formation; the structures for the reduced (green) and oxidized (yellow) forms are drawn in the ribbon presentation with disulfide bond in the ball-and-stick presentation.

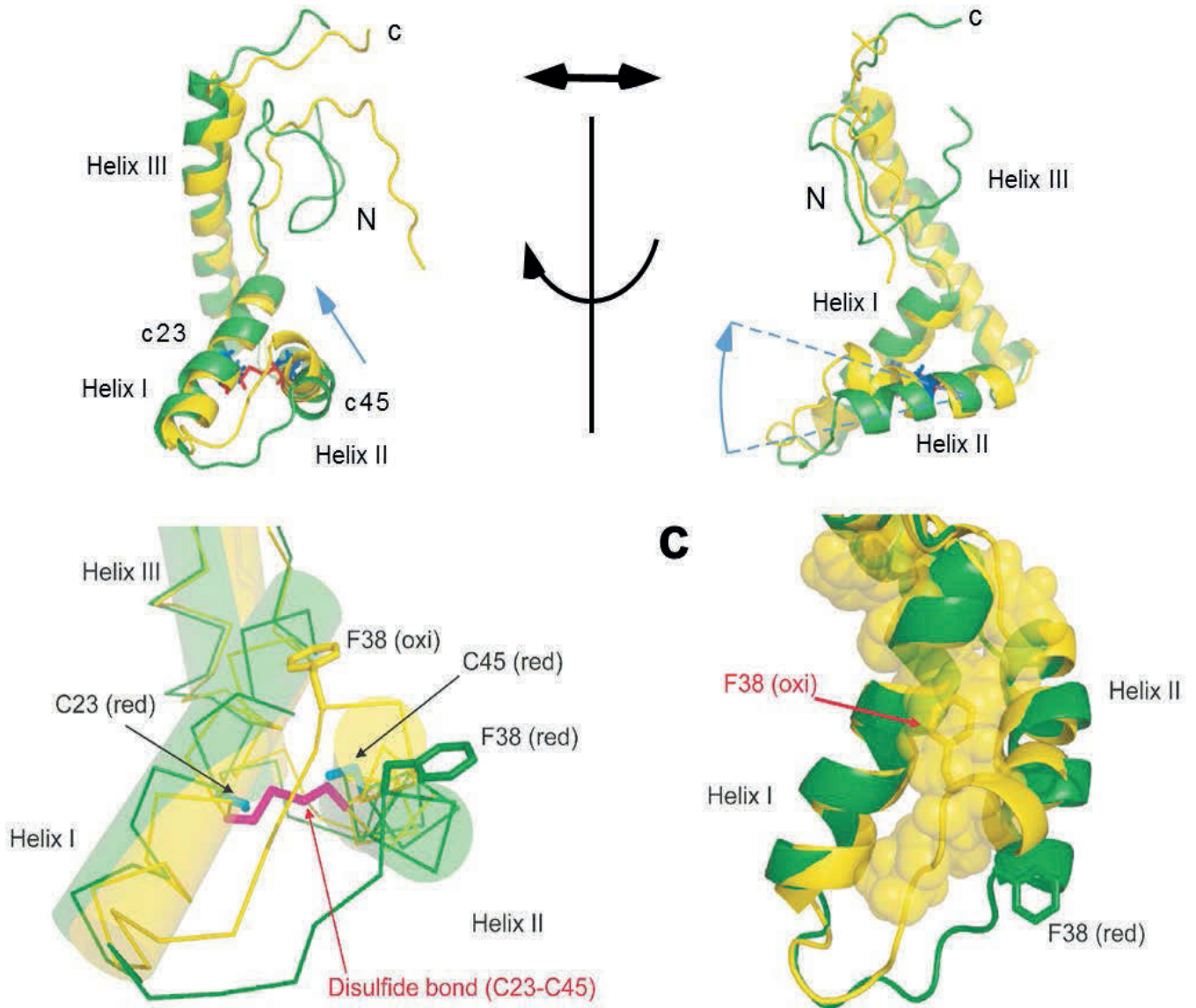


Figure III-4

Structure comparisons of the A-domains in the reduced and oxidized form. (A) Ribbon drawings for the reduced (green; PDB code 2YRQ) and oxidized (yellow) A-domains; two structures were overlaid to minimize the root mean square deviation (rmsd) of the C α positions in the helices (residues Ser15-Lys30, Phe38-Trp49, Ala54-Met75). The residues drawn in a ball-and-stick presentation are cysteine residues, Cys23 and Cys45, in the reduced (blue) and oxidized (red) forms. The apparent change in the orientation of the N-terminal part of the helix II is emphasized by arrows in blue. The right structures are the views for the left structures by 90-degree rotation. (B) The close up view of the parts comprising helices I and II with interhelix linker in the reduced and oxidized A-domain, which demonstrates the flipped Phe38 ring in the oxidized structure (yellow) relative to that in the reduced form. (C) The other close up view to show the hydrophobic contacts between the flipped Phe38 in the reduced A-domain (yellow) with the overlaid reduced form (green). The hydrophobic residues (residues F18, F19, F38, F41, F60, V20, V36 and W49) between the helices I and II are drawn by the yellow space filling atoms. The figures were prepared by the program PyMOL (Schrödinger, LLC).

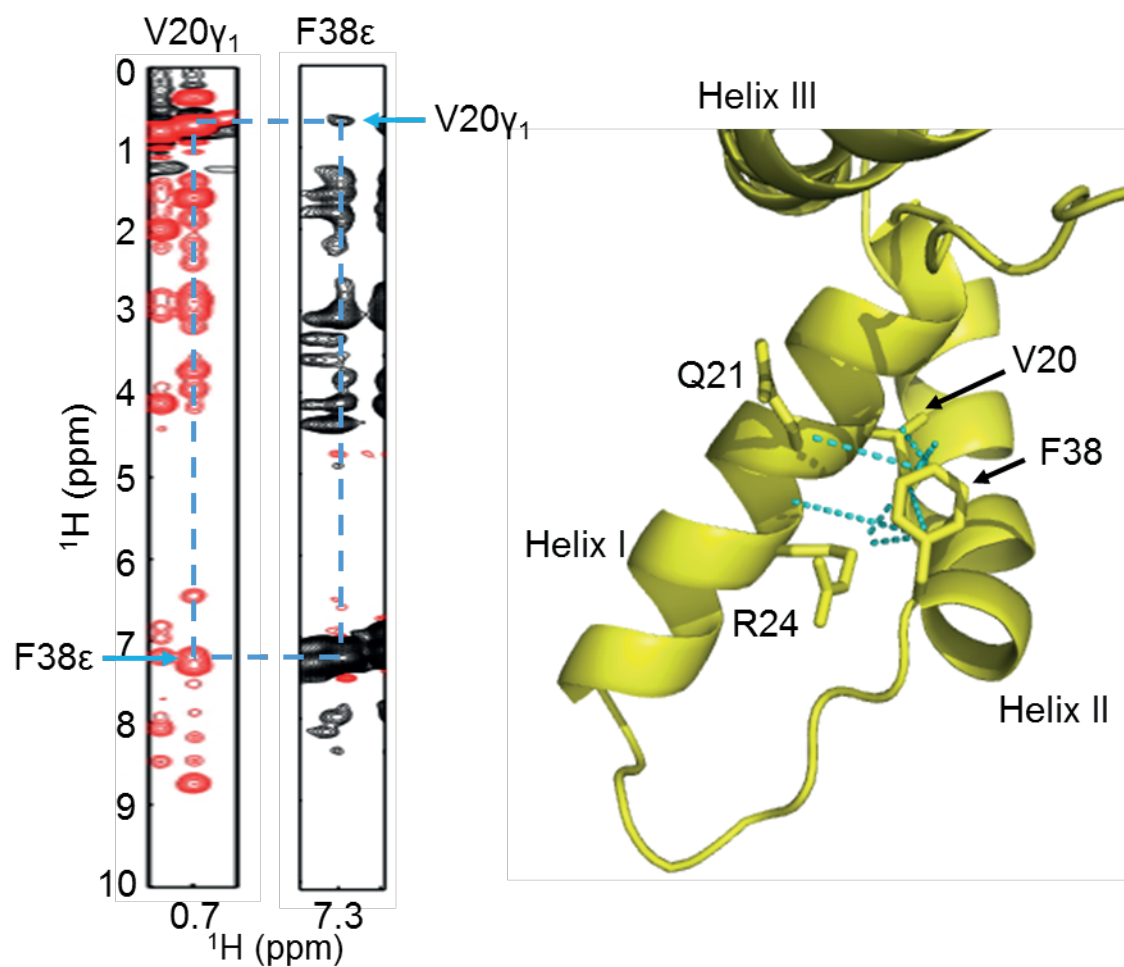


Figure III-5

The NOEs to define the flipped ring orientation of Phe38 in the reduced A-domain. (A) The representative strips from the 3D ^{13}C -edited NOESY data for the reduced A-domain. Val20 γ -methyl protons showed clear NOE to Phe38 ϵ ring protons (left panel) and vice versa (right panel). (B) The NOEs derived from Phe38 ring protons are drawn in the blue dotted lines on the structure of the oxidized A-domain; the observed NOEs are listed as V20 H β -F38 H ϵ , V20 H γ 1-F38 H δ , V20 H γ 1-F38 H ϵ , V20 H γ 1-F38 H ζ , Q21 H β -F38 H ϵ , R24 HN-F38 H δ , R24 H δ -F38 H δ , and R24 H δ - F38 H ζ .

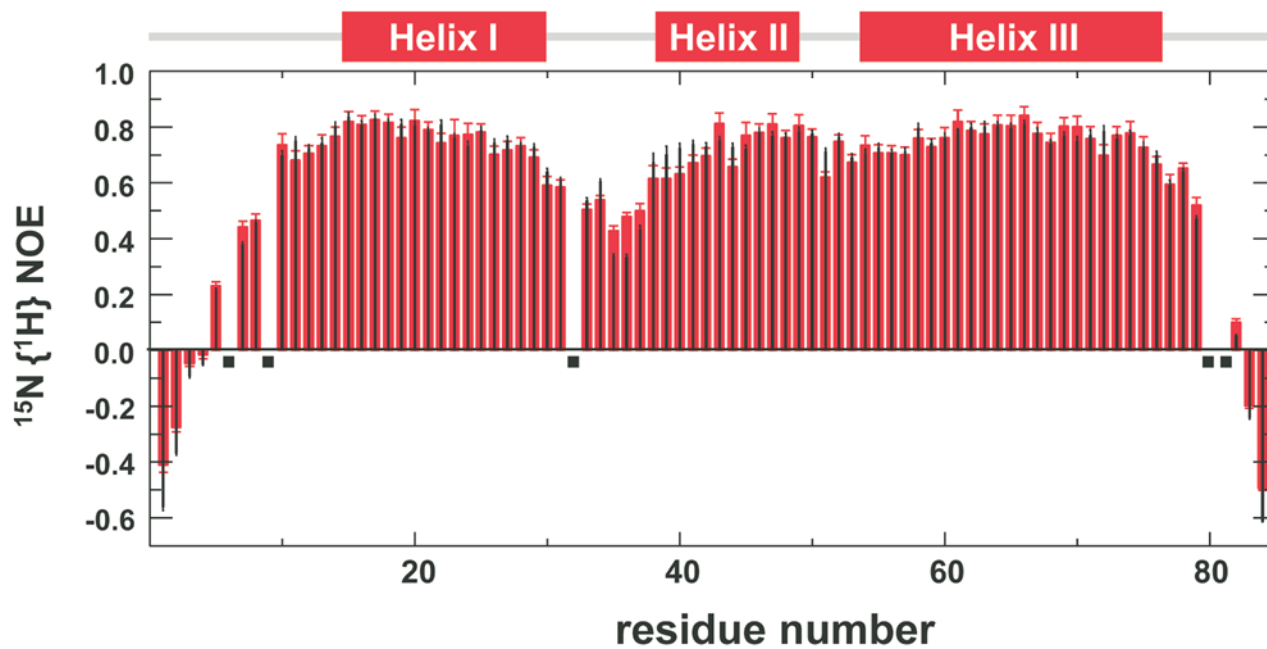


Figure III-6

The comparison of the $^{15}\text{N}(^1\text{H})$ heteronuclear NOEs between the reduced and oxidized A-domains. The values indicated by the green and yellow bar indicate the heteronuclear NOE intensities for the each corresponding residue in the reduced and oxidized A-domain, respectively.

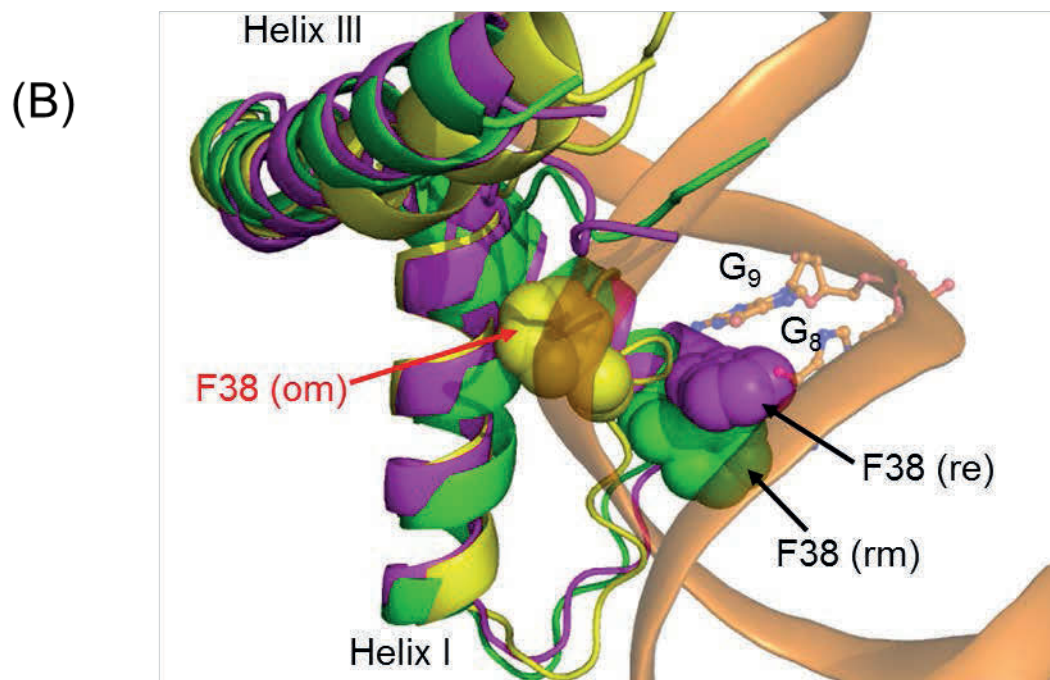
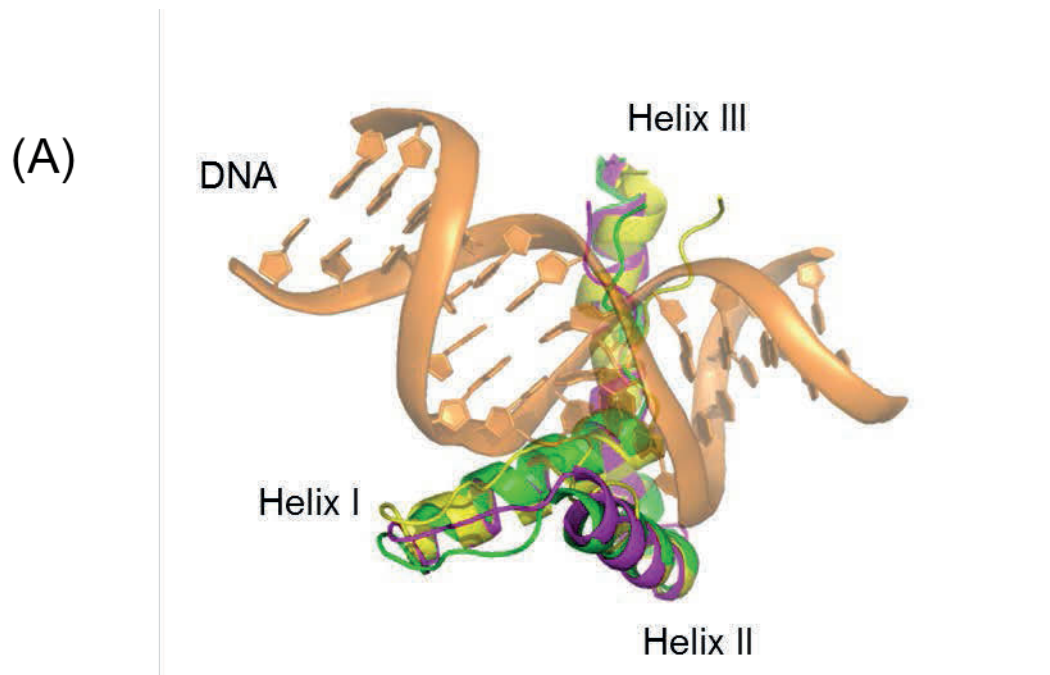


Figure III-7

Comparing the model complexes with the crystal structure of the reduced A-domain with cisplatinated DNA. (A) The modeled complex structures with the A-domains in the reduced (PDB code 2YRQ) and the oxidized forms solved in the DNA-free state are overlaid onto the X-ray complex structure (PDB code 1CKT). The cisplatin-[d(GpG)] part is marked with a red dotted circle. The A-domain structures are drawn in ribbon presentations; the reduced A-domain in the X-ray complex (magenta), the reduced (green) and oxidized (yellow) A-domains in the model structures. The displatinated DNA is drawn in pink ribbon drawing. (B) The close up views around the platinated site to compare the interactions of the Phe38 ring moiety to the cavity made by the cisplatinated-[d(GpG)]. Structures are drawn in the same color usage as in (A), with space-filling representation to the phenyl rings at Phe38. The figures were prepared by the program UCSF Camera.

Table III-1**Structural statistics of the final 20 structures of the oxidized A-domain of HMGB1**

NOE upper distance restraints	
Intra-residual ($ i-j = 0$) (402)	0.000±0.000
Medium-range ($1 \leq i-j \leq 4$) (1077)	0.010±0.003
Long-range ($ i-j > 4$) (436)	0.027±0.013
Total (1915)	0.012±0.004
Dihedral angle restraints (ϕ and ψ) (131) ^a	1.165±0.453
RMSDs from dipolar coupling restraints (Hz)	
¹ D _{NH} (55)	1.3 ± 0.1
¹ D _{NC'} (34)	2.4 ± 0.4
¹ D _{HC'} (34)	2.5 ± 0.1
RMSDs from ideal stereochemistry	
Bonds (Å)	0.0054±0.0002
Angles (°)	0.608±0.043
Impropers (°)	0.927±0.127
Ramachandran plot ^a (%)	
Residues in most favored regions	90.3
Residues in additional allowed regions	8.9
Residues in generously allowed regions	0.2
Residues in disallowed regions	0.6
Average RMSDs to the mean structure (Å)	
Backbone (N,CA,C',O)	0.76
All non-hydrogen	1.21

^a The angle restraints were from TALOS+ with the angle ranges ±30°.

^b For the residues 18-78 in the 20 lowest energy structures.

^c For the residues in the secondary structured parts (residues 18-33, 41-52, and 57-78).

Chapter IV

General Conclusions

My works have delineated the protein structure/dynamics and function relationships on different types of proteins by using artificial modification in combination with extensively various NMR methods.

In the case of Pin1 PPIase domain, we clarified the active site structure is intrinsically fragile, and the state of the residues at 113 position sensitively changes the tautomeric states of the neighboring histidines, which change the active site structure by changing hydrogen bonding network running in the active site. This gives the idea that the Pin1 PPIase active site architecture is maintained very subtle chemical bonding balance, which structural flexibility should be functionally relevant.

In the other case of the HMGB1, we found that protein allosterically changes its active loop structure by the disulfide bond formation under oxidative condition. The conformational change was unexpected based on the high-resolution structure under reductive condition as inside cells. This gives an example for showing nature uses the naturally occurring chemical modification to modulate protein function through changing the structure that is intrinsically kept by the subtle thermodynamic balance.

Protein structure/dynamics-function relationships has been focused for long time in protein science, however they still have things uncovered. Chemically and/or genetically modification to proteins is now well prevailing

approach to explore protein functions and structures. However, they are not fully applied to see the effect on the protein dynamics that is intimately relating to the structure. In my Ph.D. work, I tried to expand the horizon of the protein structure/dynamics and function relationships by extensive use of modern NMR techniques. I believe some of my intentions have been realized.

Acknowledgments

I would like to express my sincere thanks to my supervisor, Professor Tate, for giving me the opportunity to study in his lab, and for his patient guidance.

I am deeply grateful for his help in the completion of this thesis. I would like to thank associate professor Naoya Tochio for helping me in the past 3 years.

Without his help, I would not have had the ability to analyse structure and dynamics of proteins using NMR. I would like to thank Dr. Jin-ichi Uewaki

for his practical help on the mutants work and CD measurement, and his time spent to help me solve problems in protein purification works. I would like to

thank Aya Takewuchi and Yu Tamari for their support and advice in the protein purification. I would like to thank Ryosuke Kawasaki, Daisuke Aoki,

and Miyashita Yurina for their help in my experiments. I would like to thank

all my friends in the Department of Mathematical and Life Sciences in

Hiroshima University. Last but not the least, I would like to thank my family

for their never ever failing support which is beyond any words to express.

References

- [1] Galzitskaya, O. V., and Garbuzynskiy, S. O. (2006) Entropy capacity determines protein folding, *Proteins-Structure Function and Bioinformatics* 63, 144-154.
- [2] Fitzpatrick, A. W., Knowles, T. P. J., Waudby, C. A., Vendruscolo, M., and Dobson, C. M. (2011) Inversion of the Balance between hydrophobic and hydrogen bonding interactions in protein folding and aggregation, *Plos Computational Biology* 7.
- [3] Basle, E., Joubert, N., and Pucheault, M. (2010) Protein Chemical Modification on Endogenous Amino Acids, *Chemistry & Biology* 17, 213-227.
- [4] Carrico, I. S. (2008) Chemoselective modification of proteins: hitting the target, *Chemical Society Reviews* 37, 1423-1431.
- [5] Cain, J. A., Solis, N., and Cordwell, S. J. (2014) Beyond gene expression: The impact of protein post-translational modifications in bacteria, *Journal of Proteomics* 97, 265-286.
- [6] Deribe, Y. L., Pawson, T., and Dikic, I. (2010) Post-translational modifications in signal integration, *Nature Structural & Molecular Biology* 17, 666-672.
- [7] Papa, F. R., Zhang, C., Shokat, K., and Walter, P. (2003) Bypassing a kinase activity with an ATP-competitive drug, *Science* 302, 1533-1537.
- [8] Nackley, A. G., Shabalina, S. A., Tchivileva, I. E., Satterfield, K., Korchynskiy, O., Makarov, S. S., Maixner, W., and Diatchenko, L. (2006) Human catechol-O-methyltransferase haplotypes modulate protein expression by altering mRNA secondary structure, *Science* 314, 1930-1933.
- [9] Behrsin, C. D., Bailey, M. L., Bateman, K. S., Hamilton, K. S., Wahl, L. M., Brandl, C. J., Shilton, B. H., and Litchfield, D. W. (2007) Functionally important residues in the peptidyl-prolyl isomerase Pin1 revealed by unigenic evolution, *Journal of Molecular Biology* 365, 1143-1162.
- [10] Chattopadhyay, A., and Haldar, S. (2014) Dynamic Insight into Protein Structure Utilizing Red Edge Excitation Shift, *Accounts of Chemical Research* 47, 12-19.
- [11] Xiao, Y., Liddle, J. C., Pardi, A., and Ahn, N. G. (2015) Dynamics of Protein Kinases: Insights from Nuclear Magnetic Resonance, *Accounts of Chemical Research* 48, 1106-1114.
- [12] Panjarian, S., Iacob, R. E., Chen, S., Engen, J. R., and Smithgall, T. E. (2013) Structure and Dynamic Regulation of Abl Kinases, *Journal of Biological Chemistry* 288, 5443-5450.
- [13] Matsuo, T., and Hirota, S. (2014) Artificial enzymes with protein scaffolds: Structural

- design and modification, *Bioorganic & Medicinal Chemistry* 22, 5638-5656.
- [14] Yaffe, M. B., Schutkowski, M., Shen, M. H., Zhou, X. Z., Stukenberg, P. T., Rahfeld, J. U., Xu, J., Kuang, J., Kirschner, M. W., Fischer, G., Cantley, L. C., and Lu, K. P. (1997) Sequence-specific and phosphorylation-dependent proline isomerization: A potential mitotic regulatory mechanism, *Science* 278, 1957-1960.
- [15] Lu, Z., and Hunter, T. (2014) Prolyl isomerase Pin1 in cancer, *Cell Research* 24, 1033-1049.
- [16] Lu, K. P. (2004) Pinning down cell signaling, cancer and Alzheimer's disease, *Trends in Biochemical Sciences* 29, 200-209.
- [17] Lu, K. P., and Zhou, X. Z. (2007) The prolyl isomerase PIN 1: a pivotal new twist in phosphorylation signalling and disease, *Nature Reviews Molecular Cell Biology* 8, 904-916.
- [18] Lu, K. P., Liou, Y. C., and Zhou, X. Z. (2002) Pinning down proline-directed phosphorylation signaling, *Trends in Cell Biology* 12, 164-172.
- [19] Blume-Jensen, P., and Hunter, T. (2001) Oncogenic kinase signalling, *Nature* 411, 355-365.
- [20] Butterfield, D. A., Abdul, H. M., Opii, W., Newman, S. F., Joshi, G., Ansari, M. A., and Sultana, R. (2006) Pin1 in Alzheimer's disease, *Journal of Neurochemistry* 98, 1697-1706.
- [21] Lim, J. N., and Lu, K. P. (2005) Pinning down phosphorylated tau and tauopathies, *Biochimica Et Biophysica Acta-Molecular Basis of Disease* 1739, 311-322.
- [22] Balastik, M., Lim, J., Pastorino, L., and Lu, K. P. (2007) Pin1 in Alzheimer's disease: Multiple substrates, one regulatory mechanism?, *Biochimica Et Biophysica Acta-Molecular Basis of Disease* 1772, 422-429.
- [23] Theuerkorn, M., Fischer, G., and Schiene-Fischer, C. (2011) Prolyl cis/trans isomerase signalling pathways in cancer, *Current Opinion in Pharmacology* 11, 281-287.
- [24] Ranganathan, R., Lu, K. P., Hunter, T., and Noel, J. P. (1997) Structural and functional analysis of the mitotic rotamase Pin1 suggests substrate recognition is phosphorylation dependent, *Cell* 89, 875-886.
- [25] Xu, G. G., Zhang, Y., Mercedes-Camacho, A. Y., and Etzkorn, F. A. (2011) A Reduced-Amide Inhibitor of Pin1 Binds in a Conformation Resembling a Twisted-Amide Transition State, *Biochemistry* 50, 9545-9550.
- [26] Mercedes-Camacho, A. Y., Mullins, A. B., Mason, M. D., Xu, G. G., Mahoney, B. J., Wang, X., Peng, J. W., and Etzkorn, F. A. (2013) Kinetic Isotope Effects Support the Twisted Amide Mechanism of Pin1 Peptidyl-Prolyl Isomerase, *Biochemistry* 52, 7707-7713.
- [27] Fischer, S., Michnick, S., and Karplus, M. (1993) A mechanism for rotamase catalysis by

- the FK506 binding-protein (FKBP), *Biochemistry* *32*, 13830-13837.
- [28] Mueller, J. W., Link, N. M., Matena, A., Hoppstock, L., Rueppel, A., Bayer, P., and Blankenfeldt, W. (2011) Crystallographic Proof for an Extended Hydrogen-Bonding Network in Small Prolyl Isomerases, *Journal of the American Chemical Society* *133*, 20096-20099.
- [29] Xu, N., Tochio, N., Wang, J., Tamari, Y., Uewaki, J.-i., Utsunomiya-Tate, N., Igarashi, K., Shiraki, T., Kobayashi, N., and Tate, S.-i. (2014) The C113D Mutation in Human Pin1 Causes Allosteric Structural Changes in the Phosphate Binding Pocket of the PPIase Domain through the Tug of War in the Dual-Histidine Motif, *Biochemistry* *53*, 5568-5578.
- [30] Hennig, L., Christner, C., Kipping, M., Schelbert, B., Rucknagel, K. P., Grabley, S., Kullertz, G., and Fischer, G. (1998) Selective inactivation of parvulin-like peptidyl-prolyl cis/trans isomerases by juglone, *Biochemistry* *37*, 5953-5960.
- [31] Sultana, R., Boyd-Kimball, D., Poon, H. F., Cai, J., Pierce, W. M., Klein, J. B., Markesbery, W. R., Zhou, X. Z., Lu, K. P., and Butterfield, D. A. (2006) Oxidative modification and down-regulation of Pin1 in Alzheimer's disease hippocampus: A redox proteomics analysis, *Neurobiology of Aging* *27*, 918-925.
- [32] Barman, A., and Hamelberg, D. (2014) Cysteine-Mediated Dynamic Hydrogen-Bonding Network in the Active Site of Pin1, *Biochemistry* *53*, 3839-3850.
- [33] Pelton, J. G., Torchia, D. A., Meadow, N. D., and Roseman, S. . (1993) Tautomeric states of the active-site histidines of phosphorylated and unphosphorylated IIIIGlc, a signal-transducing protein from escherichia coli, using two-dimensional heteronuclear NMR techniques, *Protein Science* *2*, 543-558.
- [34] Sudmeier, J. L., Bradshaw, E. M., Haddad, K. E. C., Day, R. M., Thalhauser, C. J., Bullock, P. A., and Bachovchin, W. W. (2003) Identification of histidine tautomers in proteins by 2D ^1H - ^{13}C ($\Delta 2$) one-bond correlated NMR, *Journal of the American Chemical Society* *125*, 8430-8431.
- [35] Zhou, X. Z., Kops, O., Werner, A., Lu, P. J., Shen, M. H., Stoller, G., Kullertz, G., Stark, M., Fischer, G., and Lu, K. P. (2000) Pin1-dependent prolyl isomerization regulates dephosphorylation of Cdc25C and tau proteins, *Molecular Cell* *6*, 873-883.
- [36] Cavanagh, J., Fairbrother, W. J., Palmer III, A. G., and Skelton, N. J. (1996) Heteronuclear NMR Experiments, *Academic Press, Inc., New York*.
- [37] Delaglio, F., Grzesiek, S., Vuister, G. W., Zhu, G., Pfeifer, J., and Bax, A. (1995) NMRpipe—a multidimensional spectral processing system based on unix pipes, *Journal of Biomolecular Nmr* *6*, 277-293.
- [38] Kobayashi, N., Iwahara, J., Koshiba, S., Tomizawa, T., Tochio, N., Guentert, P., Kigawa,

- T., and Yokoyama, S. (2007) KUJIRA, a package of integrated modules for systematic and interactive analysis of NMR data directed to high-throughput NMR structure studies, *Journal of Biomolecular Nmr* 39, 31-52.
- [39] Johnson, B. A. (2004) Using NMRView to Visualize and Analyze the NMR Spectra of Macromolecules, *In Protein NMR Techniques (Downing, A.K., Ed)*, pp 313-352.
- [40] Guentert, P. (2009) Automated NMR Structure Calculation With CYANA, *In Protein NMR Techniques (Downing, A.K., Ed)*, pp 353-378.
- [41] Guentert, P. (2009) Automated structure determination from NMR spectra, *European Biophysics Journal with Biophysics Letters* 38, 129-143.
- [42] Shen, Y., Delaglio, F., Cornilescu, G., and Bax, A. (2009) TALOS plus : a hybrid method for predicting protein backbone torsion angles from NMR chemical shifts, *Journal of Biomolecular Nmr* 44, 213-223.
- [43] Schwieters, C. D., Kuszewski, J. J., Tjandra, N., and Clore, G. M. (2003) The Xplor-NIH NMR molecular structure determination package, *Journal of Magnetic Resonance* 160, 65-73.
- [44] Laskowski, R. A., Rullmann, J. A. C., MacArthur, M. W., Kaptein, R., and Thornton, J. M. (1996) AQUA and PROCHECK-NMR: Programs for checking the quality of protein structures solved by NMR, *Journal of Biomolecular Nmr* 8, 477-486.
- [45] Koradi, R., Billeter, M., and Wuthrich, K. (1996) MOLMOL: A program for display and analysis of macromolecular structures, *Journal of Molecular Graphics* 14, 51-&.
- [46] Wilson, K. A., Bouchard, J. J., and Peng, J. W. (2013) Interdomain Interactions Support Interdomain Communication in Human Pin1, *Biochemistry* 52, 6968-6981.
- [47] Jeener, J., Meier, B. H., Bachmann, P., and Ernst, R. R. (1979) Investigation of exchange processes by 2-dimensional NMR-spectroscopy, *Journal of Chemical Physics* 71, 4546-4553.
- [48] d'Auvergne, E. J., and Gooley, P. R. (2008) Optimisation of NMR dynamic models I. Minimisation algorithms and their performance within the model-free and Brownian rotational diffusion spaces, *Journal of Biomolecular Nmr* 40, 107-119.
- [49] d'Auvergne, E. J., and Gooley, P. R. (2008) Optimisation of NMR dynamic models II. A new methodology for the dual optimisation of the model-free parameters and the Brownian rotational diffusion tensor, *Journal of Biomolecular NMR* 40, 121-133.
- [50] Platzer, G., Okon, M., and McIntosh, L. P. (2014) pH-dependent random coil ¹H, ¹³C, and ¹⁵N chemical shifts of the ionizable amino acids: a guide for protein pK (a) measurements, *Journal of Biomolecular NMR* 60, 109-129.
- [51] van de Ven, F. J. M. (1995) *Multidimensional NMR in Liquids*, Wiley-VCH.
- [52] Markus, M. A., Dayie, K. T., Matsudaira, P., and Wagner, G. (1996) Local mobility within

- villin 14T probed via heteronuclear relaxation measurements and a reduced spectral density mapping, *Biochemistry* *35*, 1722-1732.
- [53] Farrow, N., Zhang, O., Szabo, A., Torchia, D., and Kay, L. (1995) Spectral density function mapping using ¹⁵N relaxation data exclusively, *Journal of Biomolecular NMR* *6*, 153-162.
- [54] Lipari, G., and Szabo, A. (1982) MODEL-free approach to the interpretation of nuclear of nuclear magnetic resonance relaxation in macromolecules.1.theory and range of validity, *Journal of the American Chemical Society* *104*, 4546-4559.
- [55] Andrec, M., Montelione, G. T., and Levy, R. M. (2000) Lipari-Szabo mapping: A graphical approach to Lipari-Szabo analysis of NMR relaxation data using reduced spectral density mapping, *Journal of Biomolecular NMR* *18*, 83-100.
- [56] Marshall, H. E., Merchant, K., and Stamler, J. S. (2000) Nitrosation and oxidation in the regulation of gene expression, *Faseb Journal* *14*, 1889-1900.
- [57] Kim, S. O., Merchant, K., Nudelman, R., Beyer, W. F., Keng, T., DeAngelo, J., Hausladen, A., and Stamler, J. S. (2002) OxyR: A molecular code for redox-related signaling, *Cell* *109*, 383-396.
- [58] Arrigo, A. P. (1999) Gene expression and the thiol redox state, *Free Radical Biology and Medicine* *27*, 936-944.
- [59] Yano, H., Wong, J. H., Lee, Y. M., Cho, M. J., and Buchanan, B. B. (2001) A strategy for the identification of proteins targeted by thioredoxin, *Proceedings of the National Academy of Sciences of the United States of America* *98*, 4794-4799.
- [60] Lind, C., Gerdes, R., Hammell, Y., Schuppe-Koistinen, I., von Lowenhielm, H. B., Holmgren, A., and Cotgreave, I. A. (2002) Identification of S-glutathionylated cellular proteins during oxidative stress and constitutive metabolism by affinity purification and proteomic analysis, *Archives of Biochemistry and Biophysics* *406*, 229-240.
- [61] Hoppe, G., Talcott, K. E., Bhattacharya, S. K., Crabb, J. W., and Sears, J. E. (2006) Molecular basis for the redox control of nuclear transport of the structural chromatin protein Hmgb1, *Experimental Cell Research* *312*, 3526-3538.
- [62] Thomas, J. O., and Travers, A. A. (2001) HMG1 and 2, and related 'architectural' DNA-binding proteins (vol 26, pg 167, 2001), *Trends in Biochemical Sciences* *26*, 219-219.
- [63] Thomas, J. O. (2001) HMG 1 and 2: architectural DNA-binding proteins, *Biochemical Society Transactions* *29*, 395-401.
- [64] Tang, D., Kang, R., Zeh, H. J., III, and Lotze, M. T. (2011) High-Mobility Group Box 1, Oxidative Stress, and Disease, *Antioxidants & Redox Signaling* *14*, 1315-1335.
- [65] Zandarashvili, L., Sahu, D., Lee, K., Lee, Y. S., Singh, P., Rajarathnam, K., and Iwahara, J. (2013) Real-time Kinetics of High-mobility Group Box 1 (HMGB1) Oxidation in

- Extracellular Fluids Studied by in Situ Protein NMR Spectroscopy, *Journal of Biological Chemistry* 288, 11621-11627.
- [66] Sahu, D., Debnath, P., Takayama, Y., and Iwahara, J. (2008) Redox properties of the A-domain of the HMGB1 protein, *Febs Letters* 582, 3973-3978.
- [67] Park, S., and Lippard, S. J. (2011) Redox State-Dependent Interaction of HMGB1 and Cisplatin-Modified DNA, *Biochemistry* 50, 2567-2574.
- [68] Venereau, E., Casalgrandi, M., Schiraldi, M., Antoine, D. J., Cattaneo, A., De Marchis, F., Liu, J., Antonelli, A., Preti, A., Raeli, L., Shams, S. S., Yang, H., Varani, L., Andersson, U., Tracey, K. J., Bachi, A., Ugucconi, M., and Bianchi, M. E. (2012) Mutually exclusive redox forms of HMGB1 promote cell recruitment or proinflammatory cytokine release, *Journal of Experimental Medicine* 209, 1519-1528.
- [69] Pil, P. M., and Lippard, S. J. (1992) Specific binding of chromosomal protein-HMG1 to DNA damaged by the anticancer drug cisplatin, *Science* 256, 234-237.
- [70] Ugrinova, I., Zlateva, S., Pashev, I. G., and Pasheva, E. A. (2009) Native HMGB1 protein inhibits repair of cisplatin-damaged nucleosomes in vitro, *International Journal of Biochemistry & Cell Biology* 41, 1556-1562.
- [71] Huang, J. C., Zamble, D. B., Reardon, J. T., Lippard, S. J., and Sancar, A. (1994) HMG-domain proteins specifically inhibit the repair of the major DNA adduct of the anticancer drug cisplatin by human excision nuclease, *Proceedings of the National Academy of Sciences of the United States of America* 91, 10394-10398.
- [72] Mello, J. A., Lippard, S. J., and Essigmann, J. M. (1995) DNA-adducts of cis-diamminedichloroplatinum (II) and its trans isomer inhibit RNA-polymerase-II differentially in vivo, *Biochemistry* 34, 14783-14791.
- [73] Shimizu, M., and Rosenber.B. (1973) Similar action to UV-irradiation and a preferential inhibition of DNA-synthesis in escherichia-coli by antitumor platinum compounds, *Journal of Antibiotics* 26, 243-245.
- [74] Wei, M., Burenkova, O., and Lippard, S. J. (2003) Cisplatin sensitivity in HMGB1(-/-) and HMGB1 mouse cells, *Journal of Biological Chemistry* 278, 1769-1773.
- [75] Ohndorf, U. M., Rould, M. A., He, Q., Pabo, C. O., and Lippard, S. J. (1999) Basis for recognition of cisplatin-modified DNA by high-mobility-group proteins, *Nature* 399, 708-712.
- [76] Uewaki, J.-I., Kamikubo, H., Kurita, J.-I., Hiroguchi, N., Moriuchi, H., Yoshida, M., Kataoka, M., Utsunomiya-Tate, N., and Tate, S.-I. (2013) Preferential domain orientation of HMGB2 determined by the weak intramolecular interactions mediated by the interdomain linker, *Chemical Physics* 419, 212-223.
- [77] Sharma, D., and Rajarathnam, K. (2000) ¹³C NMR chemical shifts can predict disulfide

- bond formation, *Journal of Biomolecular NMR* 18, 165-171.
- [78] Sterner, R., Vidali, G., and Allfrey, V. G. (1979) Studies of acetylation and deacetylation in high mobility group proteins-identification of the sites of acetylation in HMG-1, *Journal of Biological Chemistry* 254, 1577-1583.
- [79] Ottiger, M., Delaglio, F., and Bax, A. (1998) Measurement of J and dipolar couplings from simplified two-dimensional NMR spectra, *Journal of Magnetic Resonance* 131, 373-378.
- [80] Herrmann, T., Guntert, P., and Wuthrich, K. (2002) Protein NMR structure determination with automated NOE assignment using the new software CANDID and the torsion angle dynamics algorithm DYANA, *Journal of Molecular Biology* 319, 209-227.
- [81] Cornilescu, G., Delaglio, F., and Bax, A. (1999) Protein backbone angle restraints from searching a database for chemical shift and sequence homology, *Journal of Biomolecular NMR* 13, 289-302.
- [82] Linge, J. P., Williams, M. A., Spronk, C., Bonvin, A., and Nilges, M. (2003) Refinement of protein structures in explicit solvent, *Proteins-Structure Function and Bioinformatics* 50, 496-506.
- [83] Bax, A., Kontaxis, G., and Tjandra, N. (2001) Dipolar couplings in macromolecular structure determination, *Nuclear Magnetic Resonance of Biological Macromolecules, Pt B* 339, 127-174.
- [84] Dominguez, C., Boelens, R., and Bonvin, A. (2003) HADDOCK: A protein-protein docking approach based on biochemical or biophysical information, *Journal of the American Chemical Society* 125, 1731-1737.
- [85] Wallace, A. C., Laskowski, R. A., and Thornton, J. M. (1995) LIGPLOT – a program to generate schematic diagrams of protein ligand interactions, *Protein Engineering* 8, 127-134.
- [86] De Vries, S. J., van Dijk, M., and Bonvin, A. M. J. J. (2010) The HADDOCK web server for data-driven biomolecular docking, *Nature Protocols* 5, 883-897.
- [87] Palmer, A. G. (1997) Probing molecular motion by NMR, *Current Opinion in Structural Biology* 7, 732-737.
- [88] Travers, A. (2000) Recognition of distorted DNA structures by HMG domains, *Current Opinion in Structural Biology* 10, 102-109.

公表論文

Allosteric breakage of the hydrogen bond within the dual-histidine motif in the active site of human Pin1 PPIase

Jing Wang, Naoya Tochio, Ryosuke Kawasaki, Yu Tamari, Xu Ning, Jun-ichi Uewaki, Naoko Utsunomiya-Tate, and Shin-ichi Tate

Biochemistry 54 5242-5253 (2015)

Redox-sensitive structural change in the A-domain of HMGB1 and its implication for the cisplatin modified DNA

Jing Wang, Naoya Tochio, Aya Takeuchi, Jun-ichi Uewakia, Naohiro Kobayashi, and Shin-ichi Tate.

Biochemical and Biophysical Research Communications (2013) 441,701-706.

受賞

Excellent Student Poster Award,

The chemistry Society of Japan: The regional of branch of shikoku andchugoku districts, Hiroshima University, 2013

The Best student presentation award ,

The 10th Nano Bio Info Chemistry Symposium, Hiroshima University, 2013

Excellent student scholarship,

Hiroshima University,2013

The Best student presentation award ,

The 11th Nano Bio Info Chemistry Symposium, Hiroshima University, 2014

Excellence Research Award,

The 6th TAIWAN-JAPAN Joint Workshop, Mei ji University, 2015